METHOD DEVELOPMENT FOR THE QUANTIFICATION OF SELECTED EARLY RARE EARTH ELEMENTS

S.M. XABA

METHOD DEVELOPMENT FOR THE QUANTIFICATION OF SELECTED EARLY RARE EARTH ELEMENTS

A thesis submitted to meet the requirements for the degree of
Magister Scientiae

in the

FACULTY OF NATURAL AND AGRICULTURAL SCIENCES
DEPARTMENT OF CHEMISTRY

at the

UNIVERSITY OF THE FREE STATE
BLOEMFONTEIN

by
SIBONGILE MAMUSA XABA

Promoter
Prof. W. Purcell

Co-promoter
Dr. J. A. Venter

January 2015

Declaration by candidate

"I hereby assert that the dissertation submitted for the degree Magister in Chemistry, at the University of the Free State is my own original work and has not been previously submitted to any other institution of higher education. I further declare that all sources cited or quoted are indicated and acknowledged by means of a comprehensive list of references."

Signature…… **Date**……..…….

Sibongile Mamusa Xaba

Acknowledgements

I would like to express my sincere gratitude and appreciation to the following people for their contributions towards this study:

- My *supervisor*, **Prof. W. Purcell** for his positive attitude and guidance through the research project. He was really helpful and I learnt considerably from him.

- My *co-supervisor*, **Dr J. Venter** for their guidance encouragement and constant reassurance during the time of my study.

- I wish to thank all colleagues (Ntate Nete, Dika, Hlengiwe, Gontse, Fanie and Trevor) for providing an environment that was helpful to undertake this project.

- Special thanks to family and friends (Khanya, Manana, Thembani, Thandeka and Dumisani) as well as Mr PS Sekonyela for the support and love throughout my studies especially my sister **Sarah Matopane Xaba** for the constant encouragement.

- Dedicated to the memory of **Vusi Kolber Xaba**, 27 June 1978 – 16 March 2013, a loving brother and father, lala ngoxolo Shwabade.

Sibongile Mamusa Xaba

TABLE OF CONTENTS

LIST OF FIGURES

LIST OF TABLES

LIST OF ABBREVIATIONS

ANALYTICAL EQUIPMENT

CHNS micro-analyser	Carbon, hydrogen, nitrogen, sulphur micro-analyser
FAAS	Flame atomic absorption spectroscopy
GFAAS	Graphite furnace atomic absorption spectrometry
ICP-OES	Inductively coupled plasma optical emission spectroscopy
ICP-MS	Inductively coupled plasma mass spectroscopy
IR	Infrared
UV/Vis	Ultra violet visible spectroscopy

LIGANDS

acac	Acetyl acetone
dap	Dimethylaminopyridine
imda	Iminodiacetic acid
nta	Nitrilotriacetic acid
TPPO	Triphenylphosphine oxide

SI UNITS

cm^{-1}	Reciprocal centimeter
nm	Nanometer
%	Percentage
g	Gram
°C	Degrees Celsius
ppb	Parts per billion
ppm	Parts per million
ppt	Parts per thousand/trillion

STATISTICAL TERMS

C.I.	Confidence interval
r^2	Correlation coefficient
LOD	Limit of detection
LOQ	Limit of quantification
H_a	Alternative hypothesis
H_0	Null hypothesis
RSD	Relative standard deviation
m	Slope
s	Standard deviation
S_c or S_b	Standard deviation of the intercept
S_m or S_a	Standard deviation of the slope

KEY WORDS

Cerium

Lanthanum

Neodymium

Quantitative analysis

Qualitative analysis

Accuracy

Recovery

1 STUDY MOTIVATION

1.1 BACKGROUND

The rare earth elements (REE) consist of a group of 17 metals which include scandium (Sc), yttrium (Y), and the lanthanides. The lanthanides are the 15 metals (lanthanum to lutetium) with atomic numbers 57 to 71 on the periodic table as shown in **Figure 1.1**. These REE are usually divided into two subgroups namely the light rare earth elements (LREE) which consist of the elements from lanthanum (La) to gadolinium (Gd) on the periodic table, while the heavy rare earth elements (HREE) include the elements from terbium (Tb) to lutetium (Lu). All the metals belonging to the LREE subgroup have unpaired electrons (0 to 7) in their elemental electron configuration, while the HREE have 'paired' electrons in their 4f orbitals.[1]

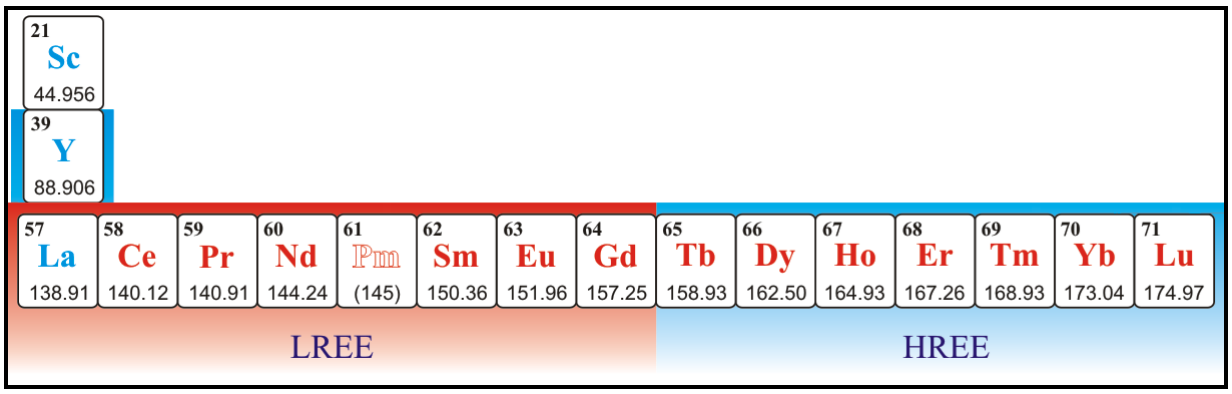

Figure 1.1: The REE in the periodic table.[1]

The global demand for REE has shown an upward trend of 7 to 9 % per annum which is in line with growth in green energy technologies since 1970.[2] This group of elements also find wide application in different sections in industry such as the electronic, optical, magnetic and catalytic fields. The REE do not occur as pure

[1] Rare earth elements, [Accessed 22-05-2013]. Available from: http://www.periodni.com/rare_earth_elements.html.

[2] Rare earth elements 101, [Accessed 22-05-2013]. Available from: http://www.iamgold.com/files/ree101_april_2012.pdf.

metals in the earth's crust, but they occur as the metal oxides with significant concentrations in several minerals such as bastnäesite, monazite and xenotime. The minerals bastnäesite and monazite contains about 95 % LREE while xenotime contains about 60 % yttrium which belongs to the HREE. Bastnäesite, which is one of the major sources of LREE, originates mainly in China and the U.S.

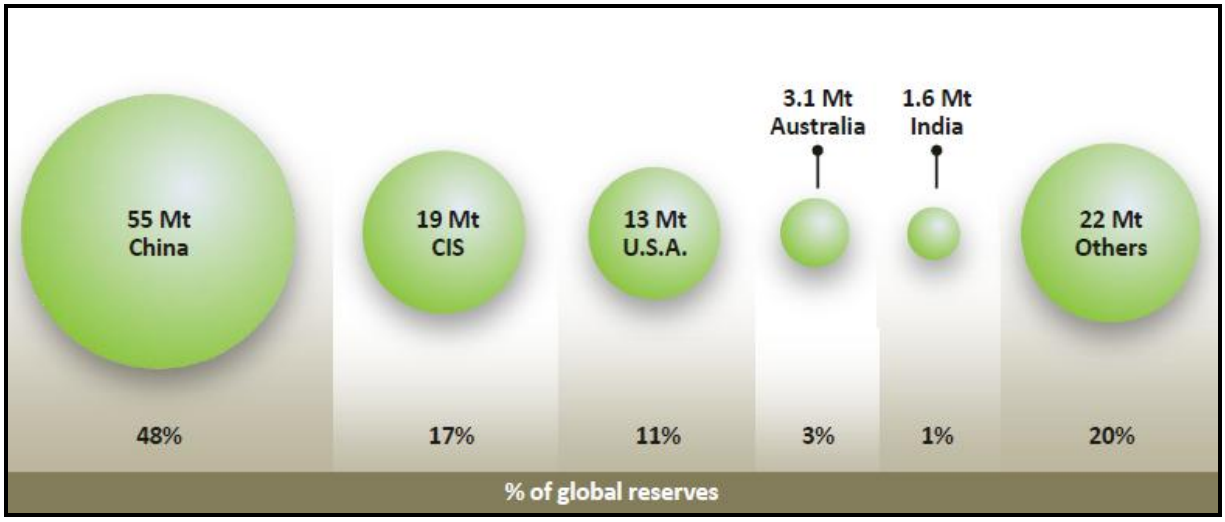

Figure 1.2: The distribution of rare earths per country.[3]

China accounts for 97 % of global REE production. Apart from that holds the country also a major percentage (~48 %) of the world's reserves which allow China to dominate the world's rare earth metals supplies. Other countries with known reserves are the CIS (Russia and former Soviet republics), U.S.A, Australia and India, while the remainder of the global reserves can be found in countries such as Africa, Brazil, Canada and Malaysia as shown in (**Figure 1.2**).[3] This monopoly of the REE pricing and export market by China are forcing other countries to adapt mitigating strategies to protect their own industries against dominance. This includes exploration for new REE sources as well as research and the development of their own REE industries.

The REE are currently in high demand due to their importance in the renewable energy industries, their application in defence as well as their use in other high-tech

[3] Rare earth elements, [Accessed 4-04-2013]. Available from: http://www.iamgold.com/files/HongKong2012REEPresentationFINAL.pdf.

products such as cell phones, television, hybrid cars and medical imaging.[4] One of the major difficulties of REE production is the presence of the radioactive elements Th and U in the majority of REE mineral deposits.[5] Radioactive minerals pose a problem with handling and transportation of large quantities since legislation only allows 0.2 Bq/g or less to be transported in 0.4 mSv/h containers. Recycling from electronic waste that contain significant amounts of rare earth metals can also be an important source of REE, which in turn will reduce the amount of REE exposed to the environment and lowers radioactivity arising in secondary REE processing.

The REE share numerous common physical and chemical properties that make them difficult to characterise or chemically separate them from each other. Such common physical properties include shiny silver-grey metallic colours, and they are good conductors of heat and electricity. Chemical properties which are very similar include their ability to be tarnished in air to form metal oxides and their ability to react quickly in hot H_2O or in diluted acids. The REE most common oxidation state is +3 and some of the separation processes utilize the stability of some of the elements in other oxidation states, e.g. (Ce(III) could be oxidized to Ce(IV) and Eu(III) could be reduced to Eu(II)). REE separation is usually carried out by a hydrometallurgical process such as solvent extraction or ion exchange which is based on the orderly difference in their basicity, which decreases from La to Lu. Major analytical problems associated with the quantification of the different REE are normally attributed to spectral or acid matrix interferences and inaccurate or poor recoveries due to changes in temperature of the nebulizer of the inductively coupled plasma (ICP) and finally to chemical interferences.

Steenkampskraal in the Western Cape is known to have one of the richest REE deposits in SA and worldwide and mainly produces monazite. It was initially operated as a thorium producing mine that exported the radioactive Th as a nuclear fuel source to the United Kingdom. With the development of uranium technology as the primary radioactive fuel source, thorium was discarded as energy fuel in 1960s and

[4] Replacing oil addiction with metals dependence, [Accessed 12-04-2013]. Available from: http://news.nationalgeographic.com/news/2010/10/101001-energy-rare-earth-metals/.

[5] Rare earth element, [Accessed 12-04-2013]. Available from: http://www.capitalco.com.au/Portals/0/Docs/Minerals_Energy/Rare%20Earth%20Elements.pdf.

Steenkampskraal mine was left abandoned. The importance of some of the REE such as Sm, Nd and La in the renewable or green energy has also prompted renewed interest by different role players in SA to explore the development of a REE industry in SA. The Great Western Minerals Group (GWMG) a leader in the exploration and manufacturing of REE based in Canada, bought the controlling interest of the Steenkampskraal monazite project (REE now main interest and Th by-product) in an effect to provide for its own separation plant the REE that were left on the surface from previous operations.[6] GWMG plans were to support Steenkampskraal with knowledge and skills to process the REE and to reduce potential hazards by mixing the thorium with concrete and storing it in blocks underground. This strategy of permanent Th waste removal is currently been re-evaluated [7] as a result of the newly developed Th/molten salt nuclear plant technology (Th-MOX) which is currently undergoing been tests in Sweden by a the Norwegian Energy Company, called Thor Energy.[8] The main goal of the Norwegians was to develop a safe, dependable and economical nuclear fuel for use in presently operating and future Light Water Reactors (LWR). Recent studies have proven that Th-MOX in LWR does not only show a possibility of fuel but it also allows the nuclear power plant to achieve longer operating cycles.[9]

The importance of REE to produce future and sustainable energy and the lack of adequate analytical and hydrometallurgical skills in SA, prompted this investigation.

[6] Rare earths mine refu, [Accessed 29-05-2013]. Available from: http://www.srk.co.za/files/File/South-Africa/pressreleases/2013/January_2013/african_mining_brief_rare_earths_mine_refub_01_jan_2013_pp36-37.pdf.

[7] A 21st century scramble: South Africa, China and the rare earth metals industry, [Accessed 2-05-2013]. Available from: http://www.saiia.org.za/occasional-papers/a-21st-century-scramble-south-africa-china-and-the-rare-earth-metals-industry.

[8] Thorium, [Accessed 29-05-2013]. Available from: http://www.world-nuclear.org/info/Current-and-Future-Generation/Thorium/#.UaXKrPXcPkI.

[9] Thorium - plutonium fuel for long operating cycles in pwrs-preliminary calculations, [Accessed 2-05-2012]. Available from: http://www.thorenergy.no/no/Topmenu/~/media/ThorEnergy/PDF/longcycles.ashx.

1.2 AIM OF THIS STUDY

With the above-mentioned in mind, the objectives of this study are to:

- Perform an in-depth literature study on the analytical techniques for the analysis of REE.
- Develop an analytical procedure that can accurately determine and quantify lanthanum, cerium and neodymium in pure REE metal, inorganic compounds as well as in organometallic complexes.
- Determine the influence of different acids on the lanthanum, cerium and neodymium recoveries.
- Comparing the results of different analytical techniques such as ICP-OES, IR and CHNS-micro analyser.
- Statistically validate these methods.

2 INTRODUCTION

2.1 INTRODUCTION

According to IUPAC (International Union of Pure and Applied Chemistry) the rare earth elements (REE) consist of a group of 17 metals which include scandium (Sc), yttrium (Y) (Group 3) and the inner transition metals (lanthanides).[10] The inner transition metals or lanthanides consist of 15 metals in the f-block series which is presented on a separate sub-table below the main part of the periodic table (**Figure 2.1**). The atomic number (Z) for these REE metals range from 57 to 71 and they are divided into two sub-groups, namely the light rare earth elements (LREE) and the heavy rare earth elements (HREE)). The LREE consists of the following metals namely, lanthanum (La), cerium (Ce), praseodymium (Pr), neodymium (Nd), promethium (Pm), samarium (Sm), europium (Eu) and gadolinium (Gd). The HREE include metals such as terbium (Tb), dysprosium (Dy), holmium (Ho), erbium (Er), thulium (Tm), ytterbium (Yb) and lutetium (Lu). The division between the REE are made according to the valence electron configuration, with the LREE subgroup having unpaired electrons from 0 to 7 in the 4f orbitals, while the HREE have paired electrons in the outer valence orbitals.[11]

Sc (Z = 21) and Y (Z = 39) are grouped with the lanthanides due to their similarity in chemical properties (high coordination number and trivalent oxidation state) and because they usually occur naturally in the same minerals with the lanthanides.[12] The REE are not that rare at all, and actually contribute to 17 % of all the naturally occurring metals, except for the element Pm, which is an artificial element created by nuclear fission. The lanthanides are part of the f-block elements in the periodic table

[10] Chemical nomenclature, [Accessed 06-06-2013]. Available from: http://en.wikipedia.org/wiki/IUPAC_nomenclature].

[11] Rare earth elements, [Accessed 22-05-2013]. Available from: http://www.periodni.com/rare_earth_elements.html.

[12] W B Jensen, *Journal of Chemical Education*, 1982, 59, p634.

(**Figure 2.1**) filling the 4f orbitals. Neither Dmitry Mendeleev nor his colleagues were able to place this group of elements in the inner transition block of the periodic table due to the absence of an identifiable atomic theory at that point in time. In 1913 Henry Moseley and Niels Bohr used elemental X-ray emission spectra and concluded from their results the order of the lanthanides from La to Lu, with atomic numbers from 57 to 71.[13] The lanthanides were then placed between barium (56) and hafnium (72) on the periodic table to obey the atomic number order.

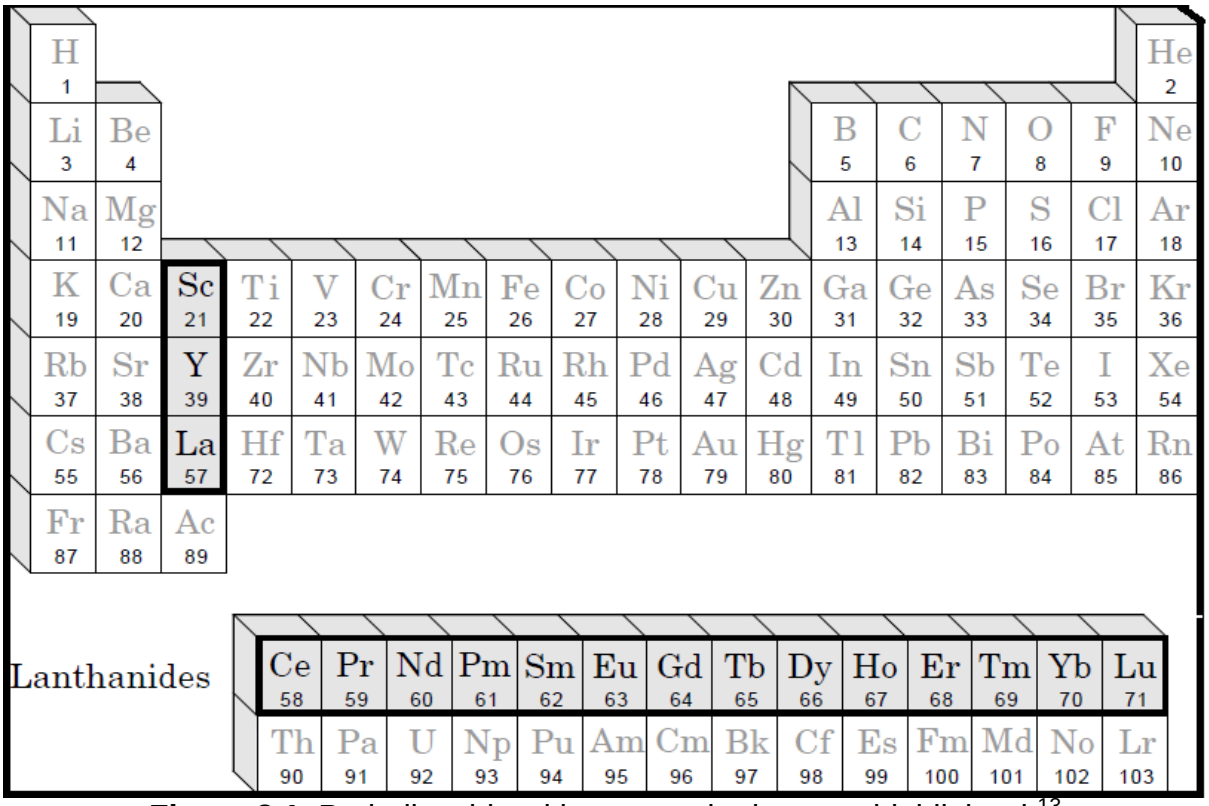

Figure 2.1: Periodic table with rare earth elements highlighted.[13]

The lanthanides, as well as Sc and Y are grouped together as REE due to the similarities in their properties such as atomic radii, ionization energies and melting points.[12,14]

[13] Introduction to the rare earths, [Accessed 10-6-2013]. Available from: www.liv.ac.uk/~sdb/Research/Chapter1.pdf.

[14] S A Cotton, Lanthanide and Actinide Chemistry, *John Wiley & Sons: Hoboken, NJ*, 2006, pp2-7.

2.2 DISCOVERY OF REE

The earliest REE were discovered in 1751 and 1787 from two minerals namely “cerite” (by Martin-Heinrich Klaproth, Jöns Jacob Berzelius, and Wilhelm Hisinger) and “gadolinite” (by Johann Gadolin) respectively and were believed to be pure metal oxides.

In 1787 a black coloured mineral, initially called ytterbite, was discovered by lieutenant Carl Axel Arrhenius.[15] He sent this mineral to Johann Gadolin in 1794 who analysed the mineral for its elemental content. He discovered that the ytterbite mineral contain a metal oxide which he called yttria. This yttria sample however contained an impure yttrium oxide, and the mineral itself was later renamed gadolinite in honour of Gadolin.

The heavy REE mineral cerite was discovered and analysed by Axel Fredrik Crönstedt in 1751, but he could only extract nickel.[16,17] Berzelius and Hisinger re-analysed the cerite from the Bastnäs iron mine near Riddarhyttan in 1794. They isolated a cerium oxide which had a yellow colour and named it ceric earth, only to discover later that the German chemist Martin-Heinrich Klaproth also analysed the same cerite mineral and named his mineral ochröite (yellow). Both research groups reported the chemical composition as $(Ce, REE)_9CaFeSi_7O_{27}(OH)_4$.[18]

[15] K A Gschneidner and J M Cappellen, 1787-1987 Two hundred years of rare earth, *Rare earth information center, Iowa State Universitv. Ames. Iowa. USA,* 1987, 2nd ed., p10.

[16] J E Jorpes and B T Kungl, Svenska Vetenskapsakademies Historis VII-Jac.Berzelius, *Regia Academia Scientiarum Suecica,* 1966, p8.

[17] A F Cronstedt, Forsok till mineralogies eller mineral-rikets upstallning, *The Gale Group, Farmington Hills, Michigan*, 1758, p3.

[18] R V Gaines, *Cambridge Geology magazine Journal*, 1997, 8, p6.

Figure 2.2: The European chemists that discovered the REE during the seventeenth and eighteenth centuries.[19]

In 1839 Carl Gustav Mosander, Berzelius's student, extracted a new metal from cerite which they called lanthanum. He pursued his investigations of the same REE mineral and in 1842 reported the discovery of another new metal which he called didymium (an inseparable twin brother of lanthanum) from the same mineral sample. In 1885 Carl Auer von Welsbach separated this so-called new element didymium into two new metals namely Nd and Pr, with neodymium meaning "new twin".

[19] Rare earth element, [Accessed 14-02-2013]. Available from: https://en.wikipedia.org/wiki/Rare_earth_element.

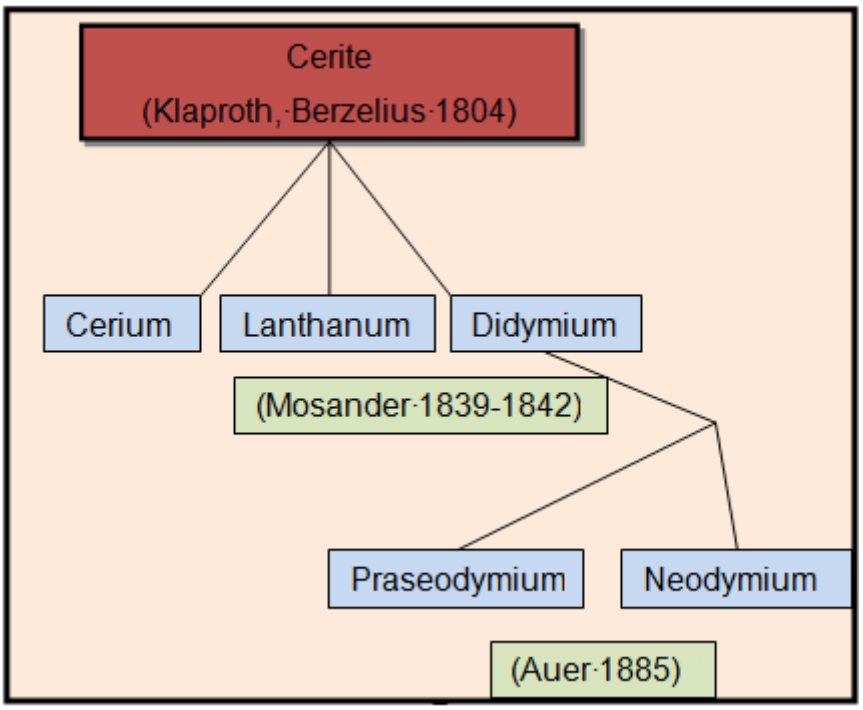

Figure 2.3: The partial scheme of the rare earth elements since 1804 to 1885.[20]

It took more than 100 years to discover and identify all 15 REE from different minerals. Colour, crystal structure, reactivity, chemical composition, occurrence and distribution in nature were the most important factors in determining the properties of the REE. Scientists still use these properties to identify which metals are present in minerals.[21]

2.3 NATURAL OCCURANCE OF REE MINERALS

The REE are not really rare, as abundance in the earth's crust of up to 70 ppm is found and more than 200 minerals have been identified that contain these REE indifferent proportions. Minerals such as bastnäesite, monazite and xenotime are the most economically viable REE minerals which are used for metal beneficiation.[22,23]

[20] K A Gschneidner Jr. and L Eyring, Handbook on the physics and chemistry of rare earths, *Elsevier Science Publishers B.V.*, 1988, p53.

[21] C Huang, Rare earth coordination chemistry fundamentals and applications, *John Wiley & Sons (Asia) Pte Ltd*, 2010, pxxiii,14.

[22] R Chi, S Xu, G Zhu, J Xu and X Qiu, Beneficiation of rare earth ore in china , *Light Metals held at the 130th TMS Annual Meeting*, 2001, pp1159-1165.

Interestingly the minerals tend to contain either LREE or HREE as major lanthanide composition, but generally include most of the REE in some quantity. The proportions of the different REE within minerals differ between deposits. Bastnäesite is a yellowish to reddish-brown carbonate mineral and it is divided into three different types of mineral groups depending on the relative proportion of REE within the mineral. These groups are bastnäesite (Ce), bastnäesite (La) and bastnäesite (Y) with a formula of (Ce, La)CO_3F, (La, Ce)CO_3F and (Y)CO_3F respectively. Bastnäesite with up to ~70 % rare earth oxide content depends on the predominant REE element (**Table 2.1**).[24] Bastnäesite is mostly found at the Bayan Obo mine in China as well as at the Mountain Pass mine in the United States (**Figure 2.5**). China is currently the largest REE economical resource in the world.

Figure 2.4: Bastnäesite and monazite minerals.[25]

The other commercially useful REE mineral monazite is a heavy, reddish-brown mineral. Similarly, there are three different kinds of monazite, depending on the relative proportion of REE within the mineral namely, monazite (Ce), monazite (La) and monazite (Nd). Unlike bastnäesite, monazite also contains up to 30 % of thorium and also 1 % of uranium which complicates its beneficiation processes considerably. The global distribution of REE deposits is illustrated in **Figure 2.5** and it is clear from

[23] C K Gupta and D K Bose, *Bulletin of Materials Science,* 1989; v 12, pp381-405.

[24] A Jordens, Y P Cheng and E Kristian, *Minerals Engineering, 2013,* 41, pp97-114.

[25] F Spedding and A H Daane, The rare earths, *John Wiley & Sons, Inc*., 1961, pp77-89.

this figure that a large number of REE deposits are located in China, the USA as well as Canada.

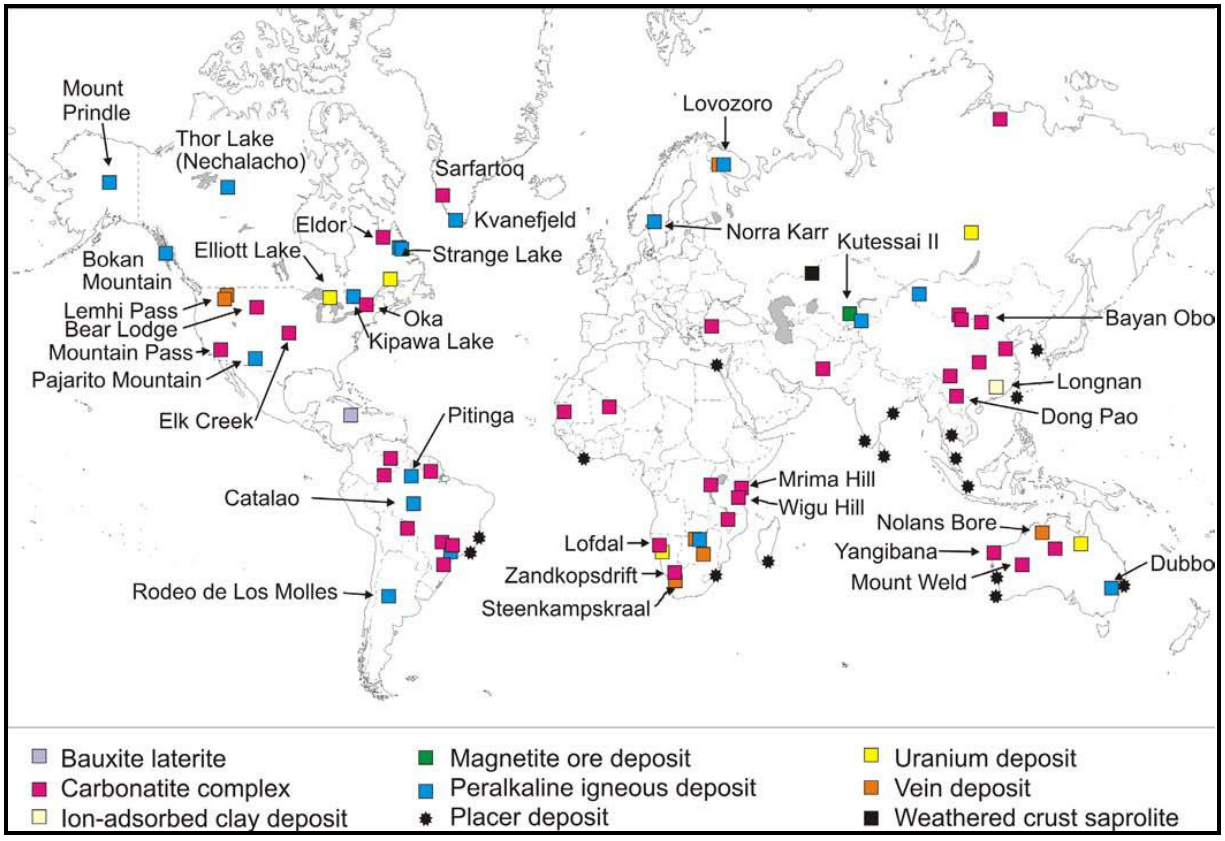

Figure 2.5: The global distribution REE resources. [26]

[26] D J Szumigala and M B Werdon, Rare-earth elements: a brief overview including uses, worldwide resources, and known occurrences in Alaska, *Alaska Division of Geological and Geophysical Surveys*, 2011, 6, pp1-13.

Table 2.1: Typical abundance of the REE in ores.[a14]

Element	Symbol	Monazite (%)	Bastnäesite (%)	Xenotime (%)
Lanthanum	La	20	33.2	0.5
Cerium	Ce	43	49.1	5
Praseodymium	Pr	4.5	4.3	0.7
Neodymium	Nd	16	12	2.2
Promethium	Pm	0	0	0
Samarium	Sm	3	0.8	1.9
Europium	Eu	0.1	0.12	0.2
Gadolinium	Gd	1.5	0.17	4
Terbium	Tb	0.05	**160**	1
Dysprosium	Dy	0.6	**310**	8.6
Holmium	Ho	0.05	**50**	2
Erbium	Er	0.2	**35**	5.4
Thulium	Tm	0.02	**8**	0.9
Ytterbium	Yb	0.1	**6**	6.2
Lutetium	Lu	0.02	**1**	0.4
Yttrium	Y	2.5	0.1	60

[a]Bold values are in parts per million (ppm)

Xenotime (**Table 2.1**) the last of the popular commercially-viable minerals, is a greenish brown mineral which is sometimes also associated with monazite. It differs from the rest of the minerals in that it belongs to an informal group of phosphate minerals that does not contain chlorides, hydroxides or water molecules as counter ions. Xenotime contains up to 60 % of yttrium oxide (**Table 2.1** and **Table 2.2**), and

trace amounts of radioactive metals such as uranium and thorium. Xenotime occurs mainly in Brazil, Madagascar, North Carolina, Norway and Sweden.

Table 2.2: REE bearing minerals.[27]

Mineral name	Chemical formula	Type	Weight (%)		
			LnO	ThO	UO
Bastnäesite (Ce)	$(Ce,La)(CO_3)F$	Carbonates	70 - 74	0 - 0.3	0.09
Bastnäesite (La)	$(La,Ce)(CO_3)F$	Carbonates	70 - 74	0 - 0.3	0.09
Bastnäesite (Y)	$Y(CO_3)F$	Carbonates	70 - 74	0 - 0.3	0.09
Monazite (Ce)	$(Ce,La,Nd,Th)PO_4$	Phosphates	35 - 71	0 - 20	0 - 16
Monazite (La)	$(La,Ce,Nd,Th)PO_4$	Phosphates	35 - 71	0 - 20	0 - 16
Monazite (Nd)	$(Nd,Ce,La,Th)PO_4$	Phosphates	35 - 71	0 - 20	0 - 16
Xenotime (Y)	YPO_4	Phosphates	52 - 67	-	0 - 5

Key: LnO - Lanthanide Oxide ThO - Thorium Oxide UO - Uranium Oxide

[27] A Jordens, A Cheng and Y P Waters, *Minerals Engineering*, 2013, 41, pp97-114.

2.4 ABUNDANCE AND RESOURCE OF REE ELEMENTS

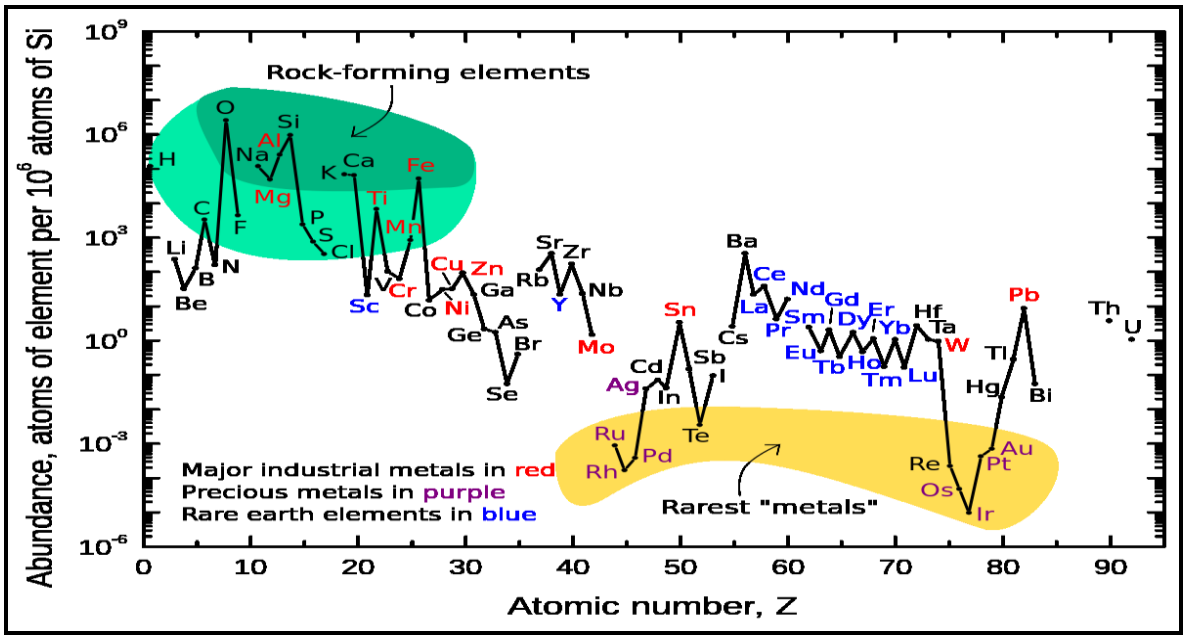

Figure 2.6: The relative abundance of the REE in Earth's upper continental crust.[28]

The LREE such as Y, La, Ce and Nd are more abundant in the earth's crust than some of the HREE such as Tm and Lu (**Figure 2.6**). Their abundance ranges from 66 ppm Ce to 0.4 ppm Lu as shown in **Table 2.3**. Interestingly it appears that the REE with an even atomic number are seven times more abundant than those with an odd atomic number according to the Oddo-Harkins rule. Pr is the only REE which is extremely scarce, highly unstable and radioactive. Main sources of REE as indicated in **Paragraph 2.3** are the minerals such as bastnäesite, monazite, and xenotime. Despite their high relative abundance, the REE minerals are difficult to mine and extract which make the REE relatively expensive metals. Recent technological breakthroughs on the application of REE have stimulated the production of high quality rare earth metals and their alloys. These products are mainly used in the production of clean or green energy.

[28] Rare earth elements-critical resources for high technology, [Accessed 21-01-2013]. Available from: http://pubs.usgs.gov/fs/2002/fs087-02/, 2002.

Table 2.3: The REE abundance in the earth's crust and the solar system.[14]

Symbol	Atomic weight	Atomic number	Crust (ppm)	Solar system
La	138.91	57	35	4.5
Ce	140.12	58	66	1.2
Pr	140.91	59	9.1	1.7
Nd	144.24	60	40	8.5
Pm	144.91	61	0	0
Sm	150.36	62	7	2.5
Eu	151.96	63	2.1	1
Gd	157.25	64	6.1	3.3
Tb	158.93	65	1.2	0.6
Dy	162.5	66	4.5	3.9
Ho	164.93	67	1.3	0.9
Er	167.26	68	3.5	2.5
Tm	168.93	69	0.5	0.4
Yb	173.04	70	3.1	2.4
Lu	174.97	71	0.8	0.4
Y	88.90	39	31	40
Sc	44.96	21	22	342

2.5 REE PRODUCTION, MARKET AND BENEFICIATION

2.5.1 THE REE PRODUCTION

The Mountain Pass mine in south-eastern United States dominated worldwide REE production from the 1960s to the 1980s, especially the production of Eu which was used in the manufacturing of colour screens. This mine contained 8 to 12 % of rare earth oxides, mainly as LREE. These deposits also contain significant quantities of radioactive elements. At that time the Mountain Pass mine was the world's main supplier of REE, which produced 33 % of the global supply of rare earth oxides and 100 % of the USA demand. The mine was closed in the early 2000s due to environmental restrictions (radio-active waste) and lower prices for REE, but largely due to competition from REE imported from China. Mountain Pass currently produces bastnäesite ores and sells separated REE from stockpiles produced before the mine was closed.

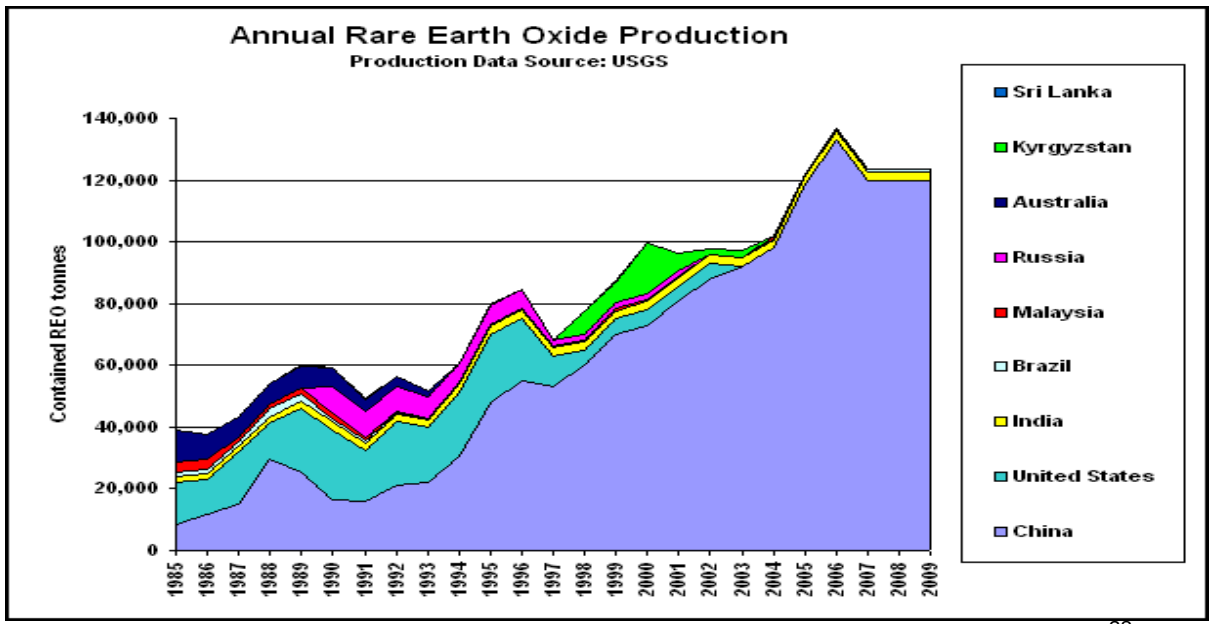

Figure 2.7: Worldwide production of rare earth oxides from 1985 to 2009.[28]

During the 1980s China emerged as a major producer of the REE while the market share of Australia and Americans decreased dramatically, mainly due to production

increase in China and a slump in market prices.[29] This dramatic shift in major REE producers is illustrated by production results in **Figure 2.7** which indicated that more than 80 % of the REE was produced by China in the late 1990s, with major deposits of REE located in the Bayan Obo mining district in the west section of the Inner Mongolia. This shift in market share continued in 2009 with China producing up to 97 % of the world REE raw materials. This dominance of the REE market enabled China to manipulate the whole REE chain with little or no competition in the market. In 2010 China restricted its REE ore exports to the rest of the world to ensure adequate supplies for its own market and to ensure economic growth in their own country. This in turn resulted in a world-wide supply shortage which affected the REE prices to skyrocket in 2010 and 2011.[30]

Figure 2.8: The high concentration REE in deep-sea mud around the island of Minami-Torishima (the rare earth minerals location are indicated by red dots).[31]

In 2011 Japan discovered high concentrations of REE in sea-mud around the island at approximately 5700 meters below the sea level (**Figure 2.8**). Their discovery includes some of the scarcest and the very expensive metals such as Dy, Tb, Eu and Yb. This discovery makes Japan the only country outside of China which has a major

[29] É S Potvin, Canada's rare earth deposits can offer a substantial competitive advantage, *Canadian Bussiness Journal*, 2012, p5.

[30] Rare earth element, [Accessed 05-09-2012]. Available from: http://www.capitalco.com.au/Portals/0/Docs/Minerals_Energy/Rare%20Earth%20Elements.pdf.

REE source with commercial viable quantities of these metals.[31] This ocean-based REE deposits can easily be extracted using pressurized air with the minimal disturbance off the seafloor. In addition it contains little or no radioactive elements which simplify the beneficiation of the ores. The high REE content in these deposits may reduce China's monopoly on the market and subsequently lead to lower prices.

In South Africa, large veins of monazite were discovered at Steenkampskraal in the Western Cape. These deposits were actively mined from 1952 to 1963. Most of these deposits contained the LREE, but also high levels of radioactivity due to the presence of Th (up to 30 %). During that time the mine operated as a primary source of monazite, contaminated with Th. The Th was exported to the UK at that time as a nuclear fuel source. Uranium later replaced thorium as nuclear fuel (and weapon manufacturing), which in turn reduced the demand for Th and led to the shutdown of Steenkampskraal.

Two attempts in 1997 and 2005 were made to restart the mine. The first attempt when the prices of REE were considered as undervalued and the second time when price manipulation problems emerged during the 2008 global recession. In 2011 the Great Western Minerals Group (GWMS) of Canada invested in a chain of up and downstream businesses relating to REE which included a joint value at Steenkampskraal with the Chinese company Ganzhou Qiandong Rare Earth Group Ltd (GQD). In the last quarter of 2012, the Steenkampskraal mine was brought back to production with its main interest the separation of the REE and Th as by-product.[32]

[31] "The U.S., China and rare earth metals" the future of green technology, military tech, and a potential Achilles‟ heel to American hegemony, [Accessed 05-09-2012]. Available from: http://dspace.nelson.usf.edu/xmlui/bitstream/handle/10806/4632/David%20Trigaux%20Honors%20Thesis%5B1%5D.pdf?sequence=1.

[32] Great Western Minerals Group and Ganzhou Qiandong Rare Earth Group sign rare earth separation agreement. Saskatoon, Canada: GWMG, Accessed 31-07-2013]. Available from: http://www.gwmg.ca/html/news/mediareleases/ index.cfm?ReportID=203424.

2.5.2 REE MARKET

China has 48 % of the world's REE deposits and supplies 97 % of the global demand, which is expected to grow between 7 - 9 % annually from 2011 to 2014 (see **Paragraph 1.1**). The growth is in products such as pure metals, REE oxides, chlorides and carbonates, and this growth is linked to the rate of growth of the low carbon technology market. China's monopoly on the REE market dictated the whole REE value chain until recently. Restriction on production and reducing export quotas were implemented by China to ensure it has enough reserves for technological and economic needs. This had an enormous influence on prices and supplies worldwide.

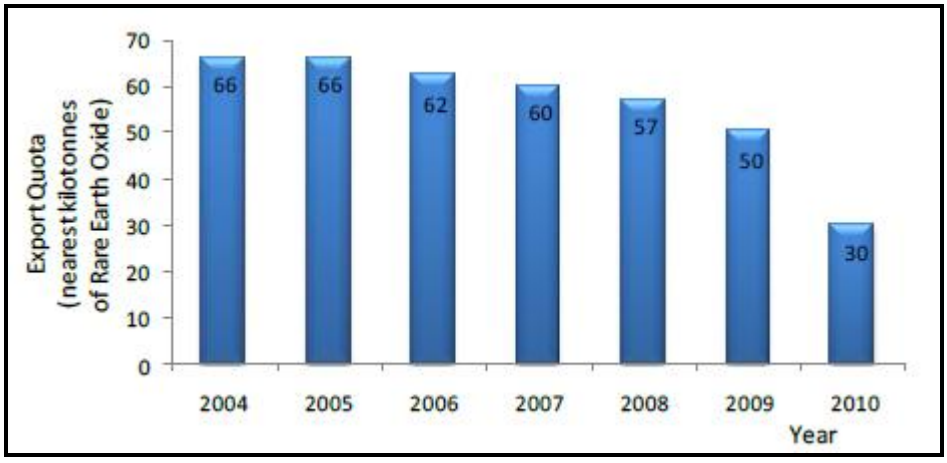

Figure 2.9: Chinese annual export quotas of REE.[33]

In April 2010 China reduced the exports of REE to other countries by almost half (see **Figure 2.9**). Greater demand for REE extraction and processing due to the development of new technologies resulted in a worldwide shortage of REE raw materials. The effect of this shortage can be seen in the price escalation of REE material in **Table 2.4**.[34]

[33] Rare earths, [Accessed 27-05-2013]. Available from: www.parliament.uk/briefing-papers/post-pn-368.pdf.

[34] Rare earth element, [Accessed 04-06-2013]. Available from: http:/ / mineralprices. com/ default. aspx#Rare).

Prices US$/kg					
Rare-earth oxide	**2007**	**2008**	**2009**	**2010**	**02/05/2011**
Lanthanum oxide	3.44	8.71	4.88	52.49	139.00
Cerium oxide	3.04	4.56	3.88	52.62	135.00
Neodymium oxide	30.24	31.90	19.12	81.38	225.00
Praseodymium oxide	29.05	29.48	18.03	78.62	208.00
Samarium oxide	3.60	5.20	3.40	36.58	120.00
Dysprosium oxide	89.10	118.49	115.67	287.85	705.00
Europium oxide	323.90	481.92	492.92	611.54	1200.00
Terbium oxide	590.40	720.77	361.67	620.38	1200.00

Table 2.4: REE prices from 2007 to 2011. [35]

Table 2.4 clearly shows the dramatic price escalation with a factor of 10 for some of the elements from 2009 to 2010 and a 2 fold increase from 2010 to 2011. These high prices for REE stimulated increased production worldwide by the opening of new and old mines (Steenkampskraal), recovery, re-use and recycling of REE.

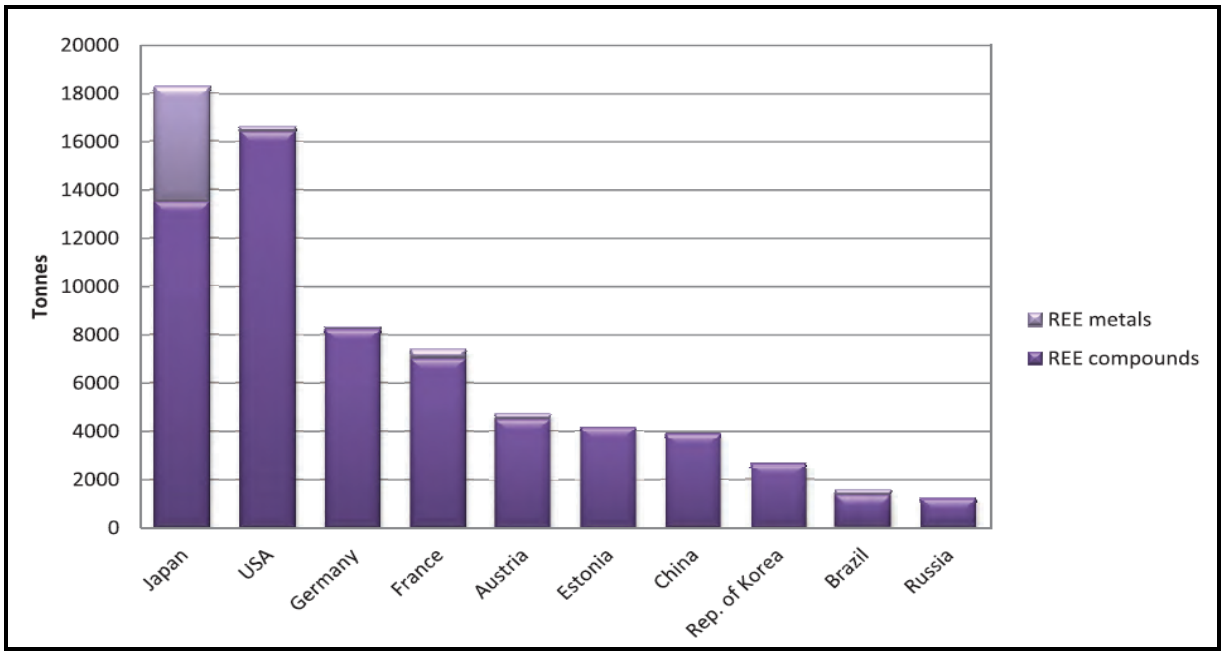

Figure 2.10: Top countries that import REE compounds and metals.[36]

[35] 2012 Annual Report, [Accessed 01-15-2013]. Available from: http://www.lynascorp.com/page.asp?category_id=1&page_id=25.

[36] UN commodity trade statistics database, [Accessed 27-05-2013]. Available from: http://comtrade.un.org/db.

In 2009 countries such as Japan and USA were the major importers of REE commodities and metals as shown in **Figure 2.10**. Japan however developed its own recycling plant for REE and recently discovered rich REE deposits in the sea mud (see **paragraph 2.7.1**) which make them less vulnerable to the imports from China.

2.5.3 REE BENEFICATION AND PRODUCTION

The production and subsequently selling and using of REE from the mineral deposits involve a number of beneficiation steps, namely mining, milling, hydrometallurgy, separation, purification and finally refining. The individual activities are as follows:

1. **Mining -** Extract the minerals from the ground to crushed ores
2. **Milling-** Grinding and beneficiation of minerals- gravity, magnetic, electronic and floatation
3. **Hydro-metallurgy-** Cracking the minerals to obtain mixed REE oxides concentrations
4. **Separation-** Separating and purifying the isolated REE oxide
5. **Refining-** To meet specific downstream technological applications

The selected processing methods for REE normally depend on the type of the minerals and economics of the operation. The recovery of REE oxides from the minerals firstly involves its crushing, grounding and classification.

The mineral bastnäesite from the Mountain Pass mine contains for example about 60 % REE oxides. In the processing of these minerals, HCI is employed to remove Sr and $CaCO_3$ to increase the REE oxide quantity to ~70 %. The next step involves calcining to remove CO_2 and this step increases the REE concentration to ~90 %. The processing of bastnäesite from the Bayan Obo mine involves the baking of the mineral with H_2SO_4 and then leaching with H_2O in a liquid-solid separation process.[37] The REE are subsequently precipitated as double sulphates, and then converted to

[37] Rare earth elements, [Accessed 12-02-2013]. Available from: http://nora.nerc.ac.uk/12583/1/Rare_Earth_Elements_profile.pdf.

the hydroxides. The final step involves the dissolution of the REE hydroxide with HCl as purification step.

Monazite and xenotime are processed differently. These minerals are firstly dissolved in hot concentrated alkaline or acidic solutions (H_2SO_4) to extract REE. H_2O is then used to dissolve and to remove the phosphate species. The alkaline treatment involves the dissolution of the minerals in NaOH at 145 °C to convert REE and Th to the hydroxides. These hydroxides are then dissolved by the addition of HCl. The ThO_2 remains as a solid under properly selected experimental conditions and is discarded as waste. A detailed flow diagram of the process is presented in **Figure 2.11**.[38]

[38] Inorganic chemistry (chemistry of lanthanoids), [Accessed 03-6-2013]. Available from: http://nsdl.niscair.res.in/bitstream/123456789/696/1/revised+Chemistry+of+Lanthanoides.pdf.

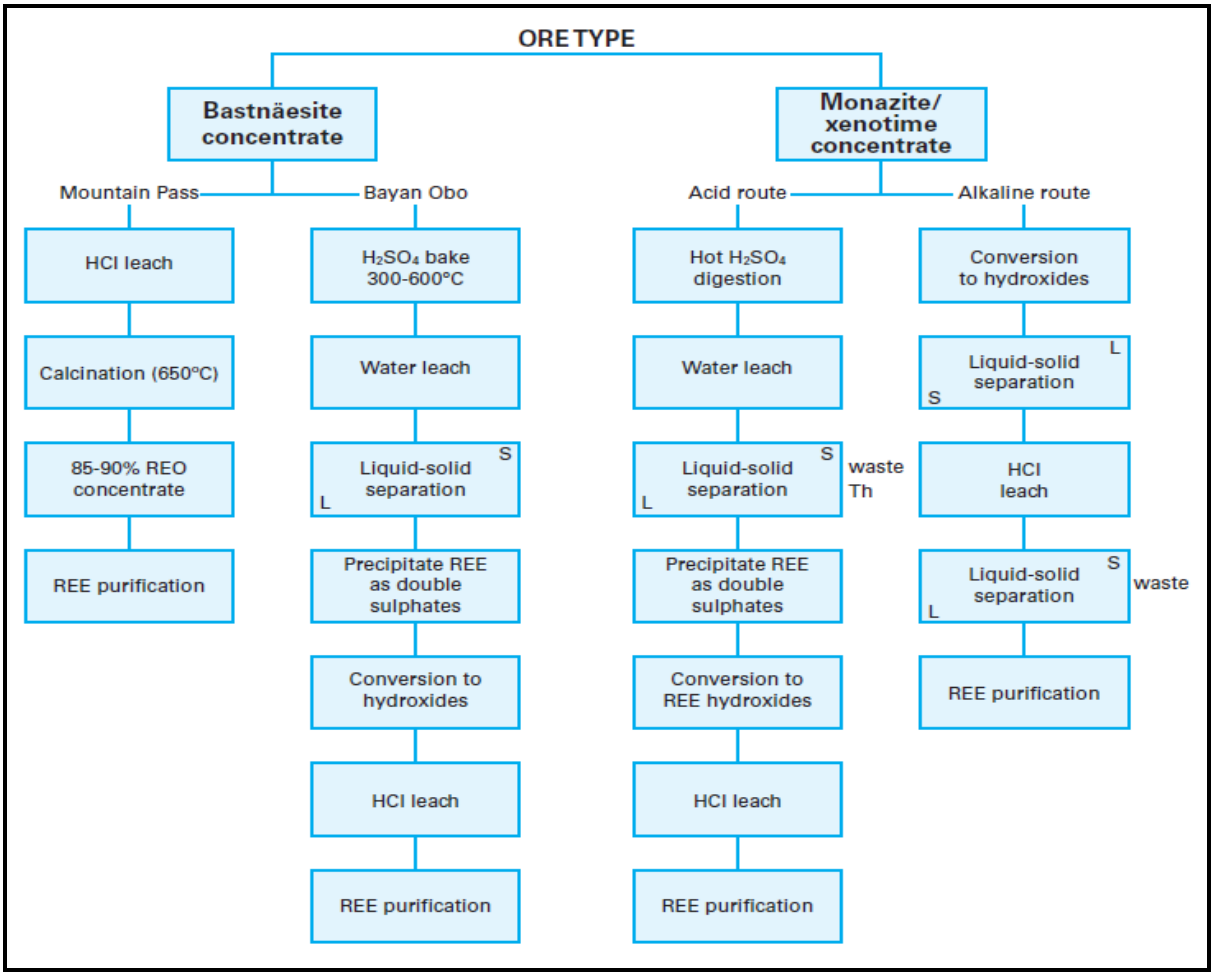

Figure 2.11: The extraction of the pure REE from minerals (bastnäesite, monazite and xenotime).[39]

2.6 EMERGING TECHNOLOGIES AND USES OF REE

The REE are generally non-hazardous and have unique properties which make them highly applicable as elements in some catalytic process, metallurgical processes and the manufacturing of ceramics and permanent magnets. Some of the REE are used to manufacture products which are extremely essential in the green technology environment, with the emphasis on renewable and non-carbon emitting materials. Many of REE currently also in high demand due to their important application in the

[39]Rare earth elements, [Accessed 13-02-2013]. Available from: http://www.reviewboard.ca/upload/project_document/EA1011-001_Rare_Earth_Elements_Profile_-British_Geological_Survey_1283466038.PDF.

medical and military environments as well as high-tech industries such as in electronics, optical applications, magnetic and catalytic uses (**Figure 2.12**).[40]

REE is currently playing a major role in the development of sustainable energy generation technology to reduce the global consumption of carbon based energy resources such as oil and coal, but also to reduce the pollution by green-house gases such as CO_2 worldwide. In addition, benefits of REE in the in green energy technology include a reduction in weight of material and increase energy efficiency in products such as electric/hybrid cars, turbines, wind-power turbines, low energy light bulbs, magnetic refrigeration and biofuels which all contain REE.

Figure 2.12: a) Neodymium-iron magnets b) samarium cobalt magnet ($SmCo_5$, Sm_2Co_{17}) c) wind turbine and d) computer screens.

Nd and Sm are extremely important in the production of permanent magnets that are used in the modern wind turbines. Neodymium-iron ($Nd_2Fe_{14}B$) magnets are more popular for this application than the samarium cobalt magnet ($SmCo_5$, Sm_2Co_{17}) because they are cheaper, have a more powerful magnetic field strength and their magnetic energy are 2 times greater than that of the samarium-cobalt magnets. Neodymium magnets are also smaller in size which also led them to be used in the speakers of earphones for MP3 players, as well as for computer hard disk and DVD drives. Samarium-cobalt permanent magnets are used in generators that produce electricity for aircraft electrical systems and in radar wave tubes to focus microwave

[40] Replacing oil addiction with metals dependence?, [Accessed 28-02-2012]. Available from: http://news.nationalgeographic.com/news/2010/10/101001-energy-rare-earth-metals/.

energy. REE also have major applications in the production of metallurgical alloys such as steel. Lanthanum on the other hand is used in nickel metal hydride batteries for hybrid cars. The colour seen on televisions and computer screens is due to the presence of terbium-fluoride-zinc sulphide, europium-yttrium compounds and cerium-strontium-sulphide in these devices. In another application cerium oxidises iron and is used as glass-decolorizing agent, in carbon-arc lights and ceramic capacitors.

REE are also used in different medical applications such as portable X-ray machines, X-ray tubes, computed tomography (CT) magnetic resonance imaging (MRI), nuclear medicine imaging and lasers (medical, surgical and dental). MRI equipment using Tb and Dy as permanent magnets generate high strength magnetic fields. This new generation of magnets are currently replacing expensive old systems which made extensive use of liquid helium to reduce electrical resistance of the coil wires.

A major concern for the US military is that these metals also have important military applications due to their extra-ordinary magnetic strength, which allows for significant reduction of component sizes. Important military applications such as jet fighter engines, missile guidance systems, night-vision goggles, smart bombs, space-based satellites, communication systems, coatings and precision-guided weapons all involve the use of REE. Production of ceramic coatings is currently not possible without gadolinium and is used as a defensive measure against neutron radiation from sun.

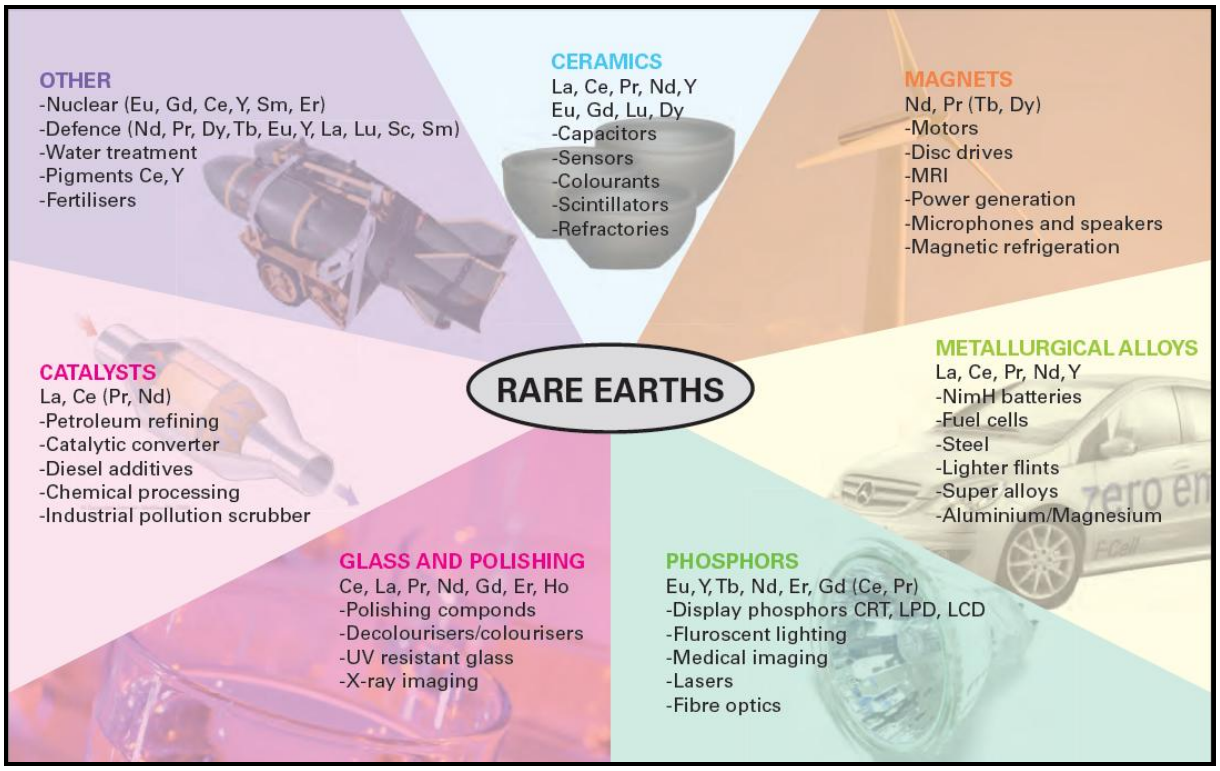

Figure 2.13: The rare earth metals and their applications.[41]

2.7 PHYSICAL AND CHEMICAL PROPERTIES OF REE

2.7.1 PHYSICAL PROPERTIES

The REE have similarities in ionic radii and oxidation states, and they occur in closely related or similar minerals which make them extremely difficult to separate and isolate. All the rare earth metals are hard, shiny silvery-white or grey in colour, but undergo colour changes when they are exposed to air to form oxides. Their density, melting and boiling points are relatively high and they are also good conductors of heat and electricity. The hardness and melting points of the REE metals increases with increase in atomic number. The REE are highly reactive towards non-metals such as N, S, H, C, halogens and chalcogens (O and S). The REE metals also react vigorously with water and acids, but do not with bases.[21] The reactivity of the metals

[41] High calibre rare earth business, [Accessed 15-03-2013]. Available from: http://www.rareearthsglobal.com/content/products/uses.asp.

however decreases with increase in atomic number due to what is called lanthanide contraction (**Figure 2.13**).

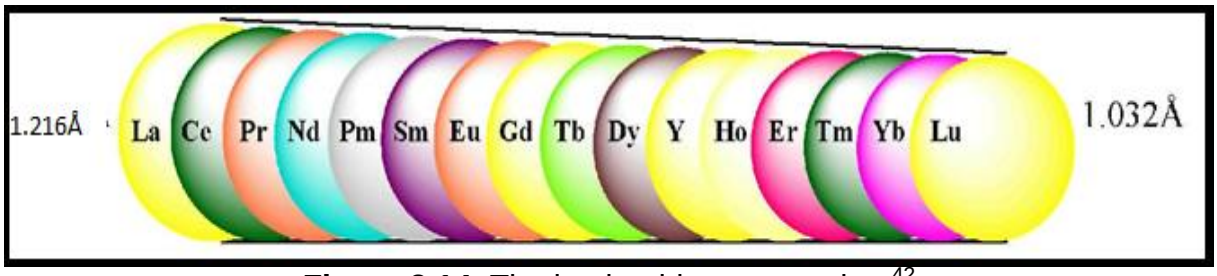

Figure 2.14: The lanthanides contraction.[42]

The lanthanide contraction is characterized by the steady decrease of the ionic radii with increase of the atomic number from lanthanum (La^{+3} = 1.216Å) to lutetium (Lu^{+3} = 1.032Å) as illustrated in **Figure 2.13**. The net effect is that all the lanthanides have very similar physical properties (ionic radii and +3 coordination number), with only a slight difference in their chemical properties.[14]

This contraction (decrease in atomic radii) is due to the addition of electrons to the inner 4f shell simultaneously to the addition of a proton to the nucleus. The addition protons then ensure a stronger force on the electrons. The increase in effective nuclear charge with decreasing atomic radii is clearly illustrated by the steady decrease in ionic radii in **Table 2.5**. The colour of the ions depend on the number of unpaired electrons (crystal field theory) in the f^n orbital and metals with the same number of the electron f^n and $f^{(14-n)}$. This phenomena is illustrated by the colours of lanthanide ions which is illustrated by La^{+3} and Lu^{+3} (colourless), Pr^{+3} and Tm^{+3} (green), Sm^{+3} and Dy^{+3} (yellow) as well as Eu^{+3} and Tb^{+3} (pink) (**Table 2.5**).

[42] E Montalvo, Expanding f element chemistry: reactivity of yttrium, lanthanide, and actinide metal complexes with diazoalkane, *Ph.D. thesis from University Of California library*, 2010, p1-4.

Table 2.5: Physical and chemical properties of the REE.[43,44]

Atomic symbol	Electron configuration		Colour(Ln^{+3})	B.P(ºC)	M.P(ºC)	Ionic radii (Å) [Ln^{+3}]	Atomic radii (Å)
	(Atom)	(Ln^{+3})					
La	$6s^24f^05d^1$	$[Xe]4f^0$	Colourless	3454	920	1.05	1.87
Ce	$6s^24f^15d^1$	$[Xe]4f^1$	Colourless	3257	798	1.03	1.83
Pr	$6s^24f^3$	$[Xe]4f^2$	Green	3127	935	0.99	1.82
Nd	$6s^24f^4$	$[Xe]4f^3$	Lilac	3127	1010	1.00	1.81
Pm	$6s^24f^5$	$[Xe]4f^4$	Pink	3000	1080	0.98	1.80
Sm	$6s^24f^6$	$[Xe]4f^5$	Yellow	1900	1072	0.96	1.79
Eu	$6s^24f^7$	$[Xe]4f^6$	Pink	1597	822	0.95	2.04
Gd	$6s^24f^75d^1$	$[Xe]4f^7$	Colourless	3233	1311	0.94	1.8
Tb	$6s^24f^9$	$[Xe]4f^8$	Pink	3041	1360	0.92	1.78
Dy	$6s^24f^{10}$	$[Xe]4f^9$	Yellow	2562	1412	0.91	1.77
Ho	$6s^24f^{11}$	$[Xe]4f^{10}$	Pale yellow	2720	1470	0.90	1.76
Er	$6s^24f^{12}$	$[Xe]4f^{11}$	Pink	2510	1522	0.89	1.75
Tm	$6s^24f^{13}$	$[Xe]4f^{12}$	Pale Green	1727	1545	0.88	1.74
Yb	$6s^24f^{14}$	$[Xe]4f^{13}$	Colourless	1466	824	0.86	1.94
Lu	$6s^24f^{14}5d^1$	$[Xe]4f^{14}$	Colourless	3315	1656	0.85	1.74

Key: B.P. - Boiling Point M.P. - Melting Point Å - 10^{-10}m

[43] Element properties, [Accessed 05-09-2013]. Available from: http://micmet.com/elementproperties.pdf.

[44] Chemistry of lanthanides and actinides, [Accessed 05-09-2012]. Available from: http://unaab.edu.ng/opencourseware/Chemistry%20of%20Lanthanides%20and%20Actinides.pdf.

The atomic radii demonstrate a smooth trend across the lanthanide series except for Eu and Yb as shown in **Table 2.5**. This discontinuity or interruption of the smooth decrease in atomic radii by Eu and Y is attributed to their contribution of 3 electrons to the metallic bonds compared to the 2 electrons by the other rare elements. Both Eu and Yb atoms are divalent, relatively stable and have a half filled [$4f^7$] and a full [$4f^{14}$] f shell respectively.

Table 2.6: Oxidation states of the REE.[21]

Symbols	Sc	Y	La	Ce	Pr	Nd	Pm	Sm	Eu	Gd	Tb	Dy	Ho	Er	Tm	Yb	Lu
+2								◊	◊						◊	◊	
+3	●	●	●	●	●	●	●	●	●	●	●	●	●	●	●	●	●
+4				□	□	□					□	□					

+2----◊ +3----● +4----□

2.7.2 CHEMISTRY OF REE

The REE are mostly trivalent (Ln^{+3}) but higher (+4) and lower (+2) oxidation states are also known for some of these elements (**Table 2.6**). They have large ionic radii compared to the rest of the elements on the periodic table, relatively small variation in oxidation states and they form complexes with a wide range of coordination numbers. This result in the formation of stable complexes or compounds with coordination numbers ranging between 6 and 12.

The lanthanide cations are considered as hard Lewis acids which form stable complexes with oxygen containing ligands. Most of the REE metals (excluding Pm) are commercially available as oxides, halides, nitrates or in pure metallic form. The nitrates and halides are all water soluble but the fluorides and the oxalates are not. The insoluble compounds, however, dissolve easily in acid. The lanthanides also show a strong affinity with fluorine, oxygen and nitrogen donor ligands (reactivity order F > O > N), from left to right on the periodic table.

2.7.2.1 HALIDE COMPOUND PREPARATION

General methods are used to prepare anhydrous and hydrous rare earth halides. These methods include the reaction between Ln(III) oxide and ammonium halide (**Reaction 1.1**) at 200 to 400 °C or by reaction of Ln(III) oxide with anhydrous hydrogen halide at 600 to 700 °C, depending on the halide.

$$Ln_2O_3 + 6NH_4X \longrightarrow 2LaX_3 + 6NH_3 + 2H_2O \qquad 1.1$$

These anhydrous REE halides are usually hygroscopic, and needs to be stored in a dry inert gas atmosphere during processing. The purity of the pure anhydrous rare earth halides prepared with NH_4X ranges from 99.12 to 99.99 %. The rare earth oxides used in this synthesis are mostly obtained by ion-exchange separation.[25] This method is the most effective in the preparation of the lanthanide (III) fluoride, as illustrated in **Equation 1.2**:

$$Ln_2O_3 + HX(aq) \longrightarrow LnX_3{\cdot}nH_2O \qquad 1.2$$

This method also produces a pure LnX_3 compound ranging from 99.90 to 99.98 % in purity, but it is not effective for Ce^{+4}. The fluorides are different from the rest of the halides (bromides, iodides and chlorides) due to their insolubility in water. The addition of hydrogen fluoride to Ln(III) oxide precipitates the fluoride compounds from the Ln(III) oxide which is very unique for the lanthanides. The HREE fluorides (with smaller Ln ions) are slightly soluble in excess HF. They dissolve in acid and in the process substitute F from the coordination sphere. The coordination number of the hydrated salts is usually 7 for the LREE and 6 for the HREE. At elevated temperatures and in the presence of water vapour the hydrated halides hydrolyse to form the oxo halides instead of the anhydrous halides as indicated in **Equation 1.3**.

$$LnX_3{\cdot}6H_2O \xrightarrow{\Delta} LnOX + 5H_2O + 2HX \qquad 1.3$$

The iodides and bromides have large radii ($F^- < Cl^- < Br^- < I^-$) hence they are easily hydrolysed and dehydrated. However, $CeX_3{\cdot}n(H_2O)$ forms CeO_2 upon heating.[44]

2.7.2.2 NITRATE CHEMISTRY OF REE

The REE nitrates are readily prepared by the addition of nitric acid (HNO_3) to pure REE metals, the oxides, hydroxides or the carbonate. Research indicated that the nitrate crystal structure of trivalent Ln(III) and tetravalent Ln(IV) contains a poly-coordinated Ln ion with 3 and 4 bidentate nitrate groups respectively. The coordination number of the hydrated salts is usually 6 for the LREE and 5 for the HREE. The hydrated nitrate loses water at 150 °C and decomposes at 200 °C. Most REE nitrates are soluble in polar solvents such as alcohols, esters, nitriles or water.

2.7.2.3 OXIDE CHEMISTRY OF REE

The Ln metals are slowly reduced to Ln_2O_3 when exposed to air at room temperature with Ce the exception which forms CeO_2, under the same conditions (**Equation 1.4** and **1.5**). The metals also rapidly ignite and burn above 150-180 °C.

$$4Ln + 3O_2 \longrightarrow 2Ln_2O_3 \qquad 1.4$$

$$Ce + O_2 \longrightarrow CeO_2 \qquad 1.5$$

Figure 2.15: Rare-earth (Pr, Ce, La, Nd, Sm and Gd) oxides powders.[45]

The oxides are usually basic and ionic and react with water to produce the hydroxides. Yb and Lu only form oxides if they are at heated at 1000 °C. CeO_2 is a yellow precipitate that dissolves easily in acid and is also formed by heating Ce metal in the presence of oxygen, by treating tetravalent Ce solution with base or by the

[45] Rare-earth oxides, [Accessed 15-04-2013]. Available from: http://www.ars.usda.gov/is/graphics/photos/jun05/d115-1.htm.

decomposition of $Ce(OH)_3$ or $Ce(C_2O_4)_3$ in oxygen or air (**Equation 1.6** and **1.7**).[44] However, Ce(IV) is easily hydrated and usually form more stable complexes than Ce(III).

$$2Ce(OH)_3 + 1/2O_2 \longrightarrow 2CeO_2 + 3H_2O \qquad 1.6$$

$$Ce_2(C_2O_4)_3 + O_2 \longrightarrow 2CeO_2 + 6CO_2 \qquad 1.7$$

2.7.2.4 COORDINATION CHEMISTRY OF REE

Rare earth elements form stable complexes with O and N donor ligands such as oxalates, citrates, ethylenediaminetetraacetic acid (EDTA), cyclopentadienyls and acetyl acetone (acac) ($Ln^{+4} > Ln^{+3} > Ln^{+2}$). The tendency of the anhydrous Ln^{+3} ions to form complexes increases from left to right in the group ($La^{+3} < Lu^{+3}$), but the formation of hydrated Ln^{+3} ions decrease in the same order. This is due to size constraints within the range of Ln^{+3} ions (decrease with the increase in atomic number). These complexes have high coordination numbers which usually ranges from 6 to 12. Research has shown that REE can form a wide variety of inorganic and organometallic compounds as indicated in **Table 2.7**.

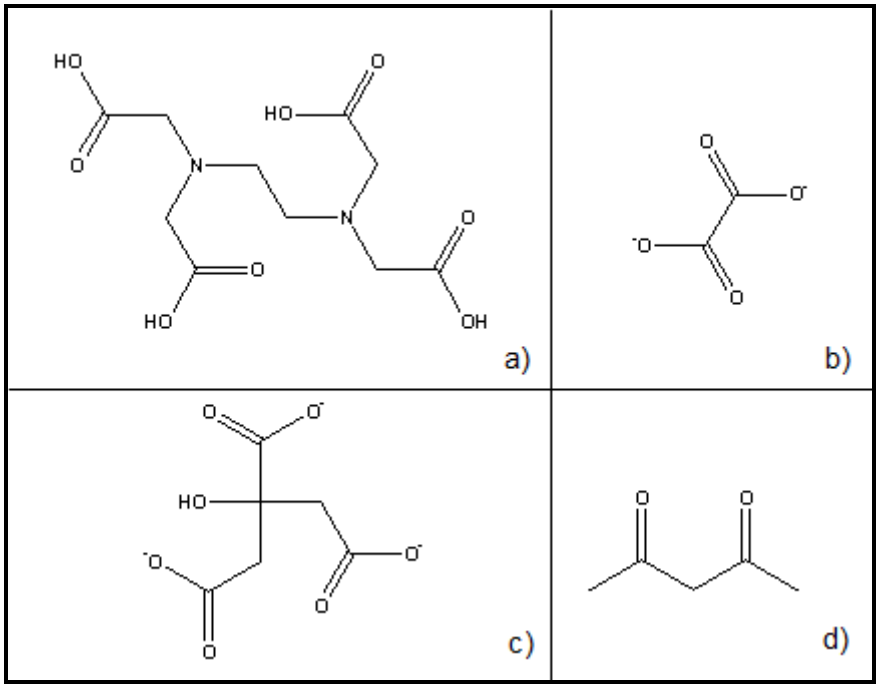

Figure 2.16: Molecular structures of a) ethylenediaminetetraacetic acid, b) oxalates, c) citrates and d) acetyl acetone.

$Ln(acac)_3$ can readily be synthesized by the addition of a lanthanide salt to a basic solution containing a β-diketonate ligand (acac) as indicated in **Equation 1.8**:

$$LnX_3 + 3Na(acac) \longrightarrow Ln(acac)_3 + 3NaX \qquad 1.8$$

These complexes are usually water soluble and they crystallize as hydrates $Ln(acac)_3 \cdot n(H_2O)$ (n = 2 for Ln = La - Ho, Y and n = 1 for Ln = Yb).

Research has shown that the most stable complexes of the lanthanides are those derived from the polyaminopolycarboxylic acids. The anions of these ligands are capable of multiple bonding using the numerous oxygen and nitrogen donors that are present in such a ligand system. It increases the number of ligand rings and also the stability of these on lanthanide complexes. In general, the ligand complex stability constant increases with decrease in radii of the metal due to lanthanide contraction. The lanthanide EDTA complex for example dissolves in water to form complexes such as $[Ln(EDTA)(H_2O)_n]^-$ with 2 to 3 water molecules bound to the metal center (see **Equation 1.9**).

$$[La(H_2O)_9]^{+3}(aq) + EDTA^{-4}(aq) \longrightarrow [La(EDTA)(H_2O)_3]^{-}(aq) + 6H_2O(l) \quad 1.9$$

Research has also shown that the REE organometallic complexes react preferentially with ligands containing either *σ* or *π-b*onding capacity. Generally these ligands are more reactive towards REE than towards the transition metals due to the high coordination number and the large ionic size of the lanthanides. A series of cyclopentadienyl (C_5H_5) complexes can readily be prepared with the dissolution of the lanthanides salts dissolved in THF (**Equation 1.10**).

$$LnCl_3 + nNa(C_5H_5) \longrightarrow LnCl_{3-n}(C_5H_5)_n + nNaCl \quad 1.10$$

The properties and geometries of these compounds not only depend on the nature of the solvent but also on the size of the lanthanide ion and the steric demand of the cyclopentadienyl group.

Table 2.7: Coordination numbers and shapes of some complex ions.[46,47]

Oxidation state	Coordination number	Geometry	Examples
+2	6	Octahedral	EuS
	8	Cubic	YbF_2
+3	6	Octahedral	$[DyBr_6]^{-3}$
	7	Capped trigonal prismatic	$[Dy(dpm)_3]\cdot H_2O$
		Capped octahedral	$[Ho[PhC(O)CH=C(O)Ph_3]\cdot H_2O$
	8	Dodecahedral	$[Ho(tropolonate)]^-$
		Square antiprismatic	$[Eu(acac)_3(phen)]$
		Bicapped trigonal prismatic	LuF_3
	9	Tricapped trigonal prismatic	$[Eu(terpy)_3]^{+3}$
		Capped square antiprismatic	$[Pr(terpy)Cl_3(H_2O)_5]\cdot 3H_2O$
		Bicapped dodecahedral	$[Eu(NO_3)_5]^{-2}$
	12	Icosahedral	$[Ce(NO_3)_6]^{-3}$
+4	6	Octahedral	$[CeCl_6]^{-2}$
	8	Square antiprismatic)	$[Ce(acac)_4$
	10	Complex	$[Ce(NO_3)_4(OPPh_3)_2]$
	12	Icosahedral	$[Ce(NO_3)_6]^{-2}$

[46] Chemistry of lanthanides and actinides, [Accessed 04-10-2012]. Available from: http://unaab.edu.ng/opencourseware/Chemistry%20of%20Lanthanides%20and%20Actinides.pdf.

[47] K Dehnicke and A Greiner, *Angewandte Chemie, International Edition*, 2003, 42, pp1340-1354

2.8 CONCLUSION

It is clear from this discussion that life in the 21st century wouldn't be the same without the 17 so-called rare earth elements. In some countries these elements have been declared as critical strategic resources due to their importance in the advanced military and space technology as well as their uses in iPads, laptop computers, television, cell phones, solar panels and hybrid cars. These elements are also extremely important to keep our society running smoothly with an efficient and rapid transfer to a clean-tech-driven global economy.

3 ANALYTICAL TECHNIQUES FOR REE DETERMINATION - LITERATURE SURVEY

3.1 INTRODUCTION

Rare earth elements (REE) occur in a variety of minerals in nature, but the highest concentrations of the LREE (Ce, La, and Nd) are mainly found in two minerals, namely bastnäesite and monazite while a major source for the HREE (Dy, Er, Tb) is xenotime.[48] The main reason for this preferential concentration of the type of REE within a mineral can be attributed to the very similar ionic radii of the LREE or cerium earths (97.0 to 103 pm for Pm to La) compared to HREE or yttrium earths (89 to 92.3 pm for Er to Tb). This dominance of the type of REE in the minerals is due to the "size-range best fit" that is possible in the structural lattice of the mineral.[49] In practice it means that elements of similar ionic radii are easily accommodated within a certain lattice structure and in this process preferential concentration in one of the types of REE is created. The tetragonal crystal structure of the mineral xenotime allows for yttrium as well as yttrium earths (Dy, Er, Tb) to be incorporated into the crystal structure while the monoclinic crystal structure of monazite easily incorporate Ce and LREE (La, Nd and Pr), with similar ionic size ,into the structure.

[48] Wicheeda lake REEs, [Accessed 05-11-2013]. Available from: http://www.aheadoftheherd.com/Newsletter/2010/wicheeda_lake_REEs.htm.

[49] Rare earth element, [Accessed 05-11-2013]. Available from: http://en.wikipedia.org/wiki/Rare_earth_element.

Figure 3.1: Monazite and xenotime minerals.[50,51]

The physical and chemical similarities between the REE not only complicate the separation of these elements, but also the accurate quantification of the different elements within a mineral ore body due to spectral interferences and coincidences. Different analytical methods are used to quantify the different REE in minerals or material samples. Flame atomic absorption spectroscopy (FAAS) was the first analytical technique that was used for the determination of REE in different samples. The disadvantages of this technique include low sensitivity, time consuming activities and the ability to quantify one element at a time. Inductively coupled plasma optical emission spectrometry (ICP-OES) was introduced in the mid-1970s as an analytical technique and was closely followed by inductively coupled plasma mass spectrometry (ICP-MS) in the early 1980s.[52] The development of these more accurate, selective and sensitive techniques prompted researchers to shift away from FAAS and GFAAS in the 1990s towards multi-element techniques such as neutron activation analysis (NAA), X-ray fluorescence (XRF), ICP-OES and ICP-MS. Common to all these techniques are higher sensitivity, large linear dynamic range, low detection limits, less prone to interference and their capability for accurate multi-element determination.[53,54]

[50] Monazite, [Accessed 05-11-2013]. Available from: http://commons.wikimedia.org/wiki/File:Monazite-169954.jpg.

[51] Xenotime-(Y)-rutile, [Accessed 05-11-2013]. Available from: http://commons.wikimedia.org/wiki/File:Xenotime-%28Y%29-Rutile-177576.jpg.

[52] A M Ghazi, D A Vanko, G Roedder and R C Seeley, *Geochimica et Cosmochimica Acta,* 1993, 57, p4513.

[53] D Kretschy, G Koellensperger and S Hann, *Metallomics*, 2011, 3, pp1304-1309.

These techniques are currently extensively used to accurately quantify the REE content in a large variety of samples which contain REE in the ultra-trace parts per billion concentration range.[55] The type of samples including biological samples, water and sediments, geological materials, soil and coal. Numerous methods have also been developed to analyse the REE content in advanced material such as nuclear material, laser crystals and luminophors. The determination of REE in complex material matrixes such as minerals can be demanding not only from an instrumental point of view but also from a separation and pre-concentration view, especially in samples containing REE at ultra-trace levels (ppb). Pre-concentration steps are normally time-, cost- and reagent consuming with demanding and difficult digestion steps. Several methods have been suggested for REE isolation and/or pre-concentration determination in samples which contain ultra-trace level REE. These include:

- Water - Sorbent extraction, ion-exchange and chelating resins as a pre-concentration. Due to low concentrations of REE in water samples the pre-concentration step improves REE analysis. The pre-concentration by co-precipitation is seldomly used due to experimental challenges and time consuming activities. Offline pre-concentration improves sensitivity and selectivity in REE analysis whilst the online pre-concentration can induce contamination of the sample and reducing the yield of the product (analyte). The hybrid (off and on-line) pre-concentration on the other hand reduces the contamination and capability of multi-sample pre-treatment at the same time and improve sensitivity.
- Sediments - Cation exchange and anion exchange chromatographic separation methods and pre-concentration. The elements (Ca, Ba, Fe, K, Na and Ti) concentrations are normally orders of magnitude higher than the REE concentrations in the sediment samples. Hence, separation is required before hand, in order to reduce the interference with the analysis.
- Rocks and minerals - Separation using cation exchange, anion exchange and extraction chromatography. Cation exchange chromatographic separation has advantages such as being cheap, fast and simple.

[54] F G Pinto, R E Junior, and T D Saint'Pierre, *A Critical Review, Analytical Letters*, 2012, 45:12, pp1537-1556.

- Ores and various geological samples - Separation and pre-concentration using resin, reversed-phase high-performance liquid chromatography (HPLC), micro-column with cation exchange resins and selective extraction chromatography. Initial separation and pre-concentration are good methods for analyzing ores and various geological samples due to its accuracy, high selectivity, sensitivity and precision.
- Soils - Extraction, decomposition methods such as microwave digestion, acid digestion and alkaline fusion. Pre-concentration of REE helps to obtain accurate and reliable results. The separation method before the analysis reduces spectroscopic and non-spectroscopic interferences.

Separation and pre-concentration methods such as co-precipitation, solvent extraction, precipitation and chromatography have successfully been employed to determine trace levels of the REE. The pre-concentration methods mostly improve sensitivity and reduce interferences from the REE, although separation methods such as ion chromatography and HPLC have shown great potential as cheap, rapid and accurate methods.

A recent article compiled the statistics on the use of different techniques or equipment in the REE determination since 2000.[55] ICP-MS and OES account for more than 70 % of all the studies that were carried out on REE determination (**Table 3.1**). NAA was also extensively used for all the different sample types while both UV/Vis and XRF produced the least amount of papers on REE quantification.

Table 3.1: Usage of spectroscopic techniques for REE determination.[55]

Sample type	ICP-OES (%)	ICP-MS (%)	NAA (%)	UV/Vis (%)	XRF (%)	Others (%)
Advanced materials	17	52	4	NU	11	16
Geological materials	16	45	18	10	11	NU
Sediments	26	52	15	NU	NU	7
Soil	12	61	15	NU	NU	12
Water	20	73	2	NU	NU	5

NU - Not used

Others - WC-OES, AAS, SIMS, EDXRF, etc.

NAA and ICP-MS are very sensitive analytical techniques but are expensive and NAA also requires access to a nuclear reactor which limits its use in this kind of determinations. The unpopularity of UV/Vis is mainly due to the non-selectivity of this technique towards the different REE as a result of the similarity of their chemistry. UV/Vis and AAS however can be used for total REE determination or with samples that contain only one REE as impurity.

The rest of this chapter contains an overview of the research that has been performed on REE using the above mentioned analytical techniques or equipment.

[55] B Zawisza, K Pytlakowska, B Feist, M Polowniak, A Kita and R Sitko, *Journal of Analytical Atomic Spectrometry*, 2011, 26, pp2373-2390.

3.2 ABSORPTION SPECTROSCOPY

3.2.1 ULTRA VIOLET-VISIBLE SPECTROPHOTOMETRY (UV/Vis)

The non-selectivity of UV/Vis as analytical technique contributes to its modern day unpopularity as analytical tool in the quantification of REE. In the early 1930s and 1940s the first UV spectroscopic study was reported on aqueous REE solutions.[56] During that time, it was discovered that some ligands such as β-diketonates, phenolate or salicylate and non-charged adducts like 1,10 phenanthroline or 2,2-bipyridine can photosensitize the luminescence of europium ions when excited in the UV region. In the 1942 Weissman discovered the luminescence properties of the trivalent Eu ion after the Eu-tris(β-diketonate) chelates was exposed to near-UV excitation in solution.[57] The advantage of using UV/Vis techniques for the characterisation of REE is attributed to the fact that REE have characteristic absorption peaks in the UV and visible regions due to f-electron transitions.

Rabie *et al*[58] separated europium from the other REE in a monazite mineral obtained from European beach sand samples by employing chemical precipitation and characterising with UV/Vis spectroscopy. The separation method involved the reduction of europium(III) chloride to europium(II) chloride using metallic zinc, followed by the selective precipitation of europium(II) sulphate by the addition of sulphate salts leaving other REE in solution. An initial product yield of about 91 % Eu was obtain and was further increased to 97 % after purification. The Eu absorption band at 394 nm using combined IC-UV/Vis, confirmed the presence of the Eu in the isolated product.

Guo *et al* [59] separated and purified the LREE and thorium present in a Baotou Iron Ore CRM mineral sample using cation exchange chromatography. The LREE and thorium were eluted with a combination of HCl and NH_4Cl followed by the addition of

[56] M H Werts, *Science Progress,* 2005, 88, pp101-131.

[57] M Singh and S Anant, *International Journal of Inorganic Chemistry*, 2012, p9.

[58] K A Rabie, S A Sayed, T A Lasheen and I E Salama, *Hydrometallurgy*, 2007, 86, pp121-130.

[59] G Guo, M Luo, J Xu, T Wang, R Hua and Y Sun, *Journal of Radioanalytical and Nuclear Chemistry*, 2009, 281, pp647-651.

5 % potassium oxalate solution. The presence of LREE and thorium were determined with tribromo-arsenzao and arsenazo III at 630 nm and 660 nm respectively using a UV/Vis commercial spectrophotometer. The results obtained were in agreement with the certified values of the CRM. The RSD of the LREE and thorium were between 0.50 - 1.70 % and 0.66 - 2.71 %, respectively, while their recoveries were above 97 %.

Wanga *et al*[60] synthesized the new [Eu(AITFBD)$_3$phen] coloured complex (**Figure 3.2**) and characterised the complex using UV/Vis spectroscopy.

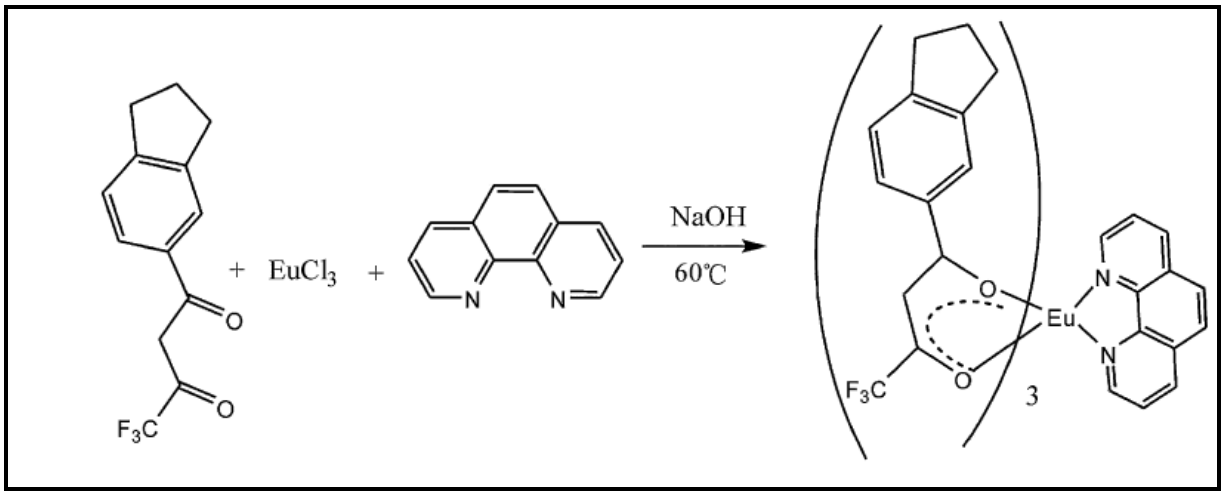

Figure 3.2: Reaction scheme of the formation of [Eu(AITFBD)$_3$phen].[60]

The UV/Vis absorption spectra of HAITFBD, phen, $EuCl_3$ and the final [Eu(AITFBD)$_3$phen] complex in alcohol solution (1×10^{-5} M) and at room temperature is shown in **Figure 3.3**. The absorption spectra of the aqueous $EuCl_3$ and phen shows no absorption maxima, but that of the [Eu(AITFBD)$_3$phen] complex is similar to HAITFBD, meaning that HAITFBD contribute to the strong absorption for the complex [Eu(AITFBD)$_3$phen] with a molar extinction coefficient in the $2.50\text{x}10^7$ - $2.80\text{x}10^7$ L mol^{-1} cm^{-1} range. The absorption band of the complex from 300 to 400 nm has been extended by transition absorption of HAITFBD. This broad absorption spectra illustrate the exact problem of UV/Vis spectroscopy in analytical chemistry namely, large or broad absorption spectra with large extinction coefficient which are very similar for all the REE in solution.

[60] H Wanga, P Hea, H Yana and M Gonga, *Sensors and Actuators B,* 2011, p156, pp6-11.

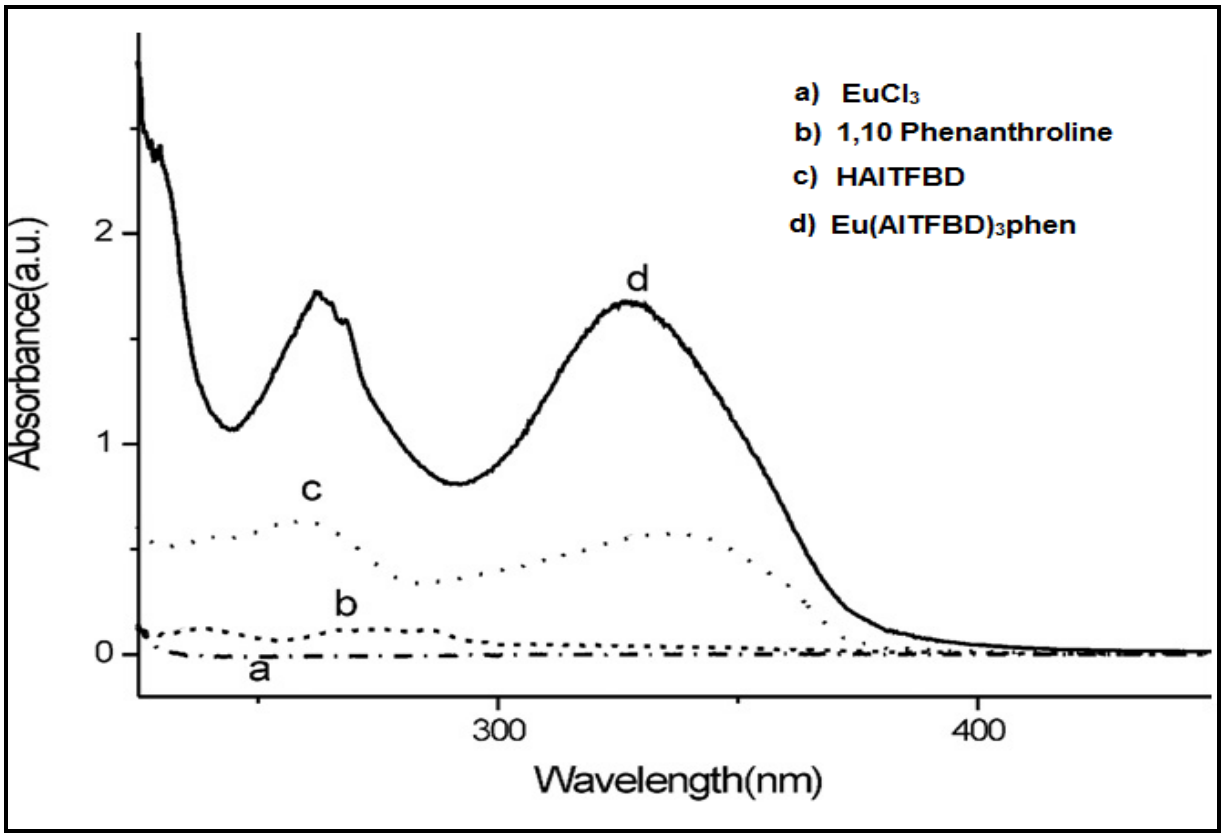

Figure 3.3: UV/Vis absorption spectra of $EuCl_3$, the ligands and the Eu^{+3} complex in alcohol solution [1×10^{-5} M].[60]

There is also no presence of metal band (f - f peaks) excitation spectra for this complex in comparison to ligand bands which is attributed to poor energy transfers from the ligand to the metal ion.

Jain *et al*.[61] developed an analytical method using a polymeric chelating resin for the quantification of lanthanum(III), cerium(III), thorium(IV) and uranium(VI) from monazite sand as well some standard geological materials. After separation from other REE and the pre-concentration, the La, Ce, Th, and U were quantified by ICP-OES and UV/Vis. The polymeric chelating resin exhibits good separating capability with maximum sorption between pH 2.5 - 4.5 for Th(IV), pH 5.5 - 7.0 for U(VI) and pH 6.5 - 8.5 for La(III) and Ce(III). The pre-concentration factors for Ce, La, Th, and U were calculated as 130, 125, 102, and 108, respectively. The average recovery for the above mentioned metals ranged between 97 and 98 %.

[61] V K Jain, A Handa, R Pandya, P Shrivastav and Y K Agrawal, *Reactive and Functional Polymers,* 2002, 51, pp101-110.

Alaa and Talaat[62] developed an analytical method for the simultaneous determination of thorium and REE in waste water without separation. The thorium and REE in the absence and presence of cetylpyridinium chloride (CPC) were reacted with 5-(2,4-dimethylphenylazo)6-hydroxypyrimidine-2,4-dione (**I**) or 5-(4-nitro-2,6-dichlorophenylazo)6-hydroxypyrimidine-2,4-dione (**II**) to form reddish coloured complexes. In the presence of CPC only the thorium complexes formed in the solution. The absorption maximum due to the formation of the thorium and Ce^{+4} or other REE complexes in the absence of CPC using reagent **I** or **II** were at 592 and 586 nm and 563 and 557 nm respectively. The complex formation of REE does not influence the recoveries in the presence of CPC. The recoveries of thorium and the REE range between 97.5 and 102.2 % and 96.5 and 101.8 % respectively. The results as in **Table 3.2** shows comparable accuracy (*t*-test) and precision (*F*-test) for Th and Ce.

Table 3.2: Analysis of waste-water samples from different locations.[62]

Location	Amount added ($\mu g\ ml^{-1}$)	Amount found[a] ($\mu g\ ml^{-1}$)			
		Th^{+4}		Ce^{+4}	
		I	**II**	**I**	**II**
Shobra El-Kema	3.0	3.05	2.90	2.90	3.07
		(t = 1.17) (F = 2.56)		(t = 1.66) (F = 3.03)	
Enshaz	3.0	3.10	2.94	2.95	3.05
		(t = 1.54) (F = 2.17)		(t = 1.39) (F = 2.40)	
10th Ramadan	3.0	3.05	2.95	2.85	2.90
		(t = 1.78) (F = 3.11)		(t = 1.83) (F = 2.73)	

[a] Average of six determinations.

Theoretical values of *t*-tests and *F*-tests at 5 d.f. and 95 % confidence limits are 2.57 and 5.05, respectively.

[62] S A Alaa and Y M Talaat, *Talanta*, 2001, 54, pp611-620.

3.2.2 FLAME ATOMIC ABSORPTION SPECTROMETRY (FAAS)/ GRAPHITE FURNACE ATOMIC ABSORPTION SPECTROMETRY (GFAAS)

Bencs *et al*[63] used both FAAS and ICP-OES to analyse the REE content in an yttrium aluminium borate ($YAl_3(BO_3)_4$) optical single crystal grown from a K_2O-MoO_3-B_2O_3 flux. The $YAl_3(BO_3)_4$ crystal was firstly washed in hot H_2O, followed by diluted HCl and then in distilled H_2O. The cleaned $YAl_3(BO_3)_4$ crystal sample was then fused with lithium metaborate ($LiBO_2$) at 950 °C. The melt was dissolved with 6 M HCl and analysed for REE (Dy, Yb and Y). The LOD ranged between 0.1 and 1.54 mg L^{-1} for FAAS and 0.024 to 0.36 mg L^{-1} for ICP-OES. A fairly good correlation was found between the results by these two independent methods (**Table 3.3**).

Table 3.3: $YAl_3(BO_3)_4$ crystals determined by FAAS and ICP-OES.[63]

Crystal sample	Concentration of analytes in the solid samples (m/m %)					
	Dy		Yb		Y	
	FAAS	ICP	FAAS	ICP	FAAS	ICP
ErYb: $YAl_3(BO_3)_4$	1.11	1.13	1.17	1.32	18.8	19.7
Er: $YAl_3(BO_3)_4$	3.39	3.71	-	-	18.7	19.6
Cr: $YAl_3(BO_3)_4$	1.24	1.37	-	-	20.1	21.0

Gardner *et al*[64] developed a method to determine REE (Sc, Y, Ho, Er, Tm, Yb, and Lu) in the absence or presence of an uranium matrix alloy using AAS without any separation. Uranium was used as a radiation buffer which enhances the REE absorbance and reduces interferences by other REE. Different acids such as HCl,

[63] L Bencs, V Horvath, I Varga, E Beregi and T Kantor, *Spectrochimica Acta Part B*, 2004, 59, pp1851-1859.

[64] R D Gardner, A L HenBisnian and W H Ashley, Determination of selected rare earths in uranium alloys by atomic-absorption spectrophotometry, *Los Alamos Scientific Lab., N.Mex. (USA)*, 1974, pp1-5.

HNO_3, $HClO_4$, H_2SO_4 and H_3PO_4 were employed to verify their influence on the absorbance of the REE. Results obtained from this study indicated that the absorbances of the REE are the largest in the presence of $HClO_4$ and that the presence of U further increases the absorbance. The uranium alloy sample was washed with water, ethanol and acetone to remove traces of oil, and allowed to dry at 25 °C. The REE samples were then dissolved the various acids, while some of the solutions were also spiked with uranium. The REE concentrations were determined in various acids employing AAS in both the absence or presence of uranium-matrix. The REE recovery ranged from 89 and 138 % in the absence of uranium and 99.5 to 101.2 % in the presences of uranium. The RSD's were calculated to be between 0.4 and 2.7 % and 4.8 to 10.6 % for Y and Lu respectively.

Diadoji and Tamura[65] developed a method to determine REE (Y, Dy and Sm) using a combination of GFAAS and a tantalum boat (metal container - see **Figure 3.4**) and FAAS.

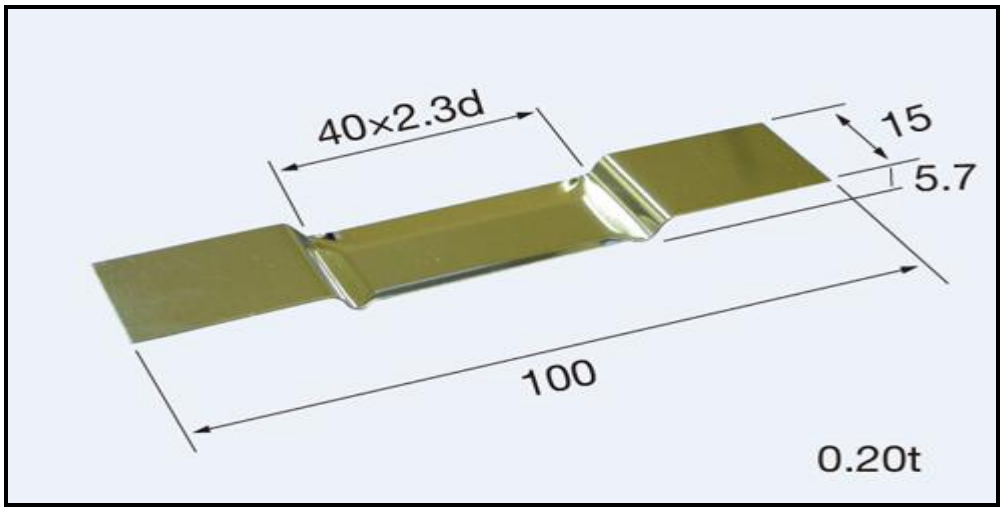

Figure 3.4: Tantalum boat.[66]

The REE could not be quantified by using a commercial graphite tube hence, the use of the tantalum boat. The use of the tantalum boat inside the graphite tube atomizer improved the sensitivity of the method as well as preventing carbide formation to

[65] H Diadoji and S Tamura, *Bulletin of the Chemical Society of Japan,* 1982, 55, pp3510-3514.

[66] Tantalum: straight boats. flat type, [Accessed 02-12-2013]. Available from: http://www.plansee.com/media/images/tantalum_boat_-_PLANSEE_-_11372994.gif.

yield improved REE quantification. The REE were dissolved in HCl or HNO_3, placed inside the metal container and analysed by GFAAS and FAAS (without the tantalum boat). The highest intensity and maximum absorbance were obtained using the atom line at 410.2 nm for Y, 421.1 nm for Dy and 429.7 nm for Sm. The standard deviation of this method ranged around 2.6 and 9.3 % for GFAAS and 1.6 to 2.5 % for FAAS. Comparable results as shown in **Table 3.4** were obtained for the sample using both GFAAS and FAAS.

Table 3.4: Quantification of Y, Dy and Sm using GFAAS and FAAS.[65]

Metal	GFAAS	FAAS
	Found (wt %)	Found (wt %)
Y	0.69	0.69
Dy	0.19	0.19
Sm	0.81	0.80

Arrebola *et al*[67] synthesised the REE-Mg-purpurin complex in order to quantify the REE content (La, Y, Pr, Nd, Sm and Ce) using AAS. The REE-Mg-purpurin complexes were extracted with isobutyl methyl ketone (IBMK) at pH 7.5. The RSD of this analysis ranged from 0.4 to 3.37 % and the recovery between 79.8 - 107 %. This method can be used to the determination for the REE content at ultra-trace levels (ppb).

Sicifiska and Michalewska[68] developed a method to determine REE (La, Pr, Nd, Sm, Eu, Gd, Tb, Dy, Ho, Er, Tm, Yb and Y) in different REE ores and concentrates. The samples were dissolved in a 5:1 mixture of H_2SO_4 and HNO_3. After filtering the product was precipitated from the filtrate by the addition of oxalic acid and HNO_3 to form REE oxalates and then heated to 700 °C. The resultant oxides were re-

[67] A Arrebola, M G Bagur, M Sanchezi-Vinas, *Journal of Analytical Atomic Spectrometry*, 1998, 13, pp765-768.

[68] P Sicifiska and M Michalewska, *Fresenius Z in Analytical Chemistry*, 1982, 312, pp530-532.

dissolved in a mixture of HCl and H_2O_2. The solution was then treated with a KCl solution and analysed using GFAAS and FAAS. The results showed that both GFAAS and FAAS methods are suitable for REE determinations in the above mentioned samples. The results in **Table 3.5** indicate that it is mainly the HREE that can be determined in lower concentrations and that the results compare well between all the methods used in this study.

Table 3.5: Determinations in REE concentrates.[68]

Component	Spectrophotometric method (%)	FAAS	GFAAS	
			Direct measurement (%)	Additive method (%)
Gd_2O_3	62.0	63.5	62.2	64.3
Dy_2O_3	20.0	20.8	20.1	19.2
Tb_2O_3	8.0	7.7	12.3	9.08
Er_2O_3	2.3	1.98	3.03	2.05
Ho_2O_3	1.4	1.47	1.57	1.36

Research results indicate the methods such GFAAS is mainly useful for single element determination of REE, but is still not very sensitive to analyse at ultra-trace levels as indicated by its use in relatively few studies.

3.3 EMISSION SPECTROSCOPY

3.3.1 ICP-OES

Statistical analysis on the use of the different techniques in the quantification of the REE clearly indicated that ICP-OES is one of more popular techniques used in research. This is mainly due to the sensitivity of this equipment, but also its ability to quantify the different REE in complicated materials (utilizing the spectral properties of the elements).

Zhang *et al*[69] employed online micro-column separation and pre-concentration to determine trace amounts of REE in environmental and food samples. Tea leaves and dried samples (pig liver, agaric and mushroom) were digested with concentrated HNO_3 while soil and sediment CRM samples were digested using a mixture of HNO_3 and HF. Secondly they employed the online micro-column separation and pre-concentration method to determine the trace amounts of REE in the samples by ICP-OES. The RSD and recoveries ranged from 1.7 % for Y to 4.4 % for Sm, 95 % to 100 % respectively, and the LOQ were determined to be 48 pg mL^{-1} for Lu to 1003 pg mL^{-1} for Sm. The method was successfully accounted for the trace amount of REE present in all the samples investigated as well as the CRMs. The method proved to be sensitive, selective, quick and valid for the determination of trace amount of REE in different samples with complex matrixes.

Renko *et al*[70] developed a new dissolution method to determine the different REE (Sm, Pr, La and Ce) as well as Nd in a NdFeB permanent magnet sample using ICP-OES. The dissolution method entailed the dissolution of a weighed sample dissolved in HCI followed by the addition of a few drops of HNO_3. The solution was analysed for Nd content at 415.608 nm after a complete dissolution. The rest of the REE nitrates (Sm, Pr and La) and Ce chloride were subsequently dissolved in deionized water. The REE (Sm, Pr, Ce and La) solution were injected onto a sulfopropyl column

[69] N Z C Huang and B Hu, *Analytical Sciences*, 2007, vol. 23, pp997-1002.

[70] M Renko, A Osojnik and V Hudnik, *Fresenius Journal of Analytical Chemistry*, 1995, 351, pp610-613.

and eluted with concentrated α-hydroxy-isobutyric acid (α-HIBA) to facilitate their separation. The separation was performed using a concentration gradient elution from 0.06 mol L^{-1} to 0.12 mol L^{-1} of α-HIBA over a period of 60 min while the pH of eluent was adjusted to 4.4. Ideal separation conditions were employed for each element to ensure the successful separation at equal or different concentrations of the particular elements. The separation of the REE by ion chromatography was deemed necessary to reduce possible spectral interference arising from line overlapping and possible matrix effects. The ICP-OES method produced REE recoveries which were compatible with those specified for the CRM as shown in **Table 3.6**. The RSD of the REE range between 0.95 and 8.0 % and the detection limits from 0.01 to 0.09 % respectively (**Table 3.6**).

Table 3.6: REE concentrations in the permanent magnet alloy NdFeB by ICP-OES.[70]

Element	Certified (%)	Results (%)	RSD (%)	Detection limit (%)	BEC
Nd	31.99	31.8	0.95	0.03	1.2
Sm	0.091	0.092	6.3	0.05	0.25
Pr	0.52	0.51	8.0	0.09	0.65
Ce	0.065	0.062	5.7	0.05	0.35
La	0.033	0.033	5.4	0.01	0.04

BEC = Background Equivalent Concentration

Darbha and Gangadharan[71] succesfully quantied the spiked REE content in a high purity Gd_2O_3 solution after their successful separation with anion exchange and employing ICP-OES. Individual REE from La to Lu oxides, except Ho, were digested in HNO_3. The individual REE were mixed and then added to the Gd_2O_3 solution. The HREE were directly quantified by ICP-OES while the LREE were determined after their separation by anion exchange. The HREE and LREE percentage recovery ranged from 95 to 110 % and 99 to 100 % respectively. These results indicated that

the elemental separation step improved the recovery and reduced possible spectral inferences.

Marathe *et al*[72] determined the HREE content (Eu - Lu) in high purity Y_2O_3 employing ICP-OES. The Y_2O_3 was spiked with the HREE which was dissolved in HNO_3. The detection limits for the HREE were determined to be in 0.22 to 4.2 ng mL^{-1} range in the absence of Y_2O_3 and from 0.22 to 5.21 ng mL^{-1} in the presence of Y_2O_3. The RSD varied between 2.3 % and 6.3 % for the different HREE and their recoveries varied from 84 to 106 %.

In another study Pei and Wenjun[73] developed a pre-concentration method to determine La, Eu, and Yb in lake water, synthetic seawater and in GBW07603 CRM samples. The REE were pre-concentrated using 1-phenyl-3-methyl-4-benzoylpyrazol-5-one on a silica gel column at pH 5. The adsorbed chelates were then eluted from the column with HNO_3 and La, Eu, and Yb were quantified by ICP-OES. The RSD for La, Eu and Yb were 3.5 %, 4.5 % and 2.4 %, respectively. The pre-concentration method proved to be very successful with the La, Eu, and Yb with recoveries in the 94.6 - 108 % range for lake water and 95.5 - 99.2 % for synthetic seawater. Metal recoveries obtained for the CRM using this method are in good agreement with the certified values as shown in **Table 3.7**.

Table 3.7: Determination of REE in GBW07603 CRM.[73]

Element	Found (µg g^{-1})	Certified value (µg g^{-1})
La	1.20	1.25
Eu	0.040	0.039
Yb	0.061	0.063

[71] L Darbha and S Gangadharan, *Fresenius Journal of Analytical Chemistry*, 1994, 348, pp284-286.

[72] S M Marathe, S S Biswas, P B Patil and P S Murty, *Microchimica Acta*, 1992, 109, pp261-268.

[73] P Liang and W Fa, *Microchimica Acta*, 2005, 150, pp15-19.

3.3.2 ICP-MS

ICP-MS is the most popular analytical method for the quantification of REE, mainly in material samples which contain very low levels of REE, due to its sensitivity, selectivity and multi-element analysis capabillities. Zhang and Nozaki[74] successfully quantified REE in different unfiltered seawater samples. They pre-concentrated and purified the REE in the seawater using solvent extraction, back extracted the REE into water and analysed them with ICP-MS. All samples were acidified with HCl (pH = 1.5) immediately after sampling. Indium as a yield monitor was added to each seawater sample and the samples were thoroughly mixed to ensure homogenization and the pH was adjusted to 1.6 with NH_3. Pre-concentration and purification of the REE and In were achieved by the quantitative extraction of the melts with a mixture of HDEHP (2-ethylhexyl hydrogen phosphate) and H_2MEHP (2-ethylhexyl dihydrogen phosphate) dissolved in heptane. The combined organic layer was washed with 3 portions of 5 mL 0.2 M HCl. The addition of $C_8H_{18}O$ to the organic phase transformed any dimeric HDEHP complexes to monomeric complexes. The REE and In were subsequantly back-extracted into the aqueous medium with 6 M HCl. The solution was washed with heptane and then evaporated to dryness. The next step involved the dissolution of the resultant precipitate by the addition of concentrated HNO_3. This solution was analyzed by ICP-MS. The recovery of the REE and In after purification were over 99.1 % and their RSD ranged bettween 2 and 5 %.

In another study Zhu *et al*[75] developed a hybrid (off-line and on-line) pre-concentration method to determine REE in natural water samples. In this method the sample loading was carried out off-line prior to the measurement. The syringe driven chelating columns (SDCC) were set into the column holder of the automatic column changing system and REE were eluted on-line and quantified with ICP-MS. The recoveries of REE varied from 96.0 % for Gd to 104.1 % for Lu while their detection limits were determined as 0.013 pg mL^{-1} for Tm and 0.15 pg mL^{-1} for Ce. The hybrid (off-line and on-line) analysis only took 3 minutes to complete. This time the duration

[74] J Zhang and Y Nozaki, *Geochimica et Cosmochimica Acta*, 1996, Vol. 60, No. 23, pp4631-4644.

[75] Y Zhu, A Itoh, T Umemura, H Haraguchi, K Inagaki and K Chiba, *Journal of Analytical Atomic Spectrometry*, 2010, 25, pp1253-1258.

compares favourable to the method developed by Fu *et al*[76]. Their overall time for analysis took 6 - 30 minutes for the on-line procedure and 5 hours for the off-line procedure. It was also found that this difference in techniques did not affect the detection limits.

Another method that employed ICP-MS for the quantification of the REE was reported by Pedreira *et al*[77]. This method involved the separation of the REE in a highly pure neodymium oxide with HPLC to determine the REE . The neodymium oxide was initially dissolved in concentrated HNO_3 while heating for 30 min at 50 °C. After dissolution, the REE solutions were diluted by the addition of diluted HNO_3. A high resolution inductively coupled plasma mass spectrometer (HR-ICP-MS) instrument was used as an element-selective detector for HPLC in highly pure REE oxide materials. The separation of the REE by HPLC was performed using sodium laurylsulfonate as modifier. It has been shown that sodium laurylsulfonate eliminates spectral interferences and enabled the determination of low amounts of REE impurities in the high-purity oxide materials. The LOD with the high performance liquid chromatography with inductively coupled plasma-sector field mass spectrometry (HPLC/ICP-SFMS) system ranged between 0.5 and 10.3 ng g^{-1}. The proposed method enabled achieving RSD ranging from 1.88 to 4.96 % together with recoveries in the range of 85.85 - 99.20 % for the different REE.

Bratz and Klem[78] used ICP-MS in combination with laser ablation to analyse geological samples for REE content. They fused the geological samples with $Li_2B_4O_7$, followed by the addition of NH_4NO_3 at 1100 °C. The samples were then analysed for the REE by laser ablation-included coupled plasma mass spectrometer (LA-ICP-MS). The same fusion was also repeated for the XRF analysis of the REE content. The method proved to be very successful and REE recoveries were obtained in the range 83 to 116 % with the RSD's that varied between 1.7 and 14.2 %. These REE

[76] Q Fua, L Yang and Q Wang, *Talanta*, 2007, 72, pp1248-1254.

[77] W R Pedreira, J E S Sarkis, C A da Silva Queiroz, C Rodrigues, I A Tomiyoshi and A Abrao, *Journal of Solid State Chemistry*, 2003, 171, pp3-6.

[78] H Bratz and R Klemd, *Mineralogisches Insititut Paper*, 2002, pp1-6.

recoveries in the geological sample are in good agreement with those reported in literature.[79]

The final example of the use of ICP-MS in REE quantification discussed in this chapter is done by Chandrasekaran *et al*[80]. They developed an extraction and pre-concentration process to determine the REE content in groundwater samples. Known quantities of REE were added (spiked) to groundwater samples. Tricaprylmethylammonium chloride and 2,6-pyridinedicarboxylic acid (PDCA) were added to these groundwater samples which subsequently complexed with the REE in the water. These complexes were then extracted with chloroform, and analysed by an inductively coupled plasma-quadrupole mass spectrometry (ICP-QMS). The limits of detection and precision ranged from 0.05 - 0.55 ng L^{-1} and 0.9 - 4.9 % respectively. The recoveries the REE in groundwater samples were reported to be between 92.1 and 108.2 % before adding PDCA and 90.2 to 110.3 % after the PDCA addition.

3.3.3 XRF, NAA AND OTHER TECHNIQUES

D'Angelo *et al*[81] used different analytical techniques to analyse apatite for REE content. In this study the researchers separated the REE (La, Ce, Nd, Sm, Eu, Tb, Yb and Lu), Hf, and Th in the apatite samples by employing cation-exchange and quantify them with ICP-OES and NAA and finally compared these results with XRF analyses. Powdered apatite samples were dissolved in concentrated HCl and HNO_3. After complete dissolution, the solution was evaporated to nearly dryness. The procedure of the elution of the REE was as follows: a) add a sample solution in 1 M HCl b) elute with 2 M HCl followed by 2 M HNO_3 and 6 M HNO_3 separately, and then analysed for REE content, c) elute only with 8 M HNO_3 for REE analysis, and d) the column was regenerated with 8 M HNO_3 to remove impurities. Quantification results indicate that the REE were initially retained the column while Fe, Ca and P were

[79] K Govindaraju, *Geostandards Newsletter,* 1994, 18, pp1-158.

[80] K Chandrasekaran, D Karunasagar and J Arunachalam, *Journal of Analytical Atomic Spectrometry*, 2012, 27, pp1024-1031.

[81] J A D'Angelo, L D Martinez, S Resnizky, E Perino and E J Marchevsky, *Journal Trace And Microprobe Techniques*, 2001, 19(1), pp79-90.

eluted with 2 M HCl and 2 M HNO_3. The REE were quantitatively desorbed with 6 and 8 M HNO_3. Apatite solid samples were then sealed in quartz and irradiated by NAA for REE determination. Finally solid apatite samples were quantitatively analyzed using XRF. Detection limits obtained for the REE ranged from 1.3 to 33.5 ng mL^{-1} and their recoveries between 90.0 - 100 %. Separating the REE from the mineral matrix successfully removed any dissolved organic compounds and inorganic salts which eliminated possible spectral interferences from other elements. After the cation-exchange separation, the only spectral interferences were among the REE themselves. Among the REE lines maintained during this studied only two compounds Sm and Eu required interference correction due to Nd interference. Advantages of this method include its fairly low cost, quick analyses and simplicity. XRF, ICP-OES, and NAA results were comparable as shown in **Table 3.8**.

Table 3.8: Comparative concentrations of selected REE, Hf, and Th content in an apatite sample.[81]

Element	ICP-OES (μg g^{-1})	NAA (μg g^{-1})	XRF (μg g^{-1})
La	191.1	187	185
Ce	498	505	501
Nd	319	330	320
Sm	173.2	173.1	-
Eu	41.6	40	-
Tb	32.4	35	-
Yb	104.5	110	-
Lu	16.4	17	-
Hf	8.4	8.1	-
Th	23.3	23	-

- = not detectable.

The REE results obtained from apatite CRM samples demonstrate that the ICP-OES and NAA techniques agrees with each other for the selected REE, Hf, and Th that are reported in **Table 3.8**. The inability of XRF to detect some of the elements illustrated its limited use for element content determination, especially at extremely low levels.

Wang *et al*[82] quantified the REE (La, Ce, Nd, Sm, Eu, Tb, Yb and Lu) in certified reference plant material (leaf, stem and root), their host soils samples as well as in reference materials of citrus leaves, pine needles and tea leaves by means of instrumental neutron activation analysis (INAA). The leaf, stem and root samples were cleaned with distilled and deionized H_2O to remove any contamination. These samples were then oven-dried for 8 hours at 65 °C. The samples were accurately weighed and ashed at 550 °C except the fern plant. The soil samples were cooled to room temperature. All the leaf, stem and root ashed samples as well as fern leaves, the soil samples and citrus leaves, pine needles and tea leaves (CRM sample) were wrapped with aluminium foil and irradiation for 8 hours and analysed by INAA. The experimental values are in good agreement with those reported for different CRM samples as indicated in **Table 3.9**. The precision of these analyses were within 10 % for most of the REE. REE concentration levels in plant material reported in literature are normally low and in the 10^{-2} - 10^{-4} µg g^{-1} range. However, the REE concentration in the plant (leaf, stem and root) and host soils in this report are relatively high (0.28 - 76.0 µg g^{-1}).

[82] Y Q Wang, J X Sun, H M Chen and F Q Guo, *Journal of Radioanalytical and Nuclear Chemistry*, 1997, Vol. 219, No. 1, pp99-103.

Table 3.9: REE contents on CRM determined by INAA (µg/kg).[82]

Elements	NIST CRM-1572 Citrus leaves		NIST CRM-1575 Pine needles		GSV-4 CRM Chinese tea leaves	
	Found	Certified	Found	Certified	Found	Certified
La	196	198	167	160	636	600
Ce	366	453	273	210	930	1000
Nd	315	317	232	164	466	440
Sm	47.3	50	23.9	20	76.3	85
Eu	13.4	13.5	8.8	5.5	16.2	18
Tb	8.9	9	6.2	31	13.5	11
Yb	9.3	11.5	12.1	17.5	44.0	44
Lu	1.4	1.55	2.2	1.6	6.8	7

Yusof[83] used INAA to determine the concentrations of La, Ce, Sm, Eu, Tb, Dy and Yb in sediment samples. A sediment sample of 45 cm height was divided into strata of 2 to 3 cm. Samples were collected from each strata and dried at 60 °C for 2 weeks in an oven, followed by grinding to yield a fine powder. The dry powdered samples were then wrapped in small polyethylene vials for irradiation. The REE concentrations of 124 µg g^{-1} at the surface sediment samples taken at different sites were found to decrease with increasing distance from the surface with 58 µg g^{-1} at 39 cm and 95 µg g^{-1} at 45 cm depth, respectively.

Cornejo-Ponce *et al*[84] used XRF analysis to determine REE (Pr, Nd, Sm and Y) in samples after pre-concentration of the REE using a silica gel that was loaded with 1-(2-pyridylazo)-2-naphthol (PAN) in the liquid-solid extraction process. The pH of the

[83] A M Yusof, S Akyil and A K H Wood, *Journal of Radioanalytical and Nuclear Chemistry*, 2001, Vol. 249, No. 2, pp333-341.

[84] L Cornejo-Ponce, P Peralta-Zamora, M I Maretti and S Bueno, *Talanta,* 1998, 46, pp1371-1378.

REE mixture was adjusted by HCI or NH_3. Modified silica was added to each solution and the mixture was stirred for 15 min and then filtered. The resulting precipitate was dried at 60 °C for 30 min and then directly analysed by EDXRF. Results indicated that extraction with modified silica improved the REE recovery obtained in this work and ranged between 70 and 100 %. The RSD of this research was about 5 % which was subsequently lower than that obtained by Rastergar *et al*[85] using the same method. It appears that the pre-concentration procedure allows for the complete recovery of the REE in the sample and improves the sensitivity in comparison with the direct quantification in the aqueous phase.

Separation and pre-concentration of the REE by different techniques such as micro-column, HPLC, extraction, anion exchange or cation exchange chromatography and separation of the REE help to eliminate interferences, improve the sensitivity and the results of REE recovery (using techniques such as NAA, ICP-OES and ICP-MS) compared to the direct analysis of the element. XRF is a multi-element technique which allows for the direct analysis of REE in solid samples but due to its low sensitivity and the presence of REE at micro and ultra-level it can seldom be successfully used for this purpose.

3.4 DIGESTION TECHNIQUES

The complete dissolution of solid samples such as mineral ore or metallic objects is vitally important for the successful chemical characterization of these compounds. The three main dissolution methods are i) mineral acid dissolution ii) flux fusion and iii) microwave dissolution. Successful dissolution normally involve one or more of the following reactions namely acid-base, oxidation and complexation reactions.

Djingova and Ivanov [86] digested CRM samples with a combination of $HClO_4$ and HF. They heated the reaction mixture to dryness and repeated this process three times to ensure the complete dissolution of the silicate matrix. They then used cation-

[85] F Rastegar, D E Hadj-Boussaad, R Heimburger, C Ruch and M J F Leroy, *Analytical Chemistry,* 1990, 18, p497.

exchange chromatography to separate the REE and other elements in the CRM. Analysis of the REE with ICP-OES proved to be very successful with a RSD below 10 % and LOD between 0.05 mg kg^{-1} for Eu and 0.5 mg kg^{-1} for Er. A comparison with previous results showed that the achieved detection limits in this study are about an order of magnitude less the normal concentrations, except for Lu.

Yoshida *et al*[87] employed digestion using HNO_3, H_2O_2, HF and $HClO_4$ individually using ICP-OES to analyse the REE content in standard rock samples and ores after separation with high-performance liquid chromatography (HPLC). The REE ore on the other hand was digested using an alkali fusion with sodium carbonate followed by the addition of a mixture of HNO_3 and H_2O_2. The addition of cupferron allowed for its complexation with REE which were finally extracted with $CHCl_3$ as the REE-cupferrates complexes (**Figure 3.5**).

[86] R Djingova and J Ivanova, *Talanta*, 2002, 57, pp821-829.

[87] K Yoshida and H Haraguchi, *Analytical Chemistry*, 1984, 56, pp2580-2585.

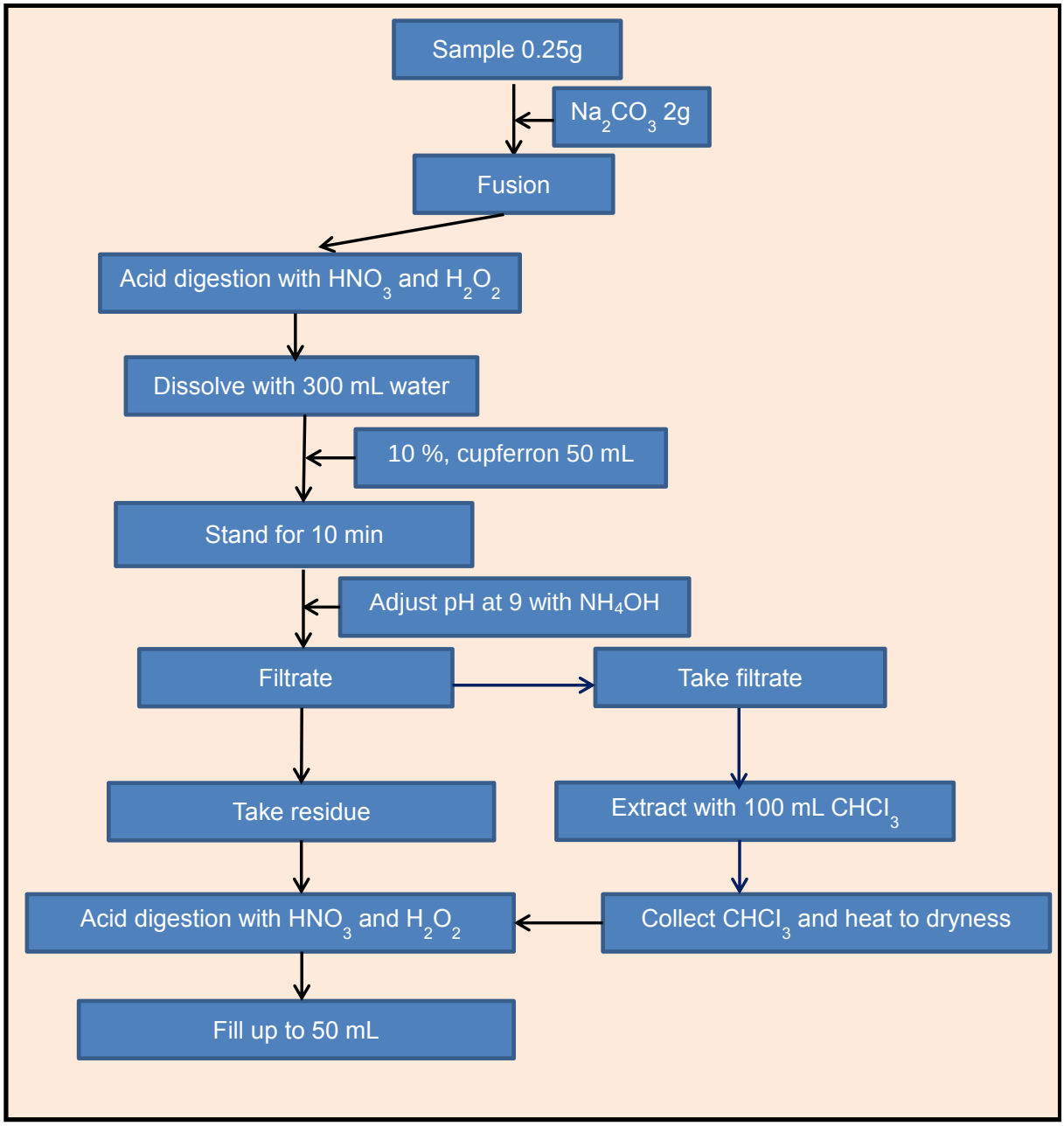

Figure 3.5: The alkali fusion for dissolution of REE ore.[87]

This method was successfully used for geological samples that contained trace amounts of REE. The recoveries ranged between 95.3 and 103.0 % for the acid digestion and 93.3 - 97.3 % for the alkaline fusion. The extraction with $CHCl_3$ improved recoveries of REE by 1 or 2 %. The REE detection limits ranged between 0.001 and 0.3 ug mL^{-1} and precision was 1.2 % for Eu and 7.4 % for Eu using a HPLC/ICP-OES combined system. The separation of REE with HPLC helped to avoid spectral interferences and clogging of ICP-OES due to the presence of large amounts of salts in the mineral.

Yenisoy-Karakaş *et al*[88] used ICP-OES to analyse the REE (La, Ce, Sm, Eu, Y, Yb, Pr and Nd) content in a bastnäesite ore as well as certified reference rock samples (CRM) without initial separation or pre-concentration of the REE. They successfully demonstrated the use of microwave-assisted acid digestion of these samples using harsh experimental conditions such as acid mixtures containing HCl, HNO_3, HF and H_3BO_3 to dissolve CRM rock samples. They successfully used HCl and HNO_3 in the microwaves to dissolve the bastnäesite ore. The acid decomposition of the bastnäesite ore samples by means of microwave digestion proved to be very successful with the REE recoveries, detection limit and RSD in the range 94.1 - 105.5 %, 0.00018 - 0.074 % and 0.11 - 2.25 % respectively. The procedure proved again to be easy and fast and the REE quantification were completed with high accuracy and precision.

Bulska *et al*[89] also employed microwave-assisted acid digestion of dissolved CRM plants samples using a mixture of HNO_3, HF and H_2O_2 under the following conditions: 5 min - 390 W, 5 min - 520 W or 10 min - 650 W. They used ICP-MS and compared the results with neutron activation analysis (NAA) and ion chromatography (IC) with UV/Vis to analyse the REE content in certified reference materials (CRM) of plant samples. The digested samples were dried and re-dissolved with the mixture of HCl and H_3BO_3 to remove the fluorides in the sample. The water was removed by evaporation and re-dissolved with HCl. Column chromatographic separation was used to separate and isolate the REE in the CRM sample as illustrated in **Figure 3.6**. REE recoveries in CRM of plant samples by ICP-MS were in excess of 99.4 %. The limits of detection (LOD) ranged between 0.1 and 0.3 ng g^{-1} using by ICP-MS. These LOD were lower than that obtained after ion exchange separation and followed by UV/Vis analysis. The LOD were between 5 - 10 ng g^{-1} and 0.1 - 50 ng g^{-1} (IC/UV/Vis) and NAA respectively. The rest of the results obtained in this study were found to be in good agreement with the certified values.

88 S Yenisoy-Karakaş, E O Gaga, A Doğangün and S G Tuncel, *Analytical letters*, 2004, Vol. 37, No. 13, pp2701-2709.

89 E Bulska, B Danko, Rajmunds, D Ski, A Krata, K Kulisa, Z Samczyn´ski and M Wojciechowski, *Talanta*, 2012, 97, pp303-311.

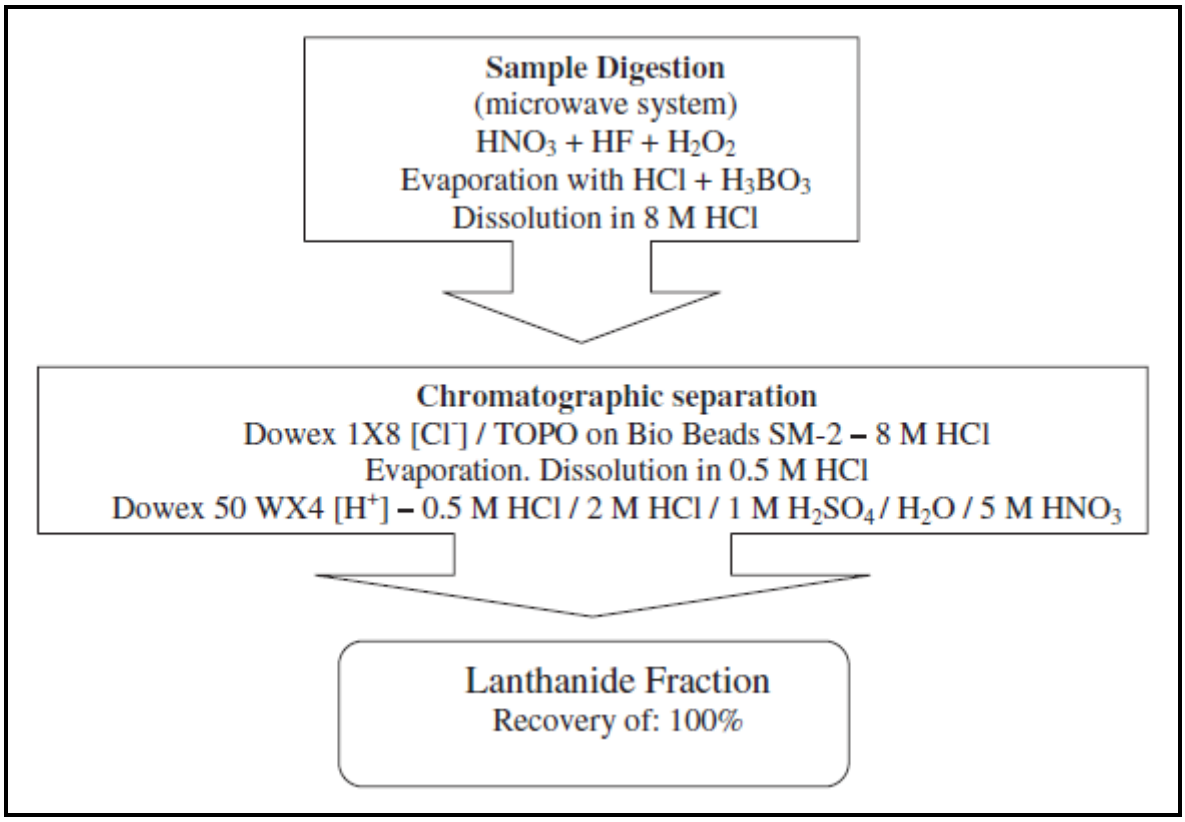

Figure 3.6: Flow chart of the selective and quantitative separation of the REE from Certified Reference Materials (CRM) of plant samples.[89]

Alvarado *et* al[90] developed different dry-ashing, wet-ashing and microwave digestion processes for the quantification of REE (Ce, Sm, Eu, Tb), U and Th in organic CRM samples such as plant tissues, orchard leaves and apple leaves. They discovered that plants have the ability to absorb trace metals such as Ce, Sm, Eu, Tb, U and Th from the air and soil. The samples were dried for 24 hours at 105 °C before performing any digestion. The product obtained after their dry ashing process were further spiked with a combination of Tm, U and Th solutions, then ashed for 1 hour at 100 °C in a muffle furnace. The temperature was then increased in steps of 50 °C up to 500 °C every 30 minutes. Tm was used as an internal standard while Th and U were used for isotope dilution. During the wet ashing process the dried samples were also spiked with a combination of Tm, U and Th. A mixture of HNO_3 and H_2SO_4 was added to these dried samples, and refluxed (boiling) for 2 - 3 hours. In the microwave digestion process the dried samples were also spiked with a combination of Tm, U and Th solutions like in the dry-ashing and wet ashing method. The microwave

[90] J S Alvarado, T J Neal, L L Smith and M D Erickson, *Analytica Chimica Acta*, 1996, 322, pp11-20.

digestion procedure involved the addition of HNO_3 and H_2O_2 to the dried samples. The mixture was then digested using different digestion programs. REE quantification was done in each step of this digestion process. The dry-ashing, wet-ashing and microwave steps had average REE percentage recoveries ranging between 80 - 90 %, 30 - 60 % and 83 - 99 % respectively using ICP-MS. The detection limits ranged from 0.1 to 0.9 ng L^{-1}. It was concluded that the microwave technique proved to be the most successful digestion process as indicated by the REE recoveries, while the wet-ashing procedure had the lowest recoveries.

Sen-Gupta and Bertrand[91] also used microwave-assisted acid digestion to determine the REE, U and Th in various silicate rock and sediment reference samples. They analysed the samples using ICP-MS without any separation of matrix elements or pre-concentration. They employed microwave-assisted digestion with a mixture of HF, HNO_3, H_3BO_3 and HCI to digest the finely powdered CRM samples. After cooling, a mixture of boric acid and EDTA were added to the solution, and then further heated for 8 min. The mixture was cooled in a water bath at 25 °C and washed with HNO_3. This solution was diluted 10 times with HNO_3 containing ruthenium (Ru) and rhenium (Re) as internal standards. Results indicated that the addition of H_3BO_3 and EDTA was extremely important in the removal of HF and played an important role in the success of the total dissolution. The recoveries of the REE in the samples ranged from 85 to 115 % and the detection limits ranged between 0.02 and 0.10 ug g^{-1}.

Shinotsuka and Ebihara[92] used microwave-assisted acid digestion to determine REE, U and Th in chondritic meteorite samples by employing ICP-MS and radiochemical NAA (RNAA). The chondrite samples were digested in the presence of an acid combination of HF, HNO_3 and $HCIO_4$. The solution was heated to dryness at 150 °C for 24 hours. The evaporation residue was re-dissolved in HNO_3 and H_2O, and this solution was divided into two portions. The first portion was further diluted to 10 mL for the determination of Y while the other portion was used for the determination of the REE, Th and U by ICP-MS. The RNAA procedure was carried out by sealing a powder meteorite sample in a quartz tube and irradiate it for 12 hours. Both techniques had excellent reproducibility of about 5 % with the exception of Lu which

[91] J G S Gupta and N B Bertrand, *Talanta*, 1995, 42, pp1595-1607.

[92] K Shinotsuka and M Ebihara, *Analytica Chimica Acta,* 1997, 338, pp237-246.

had a RSD of 10 %. The detection limit ranged between 0.28 and 5.9 ng g^{-1} for the ICP-MS analysis and 0.094 to 36 ng g^{-1} for RNAA. Both ICP-MS and RNAA techniques had similar detection limits for the REE.

In another study where microwave-assisted acid digestion was used in sample dissolution, Cao *et al*[93] determined 8 REE (La, Ce, Nd, Sm, Eu, Tb, Yb, and Lu) in human hair and wheat powder CRM samples from China. They digested the Chinese CRM samples in a mixture of HNO_3 and $HClO_4$, followed by HCl addition. After complete dissolution of the sample, HF was added to form $(REE)F_3$ precipitates. These precipitates were then analysed by RNAA. The recoveries obtained in this study varied between 97 - 101 % and the results obtained showed good agreement with the reported CRM values.

3.5 CHARACTERIZATION OF REE COMPLEXES

IR spectroscopy was extensively used to characterize REE in numerous inorganic and organometallic compounds. It provided valuable information on the successful (or not) formation of the metal complexes. In addition, elemental analysis was also used to confirm the chemical composition of organometallic compounds containing C, H, S, O and N.

3.5.1 INFRARED (IR)

Wang *et al*[94] synthesised $K_3[Dy(nta)_2]\cdot 6H_2O$ and $(NH_4)_3[Dy(nta)_2]$ complexes by reacting nitrilotriacetic acid (nta) and Dy_2O_3 in 1:2 ratio (metal:ligand) by refluxing the two reactions for 7 hours. The solution pH was adjusted to 6 by the addition of $KHCO_3$ or NH_4OH and left for two to three weeks at room temperature to allow for crystallization. The nta, $K_3[Dy(nta)_2]\cdot 6H_2O$ and $(NH_4)_3[Dy(nta)_2]$ complexes was characterized by infrared as illustrated in **Figure 3.7**.

[93] L Cao, W Tian, B Ni, P Wang and Y Zhang, *Analytical and Bioanalytical Chemistry*, 2002, 372, pp397-400.

[94] J Wang, X Z Liu, Z H Zhang, X D Zhang, G R Gao, Y M Kong and Y Li, *Journal of Structural Chemistry*, 2006, Vol. 47, No. 5, pp906-912.

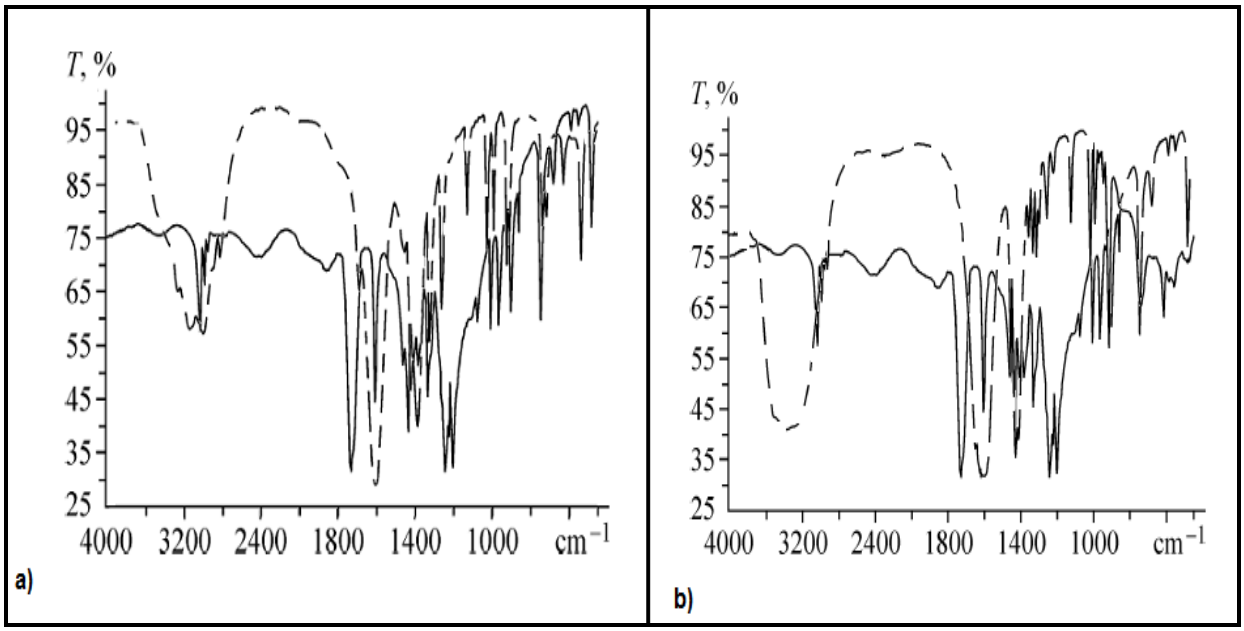

Figure 3.7: An infrared structure of **a)** (- — —) $(NH_4)_3[Dy(nta)_2]$ and (———) nta **b)** (- — —)$K_3[Dy(nta)_2]\cdot 6H_2O$ and (———) nta.[94]

The characteristic C-N stretching frequencies of the $K_3[Dy(nta)_2]\cdot 6H_2O$ and $(NH_4)_3[Dy(nta)_2]$ complexes were observed at 1140 cm^{-1} compared to the same stretching frequency of nta which was observed at 1200 cm^{-1}. The COOH vibration at 1710 cm^{-1} of the nta disappeared in the different complexes and the characteristic absorptions for the asymmetric and symmetric carboxylate vibrations of the ligand (nta) which were observed at 1610 cm^{-1} and 1340 cm^{-1} respectively, are shifted to 1600 cm^{-1} and 1410 cm^{-1} in the $K_3[Dy(nta)_2]\cdot 6H_2O$ complex. These observations confirm that the O atoms of COO^- are coordinated to the Dy ion. The OH vibrational absorption of H_2O appears as a wide peak at 3390 cm^{-1} in the complex.

Khorasani-Motlagh *et al*[95] demonstrated the complexation of $[Nd(phen)_2Cl_3]\cdot H_2O$ with nitrogen donor ligands such as phenylcyanamide, (pcyd); (2-chlorophenyl)cyanamide, (2-Clpcyd); (2,3,5-trichlorophenyl)cyanamide, (2,3,5-Cl_3pcyd); or (2,3,4,5-tetrachlorophenyl)cyanamide, (2,3,4,5-Cl_4pcyd). $[Nd(phen)_2Cl_3]\cdot H_2O$ was dissolved in H_2O and the ligands were added to react while heating the water to boiling point and stirring for 3 hours. The isolated precipitates

[95] M Khorasani-Motlagh, M Noroozifar, S Niroomand and J Saffari, *Journal of the Iranian Chemical Society,* 2010, Vol. 7, No. 4, pp807-813.

were washed with hot water. The products were dried for several hours in vacuum over P_4O_{10} and characterized by IR (**Table 3.10**)

Table 3.10: Infrared data of the cyanamide group.[95]

Complex	ν (NCN) (cm^{-1})
$[Nd(phen)_2(pcyd)_3]$	2090, 2108, 2227
$[Nd(phen)_2(2\text{-}Clpcyd)_3]$	2110, 2125, 2243
$[Nd(phen)_2(2,3,5\text{-}Cl_3pcyd)_3]$	2110, 2130, 2245
$[Nd(phen)_2(2,3,4,5\text{-}Cl_4pcyd)_3]$	2120, 2135, 2243

The C≡N stretching frequencies of neutral phenylcyanamide are in the range of 2225 to 2249 cm^{-1}, while coordination of phenylcyanamide ligands produce strong bond stretching frequencies lower than 2150 cm^{-1}. The IR spectrum of $[Nd(phen)_2Cl_3]\cdot H_2O$ showed a wide water stretching mode at 1635 cm^{-1}. The C=N absorption bands of phen at 1514, 1421 cm^{-1} shifted to lower waves upon complexation with cyanamide groups.

Babij and Mondry[96] demonstrated complexation of lanthanide (Gd^{+3}, Tb^{+3}, Dy^{+3} and Er^{+3}) complexes with S(+)-mandelic acid (ManH) by infrared characterization (**Table 3.11**). Lanthanide complexes with ManH were obtained at room temperature by the slow evaporation of aqueous solutions prepared by mixing solutions of $EuCl_3$, ManH and NaOH in a 1:1:1 molar ratio.

[96] M Babij and A Mondry, *Optical Materials*, 2012, pp1-5.

Table 3.11: Infrared data of $[Ln(Man)_3]\cdot 2H_2O$ complexes and mandelic acid.[96]

Compound	ν (COOH)	ν (OH)	ν_{as}(COO)	ν_{as}(COO)
ManH	1724	3447		
Tb-Man		3263, 3425, 3620	1620	1388
Dy-Man		3263, 3425, 3620	1620	1388
Er-Man		3263, 3425, 3620	1620	1388

The spectra of all the $[Ln(Man)_3]\cdot 2H_2O$ complexes as well as mandelic acid are significantly different from each other in the region of the characteristic carboxylic and OH group vibration. The spectrum of ManH shows the COOH vibration of the protonated carboxylic group at 1724 cm^{-1} and the OH stretching frequency corresponding to the sharp alcoholic group peak at 3447 cm^{-1}. The characteristic absorptions of the COOH of ManH at 1724 cm^{-1} disappeared in the $[Ln(Man)_3(H_2O)_2]$ complexes and the characteristic absorptions for the asymmetric and symmetric vibrations of the deprotonated carboxylic group of $[Ln(Man)_3]\cdot 2H_2O$ are observed at 1620 and 1388 cm^{-1} confirming COO^- coordination *via* the oxygen atom to the lanthanide ions. The OH vibrational absorption of H_2O for the $[Ln(Man)_3]\cdot H_2O$ complexes are present as wide peaks at 3236, 3425 and 3620 cm^{-1}.

Silva *et al*[97] demonstrated complexation of $Nd(NO_3)_3$ and polystyrene sulfonic acid (H-PSS) in a 6:1 molar ratio in a reaction mixture which was left overnight at 5 °C. The IR spectra of H-PSS and Nd-PSS were obtained in the 400 - 4000 cm^{-1} region as shown in **Figure 3.8**.

[97] M C Silva, F H Cristovan, R Ruggiero, W O Cruz and A Marletta, *Brazilian Journal of Physics*, 2006, vol. 36, no. 2A, pp499-500.

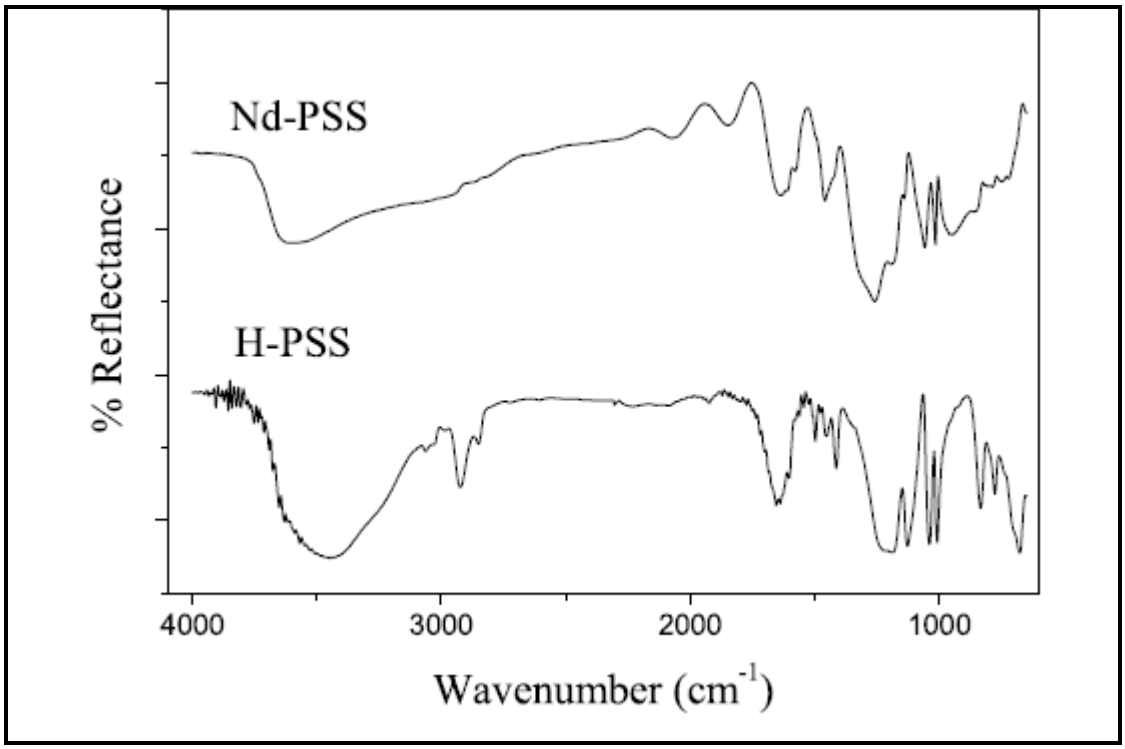

Figure 3.8: The IR spectra of H-PSS and Nd-PSS.[97]

The S=O and OS-O symmetric stretching frequencies of the ligand are observed at 1190 cm^{-1} and 1000 - 1030 cm^{-1} respectively. The angular deformation of C-H of aromatic ring at 800 cm^{-1} and symmetric stretching of O-H at 3000 - 3900 cm^{-1} are also observed on the ligand. The Nd-PSS complex also showed stretching frequencies bands in the same range with an enlargement of the % reflectance.

3.5.2 CHN-ELEMENTAL ANALYSIS

Anna Mondry and Przemyslaw Starynowicz[98] demonstrated the successful complexation of Nd_2O_3 to diethylenetriaminepentaacetic acid, (dtpa) in a 1:2 ratio (metal:ligand) mixture. The pH of the solution was adjusted to 5 using an aqueous solution of $[C(NH_2)_3]_2CO_3$ and it was left to crystallize. Elemental analysis data for the $(C(NH_2)_3)_2[Nd(dtpa)(H_2O)]\cdot 7H_2O$ complex are as follows (%): C 24.60, H 6.20, N 16.10, which are in accord with the theoretical elemental percentage calculation based on the theoretical composition of C 24.10, 5.80, N 15.80.

[98] A Mondry and P Starynowicz, *Polyhedron,* 2000, 19, pp771-777.

Wang *et al*[99] demonstrated that *trans*-1,2-cyclohexanediaminetetraacetic acid, (cydta) or ethylenediaminetetraacetic acid, (edta) reacts with Y_2O_3 in a 1:2 ratio (metal:ligand) when refluxed for 10 hours. The pH of the solution was adjusted to 6 by the addition of $NaHCO_3$ and left for two to three weeks at room temperature to crystallize. The REE complexes were characterised in percentile content using a CHNO analyser (**Table 3.12**).

Table 3.12: Characterization data of REE complexes, found (calculated).[99]

Complex	C (%)	H (%)	N (%)
$Na[Y(edta)(H_2O)_3]\cdot 5H_2O$	22.03 (22.07)	5.17 (5.19)	3.68 (3.64)
$Na[Y(cydta)(H_2O)_2]\cdot 5H_2O$	28.94 (28.98)	5.54 (5.56)	4.80 (4.83)

Shavaleev et al[100] successfully complexed $PrCl_3\cdot 6H_2O$ and benzimidazole-substituted 8-hydroxyquinolines in ethanol. The reaction mixture was stirred at 70 - 80 °C for 15 min. The isolated precipitate was filtered and washed with ethanol/water (50:50), repeated with ether and dried. This synthetic procedure proved to be successful for complex formation as the theoretical and experimental composition of $[Pr(C_{17}H_{10}N_3O)_3]\cdot 3H_2O$ is in agreement with each other namely C, 60.18 (60.04); H, 4.16 (4.06); N, 12.39 (11.82). The $[Pr(C_{17}H_{10}N_3O)_3]\cdot 3H_2O$ complex was recrystallized in acetonitrile/ethanol/isopropanol at room temperature.

3.6 LOD

A recent article compared the detection limits (LOD) on the use of separation and pre-concentration methods for different techniques such as ICP-MS, ICP-OES and NAA for the REE determination since 2000.[55] ICP-MS, ICP-OES and NAA

[99] J Wang, Y Wang, Z H Zhang, X D Zhang, J Tong, X Zh Liu, X Y Liu, Y Zhang and Z J Pan, *Journal of Structural Chemistry*, 2005, Vol. 46, No. 5, pp895-905.

[100] N M Shavaleev, R Scopelliti, F Gumy and J G Bunzli, *Inorganic Chemistry*, 2008, 47, pp055-9068.

techniques have shown the highest sensitivity and had comparable LOD values for the determination of REE in various samples, as shown in **Table 3.13**.

Table 3.13: Detection limits of REE in various samples using ICP-MS, ICP-OES and NAA.[55]

Samples	Technique	LOD		
		La	Ce	Nd
Water	ICP-OES	0.3 ppb	0.22 ppb	0.02 ppb
	ICP-MS	0.04 ppb	0.09 ppb	0.08 ppb
Geological	ICP-MS	0.01 ppb	0.01 ppb	0.05 ppb
	NAA	0.2 ppm	0.3 ppm	3.8 ppm
	ICP-OES	4.3 ppb	31 ppb	22 ppb
Biological	ICP-MS	0.1 ppb	0.02 ppb	0.2 ppb
	ICP-OES	88.1 ppb	182 ppb	264 ppb

Research also indicated that ICP-MS provides simpler spectra and lower detection limits than other techniques such as ICP-OES and NAA, allowing for the REE determination in water as well as biological and geological samples, with the need for matrix separation or pre-concentration.

3.7 CONCLUSION

The discussions in the above sections revealed that the ICP-OES and ICP-MS are the most applied techniques (**Table 3.1**) for the determination of REE in samples such as biological and geological materials. This is due to the several advantages that these techniques have over other existing analytical techniques such as UV/Vis and XRF. Both ICP-OES and ICP-MS have shown greater success in the analysis of environmental (water and plants) and geological (mineral samples) materials which have low REE contents. However, ICP-MS appears to be a more popular option for the analysis of REE, due to the fact that it is a multi-element technique, has no spectral interferences, a wide concentration range and has extensively low detection limits.

Dry ashing has several advantages, including limited supervision and high percent recoveries. The microwave procedure is a very promising and popular digestion method with relatively high percent recoveries. Other advantages of the microwave digestion include very little digestion time, almost no required supervision and a low potential for contamination.

4 SELECTION OF ANALYTICAL TECHNIQUES

4.1 INTRODUCTION

The accurate and complete chemical characterisation of any chemical compound or mineral depend on three distinct and different processes namely i) the complete dissolution of the sample, ii) identifying of the chemical compounds present in the sample (qualification) and finally iii) quantifying the elements in question (quantification). The sample dissolution preparation or steps involves the complete conversion (destruction) of the solid sample into an aqueous solution using techniques such as digestion or flux fusion to produce homogeneous solutions. Identification of chemical compounds, either in solid or aqueous phase involves techniques such as IR, NMR, spectral characterisation and CHN microanalysis. The final step in this characterization process involves the accurate quantification of the element in question using techniques such as ICP-OES, ICP-MS, AAS and UV/Vis.

This section reviews the analytical principles, equipment and techniques used throughout the study. Dissolution techniques which were successfully applied in this study will be discussed in detail. This discussion will be followed by an in-depth discussion of different characterization techniques such as UV/Vis, IR and CHN microanalysis as well as spectrometric techniques such as ICP-OES, ICP-MS and AAS which were used for the quantification of the different elements. The advantages and drawbacks of these techniques were evaluated before it was used in this study.

4.2 SAMPLE DISSOLUTION

Sample dissolution, the first step in wet analytical processes, is critically important for complete characterization of the chemical compound. This is a process which ensures a total conversion of a solid material, for example a mineral sample, into a homogenous solution suitable for the wet chemical analysis. Incomplete sample dissolution will result for example in poor recoveries, missing of important constituents and finally loss of material or the loss of much needed information for proper decision making. There are several sample decomposition methods, such as flux fusions, (wet ashing or acid dissolution) and microwave digestion, which may be appropriate for the digestion of different sample matrices. Flux fusion is usually used for the dissolution of highly inert metals or mineral samples and involves the heating of an acidic or a basic flux e.g. 1:10 sample:flux mass ratio to a temperature at or above its melting point to produce a homogenous ionic solution.[101,102,103] This fusion changes the chemical composition of the sample which makes the sample soluble in either acid/base or oxidation reaction.

Samples investigated in this study did not require this extremely robust method and only open-beaker acid digestion and microwave digestion were used for dissolution. These techniques will be discussed in detail in the next few sections.

4.2.1 MICROWAVE DIGESTION

4.2.1.1 BACKGROUND

The microwave irradiation theory was conceptualized in 1864 by James Clerks Maxwell and its existence was proved by Heinrich Hertz in 1888 when he managed to build a spark gap radio transmitter which produced microwaves in the UHF

[101] G D Christian, Analytical chemistry*, John Wiley & Sons, New York*, 1994. 5th edition, p670.

[102] J Bassette, R C Denney, G H Jeffery and J Mendham, Vogel's textbook of quantitative inorganic analysis. *Longman Scientific & Technical, 4th edition,* 1978. pp105-106.

[103] M Nete. Dissolution and analytical characterization of tantalite ore, niobium metal and other niobium compounds*. M.Sc. thesis. Bloemfontein: University of the Free State Library*, (2009). p36.

region.[104,105] Marconi and Southworth recognized and used microwave as a means of wireless communication.[106] Anomalies in communication tones observed by Taylor and Young when objects moved between the transmitter of the microwave and its receiver led to the development of radar technology systems in the late 1930's and early 1940's which was used in radar detection installations against air attacks during WW II.

It was only in 1946 that Percy Spencer, an engineer at Raytheon Corporation noticed the heating ability of the microwave generated by a magnetron. The first commercial microwave oven, weighing 300 kg and more than 1.5 m tall, was produced in 1947 (**Figure 4.1**).[107] Microwaves are currently mostly used in telecommunication, RADAR systems and TV broadcasting *via* satellites as well its widespread use as microwave ovens in households all over the world.[108]

Figure 4.1: The first microwave oven.[109]

[104] J J Carr, Practical antenna handbook*, McGraw-Hill*, 2001, 4th Edition, p5.

[105] M D Pozar , Microwave engineering*, John Wiley & Sons, Inc*. 1998, 4th edition, p4.

[106] A Loupy, Microwaves in organic synthesis, *WILEY-VCH Verlag GmbH & Co. KGaA, Weinheim*, 2nd edition, 2006, p5.

[107] N G Tai-Kai and C W CHAN, Microwaves and microwave oven, *Department of Physics, Hong Kong University of Science and Technology,* pp1-6.

[108] H Rajak and P Mishra, *Journal of Scientific and Industrial Research*, 2004, vol 63, pp641-654.

[109] The microwave on everyone's radar, [Accessed 04-10-2013]. Available from: http://news.investors.com/management-leaders-in-success/010511-558851-percy-spencer-put-the-microwave-on-everyones-radar.htm#ixzz2uDyh5sh6.

The use of microwave ovens for laboratory purposes started in 1978 and was mostly used as open system reactors without pressure control for organic and inorganic syntheses. These poorly controlled reaction conditions led to numerous explosions and fires and the first commercially laboratory microwave, with temperature and pressure control, was introduced to the market in 1989.

Microwaves are electromagnetic radiation with wavelengths in the range 0.001 - 0.3 m and frequencies between 300 MHz to 300 GHz and are located between the infrared and radio spectra in the electromagnetic wave spectrum (**Figure 4.5**).[110] The preferred frequency is 2.45 GHz for laboratory reactions.[111] Apart from that, microwave technology is used for communications (satellite, radio, television and wireless phone) and medical applications.[112]

4.2.1.2 BASIC PRINCIPLES BEHIND MICROWAVE DIGESTION

The interaction of microwave radiation with samples and reagents such as acids cause both ionic conduction and dipole rotation, resulting in the fast heating of the mixture with consequent decomposition.[113] Microwave heating is able to heat only the sample and not the apparatus, improving the energy transfer and reducing digestion duration. Another advantage of microwave heating is the provision of uniform heating throughout a reaction mixture, unlike conventional heating (**Figure 4.2 a**) which main energy transfer occurs at the interactive surface between the reaction mixture and the source.

[110] E D Neas and M J Collins, *American Chemical Society*, 1998, pp7-32.

[111] M Gaba and N Dhingra, *Indian Journal Pharmaceutical Education and Research*, 2011, Vol 45, pp175-183.

[112] H Gunzler and D Williams, Handbook of analytical techniques, *OWILEY-VCH Verlag GmbH*, 2001, pp77-104.

[113] Z Mester and R E Sturgeon, *Critical Reviews in Analytical Chemistry*, 2003, vol XLI, p296.

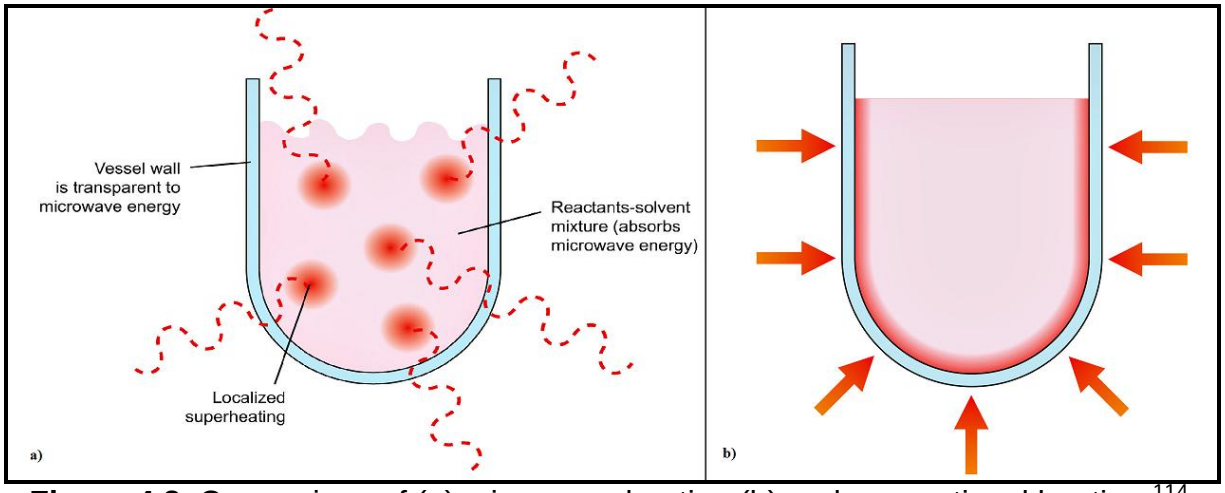

Figure 4.2: Comparison of (a) microwave heating (b) and conventional heating.[114]

Conventional heating usually involves the use of external heat sources such as an oil-bath or heating mantle which are first heated with the subsequent energy transfer to the solvent, resulting in a temperature difference between the solvent at the walls of the container (beaker) and the solvent in the interior of the container.[115]

Table 4.1: Advantages and disadvantages of microwave as digestion technique.[116]

Advantages	Disadvantage
Reduces cross-contamination	Lack of scalability
Increase dissolution rate	Limited applicability
Complete decomposition	No direct reaction monitoring or visual inspection
Uniform heating	
Avoided heat loss	
Reduce waste	
Improve reaction control	

[114] B l Haveys, Microwave synthesis*, CEM publishing*, 2002, pp15-17.

[115] Developments in microwave chemistry, [Accessed 04-10-2013]. Available from: http://www.rsc.org/images/evaluserve_tcm18-16758.pdf.

[116] S Ravichandran and E Karthikeyan, *International Journal Chemistry et Techniques Research,* 2011, vol 3, pp466-470.

4.2.2 MICROWAVE APPARATUS

Recent developments in microwave equipment technology enables researchers to use either single-mode or multi-mode apparatus for their research.[115]

The difference between the two techniques involves the build-up of energy within the system. In both cases, a magnetron generates the microwaves and is directed into the reaction chamber (cavity) through a wave guide. In multi-mode technology, microwaves entering the cavity are reflected by the walls, generating 3 standing micro-wave patterns within the cavity (**Figure 4.3**). The standing wave patterns consist of nodes (cold) and antinodes (high). This results in drastic variations (chaos) in the heating efficiency of numerous samples at different positions of the load. Another disadvantage of a multi-mode apparatus is that the temperature cannot be monitored *via* thermocouple or any other device during the heating process of the samples, since the irradiation power is controlled by the on-off cycles of the magnetron.

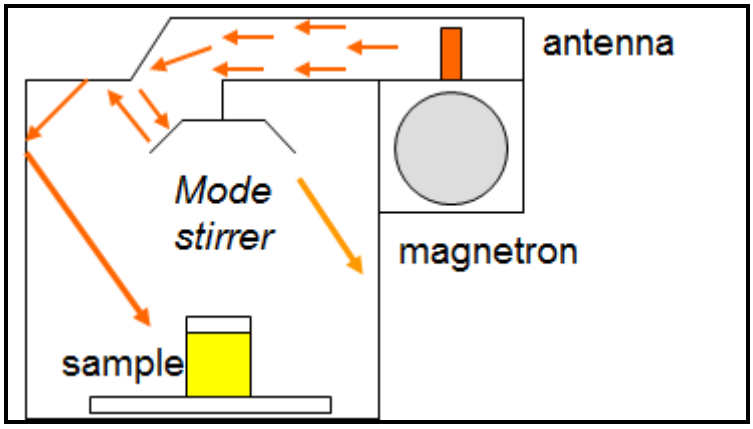

Figure 4.3: Schematic presentation of a multi-mode apparatus.[117]

In the single-mode apparatus the microwaves enter the cavity with the formation of one standing wave which has the same amplitude but with different oscillation directions (**Figure 4.4 b**). An appropriately designed cavity prevents the formation of hot and cold spots within the sample, resulting in a uniform heating of small quantities.

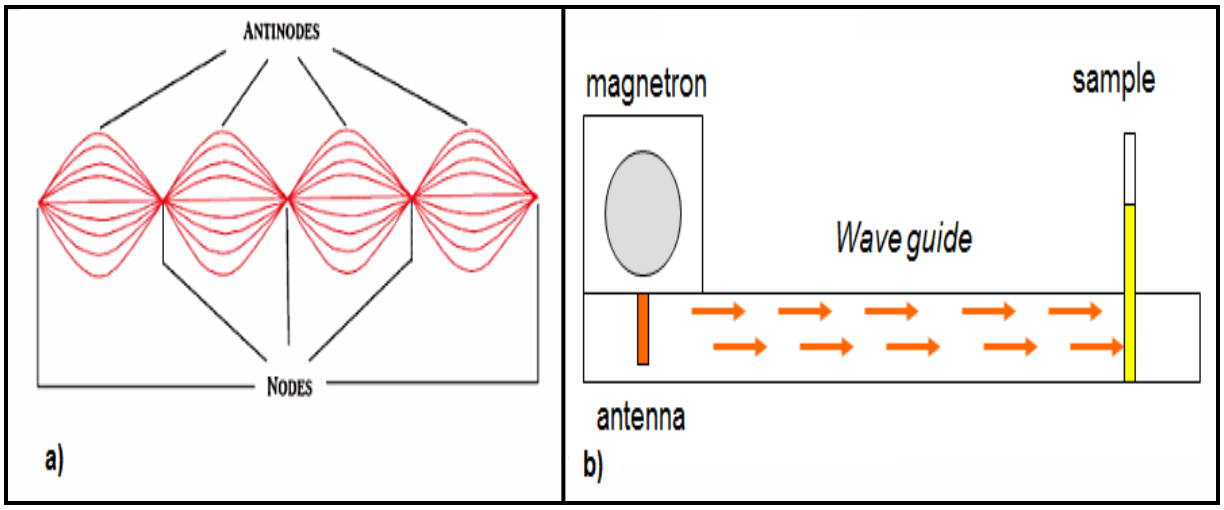

Figure 4.4: a) Generation of a standing wave pattern and b) single-mode heating apparatus.[117]

Single-mode reactors can process reaction volumes ranging from 0.2 to 50 mL while multi-mode equipment are designed to process samples with volumes between 5 to 1000 mL. The disadvantage of the single-mode digesters is that it can irradiate only one vessel at a time. Another advantage of single mode microwave digesters is that it can rapidly cool the reaction mixture with compressed air after completion of the irradiation.

4.2.3 OPEN VESSEL ACID DIGESTION

Acid dissolution in the open beaker is a relatively simple sample dissolution process at relatively low temperatures which only involves a hotplate with stirring capacity and a glass beaker. The dissolution of the samples with acids such as HF, HCI, HI, H_2SO_4, H_3PO_4, HNO_3, $HCIO_4$ and aqua regia are used to release the metals of interest from the sample matrix and convert them into a homogenous solution suitable for wet chemical analysis.

The solubilisation of different elements using any of the dissolution techniques involve the chemical attack/interaction with the compound in question and may involve either one, or a combination of the three main types of reactions, namely

[117] A Stadler, Synthos 3000 microwave assisted organic synthesis meanings model application, 2005, pp1-34.

acid/base reactions, oxidation/reduction reactions and complexation. Neutralization normally involve the protonation of an oxygen atom bonded to a metal ion as presented in **Equation 4.1**[118].

$$H_2SO_4 + Nb_2O_5 \rightarrow Nb_2O_4(SO_4) + H_2O \quad 4.1$$

Oxidation involves the change of the metallic element or a metal ion in a low oxidation state into the more soluble hydrated metal ion as indicated in **Equation 4.2**[119].

$$Zn_{(metal)} + HCl \rightarrow Zn(H_2O)_6^{2+} + H_{2(g)} + 2Cl^- \quad 4.2$$

Metals such as cerium and silver with standard electrode potential (E^0) values greater than hydrogen (E^0 = 0 V) require acids with a higher redox potential/ability such as HNO_3, hot H_2SO_4 or hot $HClO_4$ to convert (oxidize) them to soluble entities.[120]

Complexation involve the formation of strong metal-ligand bonds to form soluble metal complexes as indicated in **Equation 4.3**[121].

$$Ta_2O_5 + 7NH_4F{\cdot}HF \rightarrow 2(NH_4)_2TaF_7 + 3NH_3 + 5H_2O \quad 4.3$$

[118] L Bogard, Traitements et analyses de surface du niobium supraconducteur, *Spectrochimica Acta, Part A: Molecul ar and Biomolecular Spectroscopy,* 2001, p16.

[119] Redox reactions-(oxidation- reduction reactions) [Accessed 04-10-2013]. Available from: http://www2.palomar.edu/stem/WorkshopMaterials/Chem115b/HO%2013-Redox%20Reactions.pdf

[120] Multi-agency radiological laboratory analytical protocols manual (MARLAP). [Accessed 04-10-2013]. Available from: www.epa.gov/radiation/marlap.

[121] M Nete. Separation and purification of niobium and tantalum from synthetic and natural compounds*. PhD. thesis. Bloemfontein: University of the Free State Library*, (2013). p162.

Table 4.2: Different acids used for sample dissolution.[122,123,124,125]

Acids	Uses
HCl	• Converts the metals to soluble salts • Dissolve silicate to produce Si-O-Si bonds • Dissolve the oxides except CeO_2 • Dissolve sedimentary rock (oolite) to remove the organic material
H_2SO_4	• Converts oxides, hydroxides or carbonates to sulphate • Used for treatment of xenotime and monazite
HNO_3	• Converts oxide, hydroxide, chlorides, carbonate or metal to nitrates • Remove barium from REE sample
HF	• REE oxides converts to REE fluorides • Digest silicate containing REE
Aqua regia	• Digest various apatites
$HClO_4$	• Convert Ce(IV) hydroxide to Ce(IV) perchlorate • Dissolve insoluble organic material from sedimentary rocks

[122] C Huang, Rare earth coordination chemistry: fundamentals and applications, *John Wiley & Sons (Asia) Pte Ltd*, 2010, p994.

[123] G Adachi, N Imanaka and Z C Kang, Binary rare earth oxides, *Kluwer Academic*, 2004, p166.

[124] Overview of Microwave Assisted Sample Preparation, [Accessed 03-10-2013]. Available from: http://www.sampleprep.duq.edu/dir/Chapter2/Chapter2.htm.

[125] R V Spirn, Distributions in the marine environment, *PhD thesis Massachusetts Institute of Technology*, 1965, pp2-136.

Open vessel digestion in this study was exclusively used to convert water insoluble organometallic complexes to the hydrated metal by the simple protonation and subsequent destruction of the organometallic compound as illustration by **Equation 4.4**[126].

$$[FeCl_2(acac)]\cdot H_2O + HCl \rightarrow [FeCl_3\cdot n(H_2O)]^{3+} + Hacac \qquad 4.4$$

4.3 IDENTIFICATION (QUALIFICATION) TECHNIQUES

The second step in the complete chemical characterization of chemical species involves the identification or qualification of the compounds using a variety of methods. Identification is required for a variety of reasons which include i) to determine if the product meet the required specification, ii) to determine if the reaction between different reagents were successful or iii) to determine the composition of samples. Numerous methods for chemical compound identification exists which include techniques such as NMR, MS, Raman X-ray diffraction or X-ray fluorescence spectroscopy. In this study the main techniques utilized for product characterization incude IR, UV/Vis and CHN micro-element analyses.

IR uses vibrational spectroscopy to identify particular unique bond vibrations within an isolated product, while UV/Vis spectroscopy provides information on the electronic bonding in a molecule. CHN micro-analyses charaterize the compounds in percentile levels of elements, such as carbon, hydrogen and nitrogen in milligram (mg), or as percentage present in the analyzed product.

4.3.1 UV/Vis SPECTROPHOTOMETRY (COLORIMETRY)

4.3.1.1 INTRODUCTION

Colorimetry in general includes all the physical-chemical methods which utilizes light absorption of a coloured solution for qualification or quantification of chemical

[126] K Takeda. K Isobe, Y Nakamura and S Kawaguchi, *Bulletin of the Chemical Society Of Japan*, 1976, 49, pp1010-1016.

compounds. UV/Vis is one of the most common and well known methods in this category.

Ultraviolet (UV) and visible radiation comprise only a small part of the electromagnetic spectrum ranging from 160 nm to 780 nm (**Figure 4.5**).[127] It is divided into an ultraviolet light section which comprises the wavelength between 160 and 400 nm and visible part of the spectrum which is allocated to the wavelength range of 400-780 nm. UV/Vis spectroscopy is a very useful method of qualitative analysis in various fields such as chemistry, physics, biochemistry, material science and chemical engineering.

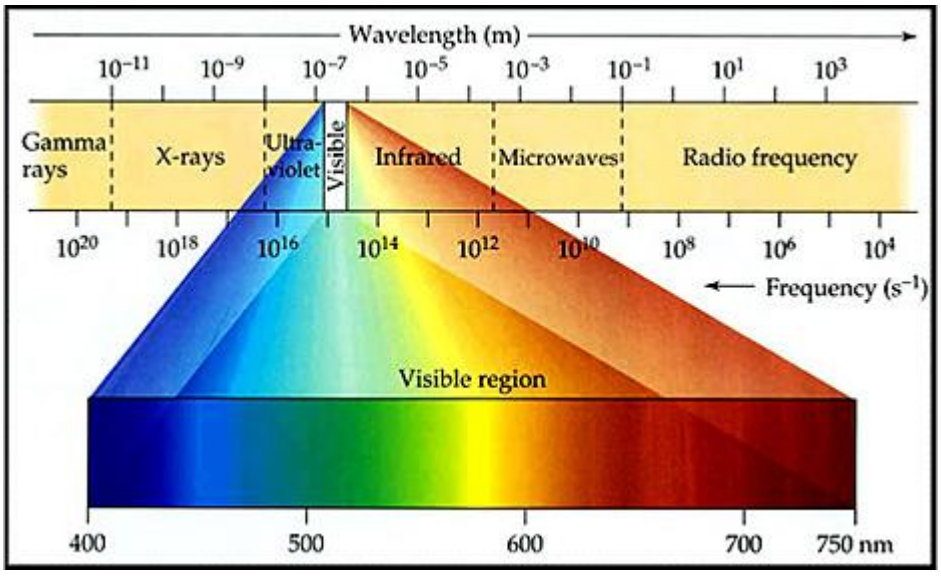

Figure 4.5: The electromagnetic spectrum.[128]

4.3.1.2 BASIC PRINCIPLES

Absorption spectroscopy with advantages such as high sensitivity and wide applicability involve the absorption of light that travels through a solution containing a colored compound. The spectrophotometer measures the difference between the

[127] D A Skoog, F J Holler and T A Nieman, Principle of instrumental analysis, *Thomson learning*, 1998, 5th edition, p302.

[128] About far infrared rays, [Accessed 03-10-2013]. Available from: http://www.air-boom.com/products_far.htm.

incident radiation (I_o) and the transmitted radiation (I) (**Figure 4.6**). The amount of light absorbed is expressed as either transmittance or absorbance.[129]

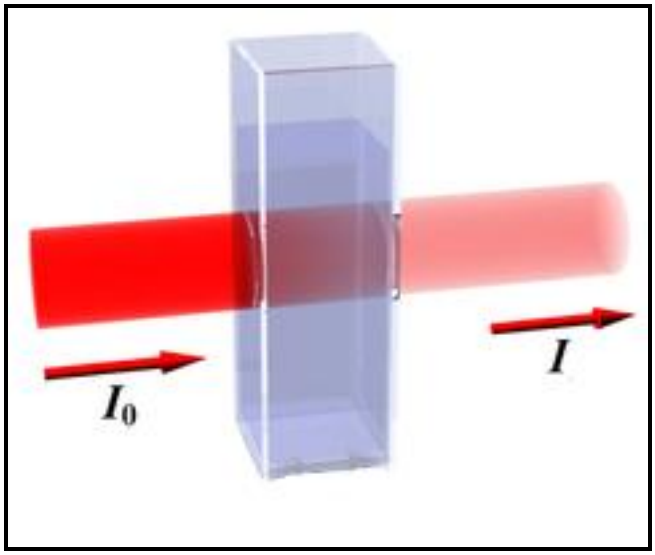

Figure 4.6: Transmittance.[130]

Transmittance is expressed as the ratio of I_o and I, or as a percentage and is defined as follows

$$T = \frac{I}{I_0} \qquad 4.5$$

or

$$T = \frac{I}{I_0} \text{ x } 100\,\% \qquad 4.6$$

I = Intensity of transmitted light

I_0 = Intensity of incident light

T = Transmittance

[129] R A Meyers, Encyclopedia of analytical chemistry, *John Wiley & Sons Ltd, Chichester*, 2000, pp1699-1714.

[130] CO_2 – An insignificant trace gas? part four, [Accessed 04-10-2013]. Available from: http://scienceofdoom.com/2010/02/05/co2-an-insignificant-trace-gas-part-four/.

The relationship between absorbance and transmittance at a given wavelength is defined by **Equating 4.7** as follows:

$$A = \log_{10}\left(\frac{I_0}{I}\right) = \log_{10}\left(\frac{1}{T}\right) = -\log_{10}(T) \qquad 4.7$$

$A = \text{Absorbance}$

The I_o and I are respectively referred to as the intensity of a beam of light before and after it has passed through cells containing the solvent and the analyte solutions.

Absorptions in the UV/Vis region occur due to electronic transitions from the ground state to the excited state. In a molecule, the different atoms can rotate and vibrate freely with respect to each other and numerous, separate absorption lines appears because of the large number of rotational and vibrational transitions. In the solution, however, molecules have less freedom to rotate due to the presence of large numbers of solvent molecules, hence the numerous separate absorption lines merge together as a result of the difference in vibrational transition to form a single broad absorption peak. The ions of lanthanide and actinide elements have a different absorbance response to these activation as indicated in **Figure 4.7**. The 4f and 5f electrons in these element groups are responsible for the shielding of electrons with higher quantum numbers and hence produce narrow absorption bands, relatively unaffected by ligands.

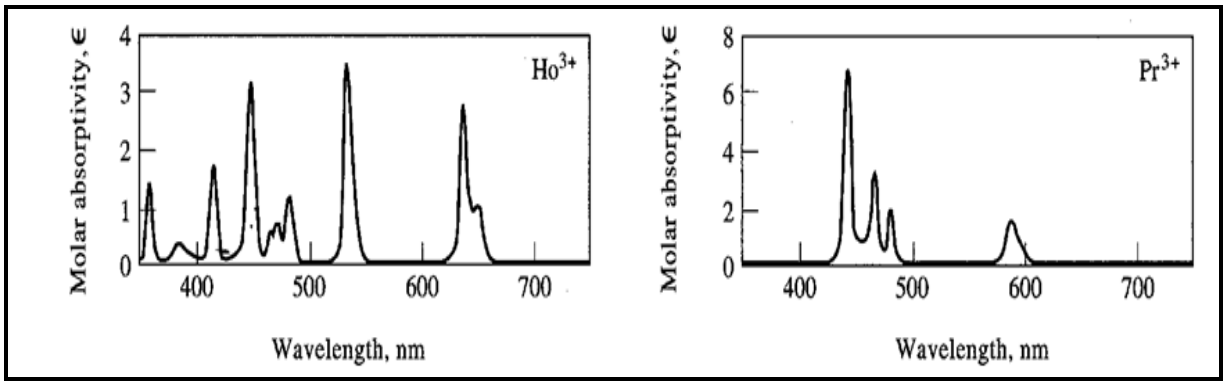

Figure 4.7: Absorption spectra of aqueous solutions of selected lanthanide ions.[131]

[131] D A Skoog, F J Holler and T A Nieman, Principles of the instrumental analysis, *Thomson learning*, 5th edition, pp336-338.

At least one of the oxidation states of elements of the first and second transition series tend to absorb visible radiation (**Figure 4.8**). Absorption involves the transition of electrons between occupied and unoccupied d-orbitals with energies which is strongly influenced by the type of ligands which is bonded to the metal ions. The resultant broad spectrum which is obtained is the result of the differences in energy between these d-orbitals. This energy difference is a function of the oxidation state of the element, the type of ligands bonded to it as well as the element's position on the periodic table.

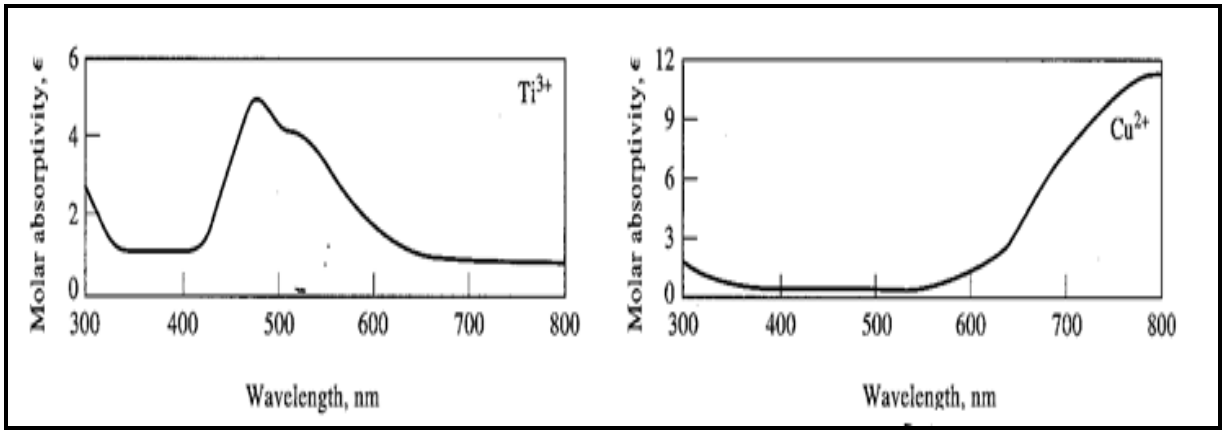

Figure 4.8: Absorption spectra of aqueous solutions of some transitional metal ions.[131]

Absorbance of organic molecules in the UV/Vis range is often the result of color bearing groups (chromophores) present within the molecules. **Table 4.3** provides an overview of color bearing groups or molecules their absorbance wavelengths as well as the type of transition. Four different types of transitions between the quantized energy levels account for most molecular UV/Vis spectra, which includes n $\rightarrow$ π^*, π $\rightarrow$ π^*, n $\rightarrow$ σ^* and σ $\rightarrow$ σ^* transitions.

Table 4.3: Absorption characteristics of some chromophores.[132,133]

Chromophore	Example	Solvent	λ_{max} (nm)	Transition
Alkene	$C_6H_{13}CH=CH_2$	n-Heptane	177	$\pi \rightarrow \pi^*$
Alkyne	$C_5H_{11}C\equiv CCH_3$	n-Heptane	178	$\pi \rightarrow \pi^*$
			196	-
			225	-
Carbonyl	CH_3COCH_3	n-Hexane	186	$n \rightarrow \sigma^*$
			280	$n \rightarrow \pi^*$
Carboxyl*	CH_3COOH	Ethanol	204	$n \rightarrow \pi^*$
Amido	CH_3CONH_2	Water	214	$n \rightarrow \pi^*$
Azo	$CH_3N\equiv NCH_3$	Ethanol	339	$n \rightarrow \pi^*$
Nitro	CH_3NO_2	Isooctane	280	$n \rightarrow \pi^*$
Nitroso	C_4H_9NO	Ethyl ether	300	-
			665	$n \rightarrow \pi^*$
Nitrate	$C_2H_5ONO_2$	Dioxane	270	$n \rightarrow \pi^*$

The energy of these electronic transitions is generally in the following order: $n \rightarrow \pi^* < \pi \rightarrow \pi^* < n \rightarrow \sigma^* < \sigma \rightarrow \sigma^*$ and is described in more detail in the next few paragraphs.

[132] D Harvey, Modern analytical chemistry, *The McGraw-Hill Companies, Inc*. 1st ed, 2000, p559.

[133] D A Skoog, F J Holler and T A Nieman, Principle of instrumental analysis, *Thomson learning*, 1998, 6th edition, p369.

$n \rightarrow \pi^*$ and $\pi \rightarrow \pi^*$ transitions

The transitions of n or π electrons to the π* excited state are normally observed/present in unsaturated compounds which also contain atoms with unshared electron pairs. Absorption for both $\pi \rightarrow \pi^*$ as well as $n \rightarrow \pi^*$ may be observed at wavelengths between 200 and 700 nm.[134]

$n \rightarrow \sigma^*$ transitions

This type of transition requires less energy than the $\sigma \rightarrow \sigma^*$ transition and is normally observed when saturated compounds contain atoms with unshared electron pairs. The $n \rightarrow \sigma^*$ transitions are normally observed in the 160 and 260 nm range. Compounds containing O, S, N and halogens can absorb energy through this type of transition.

$\sigma \rightarrow \sigma^*$ transitions

In this type of transition an electron get excited from a sigma bonding orbital (σ) to sigma anti-bonding orbital (σ*) which require a large amount of energy. The $\sigma \rightarrow \sigma^*$ transitions normally give absorption bands below 200 nm. This type of absorption corresponds to the breaking of bonds such as C-C, C-O, C-H and C-X.

Visible light includes the rainbow colors red, orange, yellow, green, blue, indigo and violet.[135] Absorption occurs when visible light strikes a colored solution. Photons with the appropriate amount of energy activate electrons at the lower levels to higher levels which removes those photons from the spectra and only emit photons with complementary colours. For example, a yellow-green solution will absorb light in the purple range as shown in **Figure 4.9**.

[134] S B Brown, An introduction to spectroscopy for biochemists, *Academic Press*, 1980, pp150-170.

[135] Visible and Ultraviolet Spectroscopy, [Accessed 17-10-2013]. Available from: http://www2.chemistry.msu.edu/faculty/reusch/VirtTxtJml/Spectrpy/UV-Vis/spectrum.html.

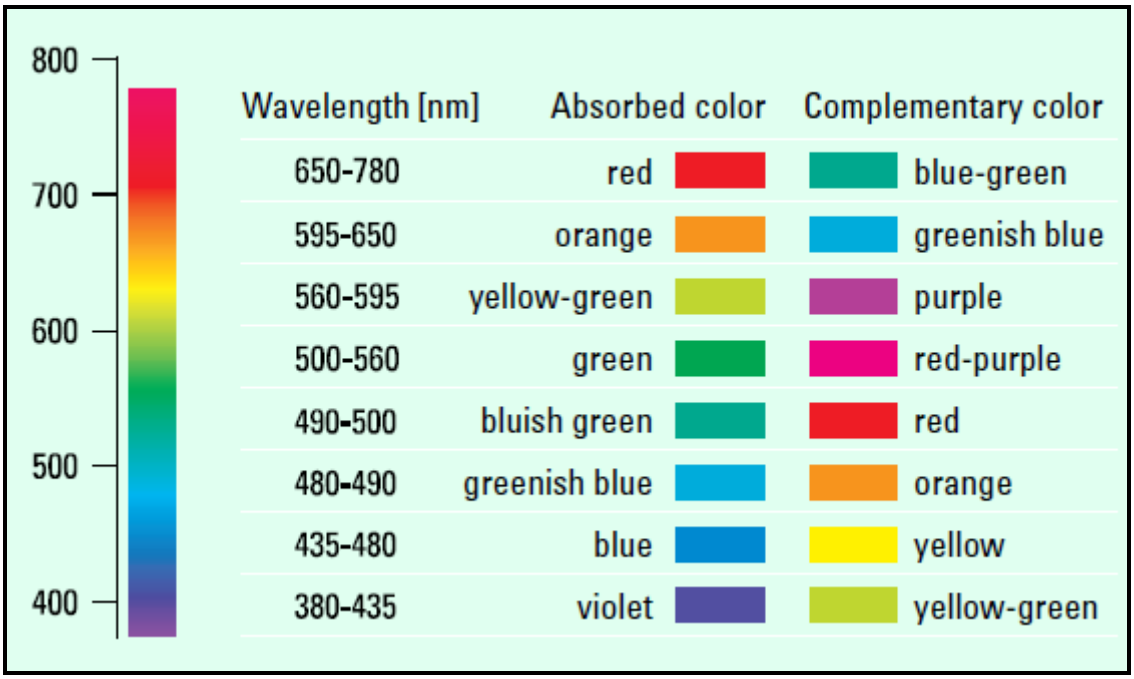

Figure 4.9: The visible spectrum, its colour absorbance and transmission distributions.[136]

The advantage of the UV/Vis technique is that it is simple, fast, versatile and cost effective. The disadvantage is that the samples should always be in solution and be a coloured solution. Another disadvantage of this analytical technique is that a mixture of materials makes it difficult to analyse and requires prior separation. Interference from the sample's matrix also makes the analysis of samples problematic.

4.3.2 INFRARED SPECTROSCOPIC METHOD

4.3.2.1 INTRODUCTION

Infrared spectroscopy is extremely useful to obtained qualitative (identity) information about chemical species. The IR region of the electromagnetic spectrum is lying to the lower energy side of the UV/Vis region (see **Figure 4.5**) and exists between 10 to 12500 cm^{-1} ($8x10^2$ to $1x10^6$ nm). The IR spectrum is further divided into three different regions, namely

[136] T Owen, Fundamentals of modern UV-visible spectroscopy, *Agilent Technologies*, 2000, pp2-28.

- Near-IR 12500 - 4000 cm^{-1} ($0.8x10^3$ - $2.5x10^3$ nm)
- Middle-IR 4000 - 200 cm^{-1} ($2.5x10^3$ - $50x10^3$ nm)
- Far-IR 200 - 10 cm^{-1} ($50x10^3$ - $1000x10^3$ nm)

But it is only the middle IR (200 - 4000 cm^{-1}) which is useful for chemical qualification. The energy (photons) associated with the middle IR region have energy in the region of 15 kcal/mol which is not high enough to induce electron transfer to higher orbitals (excitation), but only enough to cause vibration activation in covalently bonded molecules.

IR spectroscopy is widely used in industrial hygiene and air quality control. It is also exclusively used in forensic science in the analysis of polymers, fibres, paints and drugs. It is also used to analyze emission gases as well as to test for alcohol (breath analyzer) in potential DUI (DWI) suspects.

4.3.2.2 BASIC PRINCIPLES

Molecules need to have permanent dipole moments to be IR active. A change in dipole moment occurs after energy absorption. The change in dipole moment is accompanied by either bend stretch, bending or rocking and these bond vibrations create different absorption bands which are characteristic of the type of bonds present in the molecule. In this process a complicated spectrum with a large number of peaks is obtained which can be used for characterization (“finger printing”) or quantification purpose since the absorption peaks are much sharper than those obtained during UV/Vis spectroscopy.

Vibrations fall into two basic categories namely stretching (symmetric and asymmetric stretch) and bending vibrations (scissoring, rocking, wagging and twisting) as shown schematically in **Figure 4.10**. A stretching vibration involves a change in the bond angle between two bonds due to energy absorption. Bending vibrations, are due to the movement of hydrogens with respect to the carbons as a result of energy absorption. These movements can be in the same direction or in opposite directions due to energy absorption differences.

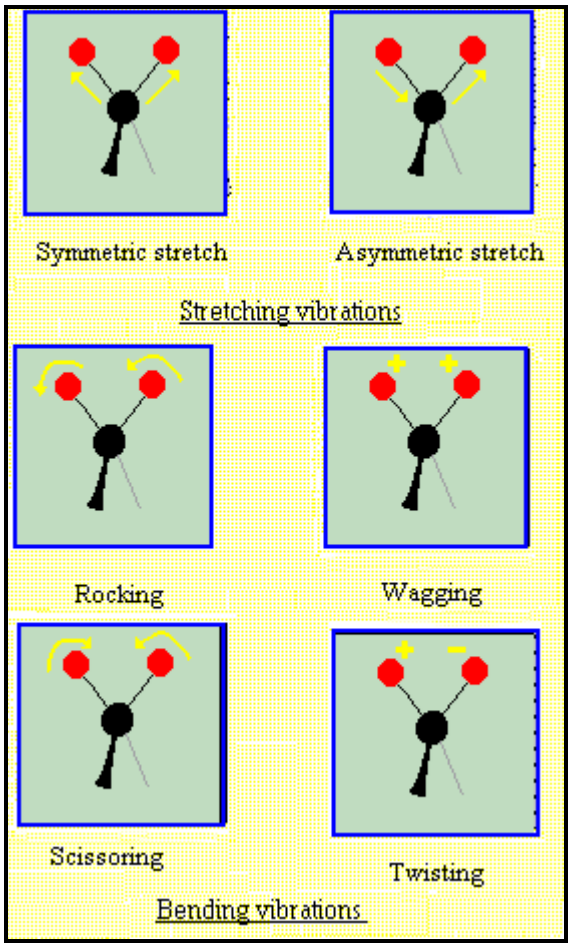

Figure 4.10: Types of molecular vibrations.[137]

Interpretation of IR spectra is relatively straightforward since the peaks obtained in the 1000 - 4000 cm^{-1} region is characteristic of the types of bonds present in the molecule as indicated in **Figure 4.11**. The assignment of the peaks gives both the type of bond and the type of vibration. For instance C=O stretching and C-H bending vibrations are at 1680 - 1750 and 2800 - 3200 cm^{-1} respectively.

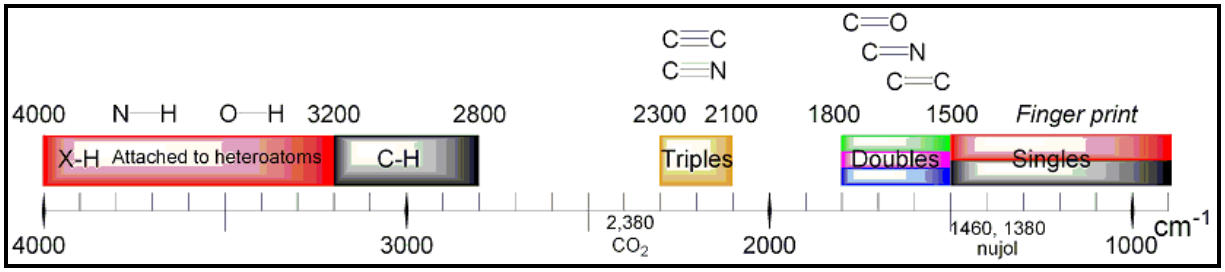

Figure 4.11: IR spectroscopy correlation table.[138]

[137] Infrared spectroscopy and modes of vibrations, [Accessed 17-10-2013]. Available from: http://wwwchem.uwimona.edu.jm:1104/spectra/unknowns/uif000.html.

The typical IR absorption is presented by wavenumber ($\bar{\nu}$), measured in reciprocal centimeter (cm^{-1}) or wavelength (λ) expressed in nanometer (nm) for covalent bonds. It mostly provides information about certain functional groups or the structure of a compound.

Disadvantages of IR spectroscopy include that the technique does not allow mixture of materials or water to be analysed. IR spectroscopy of aqueous solutions is characterized by the strong absorbance of H_2O in the mid-IR spectral region. An advantage of IR spectral is that it provide a “fingerprint” spectrum which is unique for the compound that is analysed. Another advantage of the IR technique is that it is normally non-destructive and requires a relatively small amount of sample.

4.3.3 C, H AND N QUANTIFICATION USING A CHNS-MICROANALYSER

4.3.3.1 INTRODUCTION

In the 1780s Antoine Laurent Lavoisier accurately determined the composition of organic compounds by elemental analysis. Lavoisier burned alcohol and other combustible organic compounds containing C, H and O in oxygen to form product such as H_2O and CO_2. He used an ice calorimeter to measure the quantity of CO_2 and heat given off during combustion as well as the melt of ice (H_2O) that was formed during the combustion process. Although the amount of the H_2O and CO_2 measured in this process were inaccurate, it opened the door to improvements in combustion techniques. In the 1800’s Berzelius and Liebig used the combustion train (the *Kaliapparat*) to absorb H_2O vapour and CO_2 from the combustion process with pre-weight $CaCl_2$ and KOH (Kali) to determine the sample composition. The C and H % content of the original substance could be calculated from the mass difference absorbed during the combustion process. Fritz Pregl refined the elemental analysis technique by the introduction of micro-chemical techniques (sample sizes in mg

[138] Infrared spectroscopy, [Accessed 10-9-2013]. Available from: http://en.wikipedia.org/wiki/Infrared_spectroscopy.

range) and succeeded in the accurate determination of C and H. He received the Nobel Prize in 1923 for the development of this process.[139]

During the next 40 years the use of the technique expanded from being used exclusively for organic compounds to nowadays where it is used in the synthetic chemical industries for compounds such as petrochemicals, fine chemicals and pharmaceuticals. The first automated elemental analysers were introduced to the market in the early 1960s and gained rapid acceptance in laboratories worldwide.[140] Automated elemental analysers such as the LECO TruSpec Micro CHNSO is used to determine the percentile carbon, hydrogen and nitrogen content in various samples such as in soil, waste or drinking water, minerals and chemical compounds. The percentile content also helps to determine the elemental composition of an unknown or known compound, as well as to verify the purity of a synthesized compound. These analyzers usually use very small quantities (2 to 3 mg) of the sample material. The gaseous combustion products are purified, separated into their various components (gas chromatography etc.) and analyzed with a suitable detector such as a thermal conductivity (TCD) or IR detector.

4.3.3.2 PRINCIPLES OF OPERATION

The most common form of elemental analysis, namely CHN analysis, is accomplished by a combustion process (**Figure 4.12**).

[139] U Kottenstette, D A Schneider and D A Loy, Absolute hydrogen determination in coal-derived heavy distillate samples, *Sandia national laboratories*, 2000, pp1-5.

[140] P E Hemming, C,H,N micro-analysis: a comparative review of the effects of instrument design on analytical performance, *Exeter Analytical (UK) Ltd*, pp1-14.

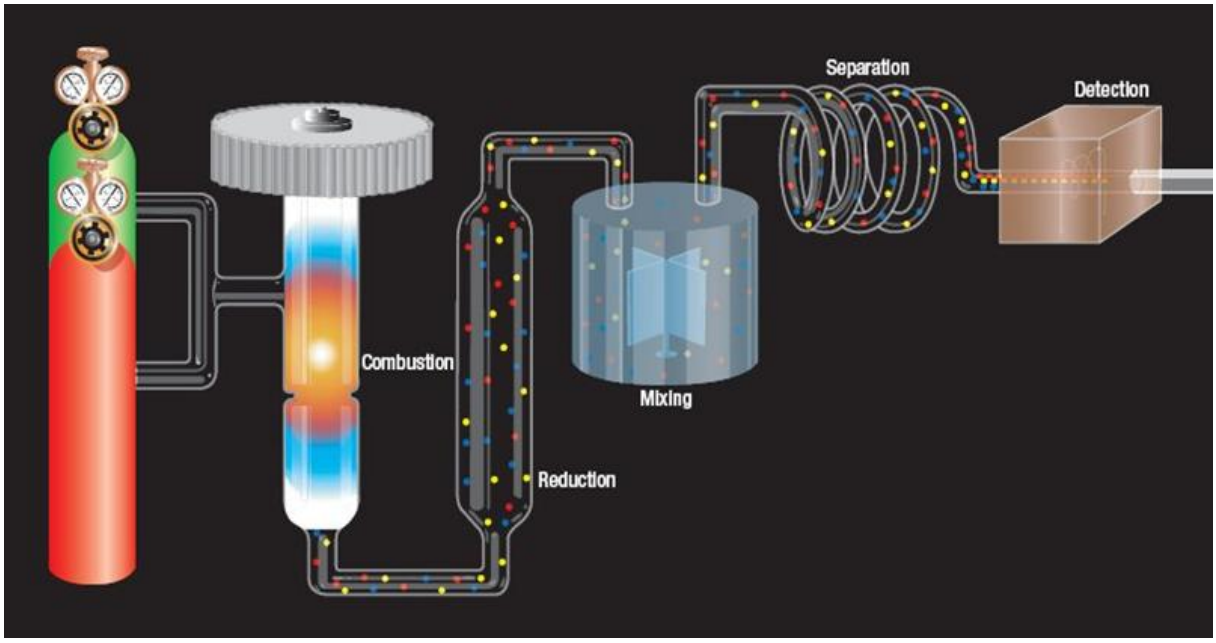

Figure 4.12: The basic set up for a CHN micro-analyser.[141]

This combustion process of organic or organometallic compounds in excess O_2 involve the conversion of C, H, N and S in the compound into gasses such as CO_2, H_2O, N_2 and N-oxides as indicated by the combustion reactions of sulfamethazine in **Equation 4.8** and (**Figure 4.12**).

$$C_{12}H_{14}N_4O_2S \xrightarrow[\Delta]{O_2} 6CO_2 + 7H_2O + 2N_2 + SO_2 \qquad 4.8$$

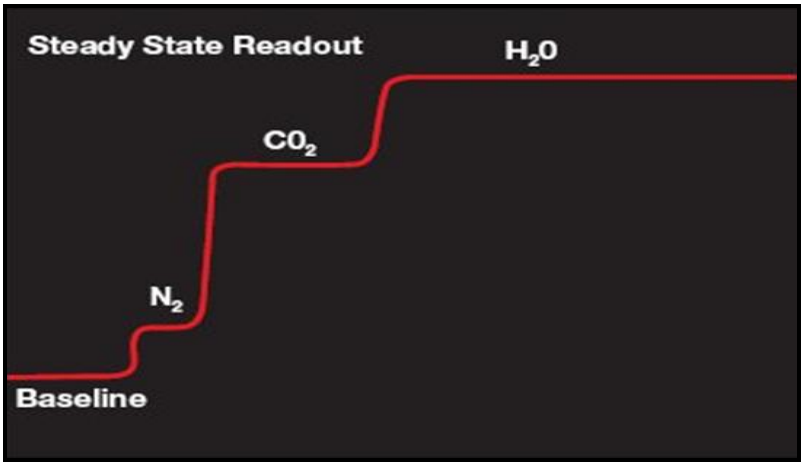

Figure 4.13: Stages in the formation of CO_2, H_2O, N_2 and N-oxides.[141]

[141] Instruments and techniques, [Accessed 03-02-2014], Available from: http://scs.illinois.edu/microanalysis/docs/440info.pdf.

In this technique, a precisely weighed sample in a tin capsule is introduced into a furnace at 950 °C. The sample is burned in the presence of oxygen using WO_3 as catalyst in the combustion tube. The tin capsule gives the benefit of a strong exothermic combustion reaction ensuring complete sample oxidation. These gasses are then transported by helium (carrier gas) through the reduction tube (containing copper granules kept at 650 °C) into the gas chromatographic column which is connected to a thermal conductivity detector (TCD). The hot Cu reduces the excess oxygen as well as nitrogen oxides to nitrogen. The chromatographic column then separates the gasses into CO_2, H_2O and N_2 fractions. The CO_2 and H_2O gasses are measured quantitatively by an IR absorption detection system, while the N_2 is determined via a TCD.[142] The gasses are then desorbed and are identified by a TCD, which provides an electrical signal related to the concentration of the gasses in the sample. Standards such as EDTA, acetanilide and cystine are used to calibrate the instrument and quantify the content of N, H and C.

Table 4.4: Advantages and disadvantages of the CHN micro-analyser.[143,144]

Advantages	Disadvantages
Operational modes CHN, CH, N and O elemental analyser	Accurately weighing small amount of sample (2-3 mg)
Simultaneous determination of C, H and N under identical conditions	Cover sample in capsule
Automated	
Less than 8 min analysis per sample	

[142] R A Nadkarni, Modern instrumental methods of elemental analysis of petroleum products and lubricants, *ASTM International*, 1991 Issue 1109, pp35-38.

[143] Elemental analysis and biological characterization, [Accessed 13-01-2014]. Available from: http://shodhganga.inflibnet.ac.in/bitstream/10603/10157/16/17_chapter%206.pdf.

[144] D Margraf, Argon as carrier gas in total C(N) elemental analysis of soils, *Elementar analysen systeme GmbH*, pp1-22.

4.4 QUANTIFICATION TECHNIQUES

The final step in the analytical process involves determining the concentration (amount) of specific elements in solution using a variety of spectrometric methods. Spectrometric methods for quantification are very popular as analytical techniques due to their i) capability to quantify all the elements in the sample matrix, ii) ability to withstand many types of interference and iii) their ability to quantify at low levels (lower detection limits). Numerous spectrometric methods for the quantification of the different elements include techniques such as AAS, ICP-OES or ICP-MS. In this study the main technique utilized for quantification of the different elements was ICP-OES, but AAS will also be discussed in detail in the next few sections.

4.4.1 ATOMIC ABSORPTION SPECTROSCOPY (AAS)

4.4.1.1 BACKGROUND OF AAS

In 1860 Guystav Kirchhoff and Robert Bunsen used atomic absorption spectroscopy (AAS) to determine sodium in flames and hot gases. The phenomenon was further explained by Kirchhoff by stating that the wavelength of the light emitted was the same as the wavelength absorbed when sodium salts were added to a flame. It was only in 1955 that atomic absorption spectroscopy as analytical technique was improved by A Walsh and C T J Alkemade.[145,146] In the early 1960s the first AAS was commercially introduced to the market. This instrument was highly in demand due to its advantages such as ease of use, flexibility, trace element analysis etc. (**Table 4.6**). Prior to ICP discovery, AAS was the most used technique for determining the concentration of a particular metal concentration in a sample. Today AAS can analyse over 62 different metals at very low concentrations in solution.

[145] F A Settle, Handbook of instrumental technique for analytical chemistry, *Prentice Hall*, 1997, pp239-506.

[146] A Walsh, *Analytical Chemistry*, 1991, 63, pp933A-941A.

4.4.1.2 INTRODUCTION

AAS is an analytical technique which utilizes the absorption of light to measure the concentration of the analyte at a specific wavelength. AAS quantifies the absorption of energy at ground state atoms in the gaseous state. The valence electrons in atoms absorb energy in the UV or visible range which allows them to make transitions to higher energy levels. The analyte concentration is determined from the amount of energy (h*v*) absorbed during the quantification process. Concentration measurements are usually determined from a working curve after calibrating the instrument with standards of known concentration. AAS is a very common technique for detecting metals and metalloids in biological, environmental, marine and geological samples.

4.4.1.3 INSTRUMENTATION

AAS main components include a radiation source (hollow-cathode lamp), atomization cell (flame or graphite furnace), monochromator and a detector (**Figure 4.14**). The atomic absorption technique uses the hollow cathode lamp (HCL) as its light source. The HCL usually contains a tungsten anode and a hollow cylindrical cathode which is sealed in a glass tube filled with an inert gas (Ne or Ar). The cathode is constructed of the pure metal of interest. When a potential difference (300 V) is applied across the electrodes, (anode and cathode) it causes ionization of gas particles at the anode. The ionized gas particles are accelerated in the direction of the cathode, then the ions strikes the cathode with sufficient kinetic energy to cause the metal ions be removed (sputtered) from the surface of the cathode. The sputtered metal atoms are further excited and the excited metal ions emit an intense characteristic spectrum (wavelengths) of the metal of interest, before they return to ground state. After a period of time, these atoms are diffused back to the surface of the cathode.

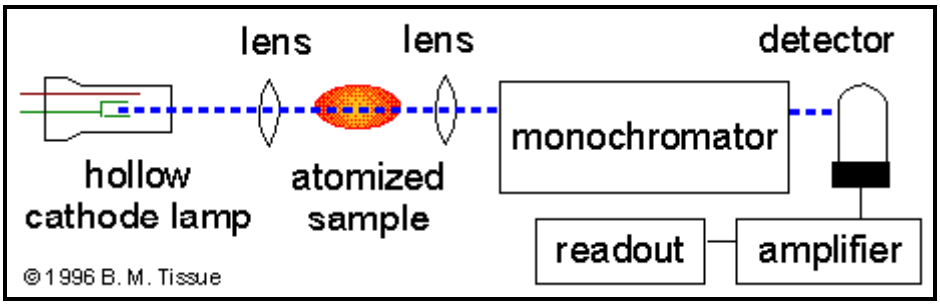

Figure 4.14: Schematic diagram of an AAS.[147]

Figure 4.15: Varian coded 37mm hollow cathode lamp for Nd analysis.[148]

The first step in the analytical process using AAS involves the introduction of the sample solution by nebulizer. The nebulization converts the solution into a fine aerosol spray which is then introduced into the atomization cell and chamber (flame or graphite furnace). Three different steps are involved in turning the solution into an atomic gas namely i) desolvation, ii) vaporization iii) volatilization. The aerosol is then mixed with a combination gas mixture (e.g. fuel and oxidant) where excitation takes

[147] Atomic-Absorption Spectroscopy (AA). [Accessed 13-01-2014]. Available from: http://www.files.chem.vt.edu/chem-ed/spec/atomic/aa.html.

[148] Varian coded 37mm hollow cathode lamp for neodymium analysis, [Accessed 03-10-2013]. Available from: http://www.labhut.com/varian-coded-37mm-hollow-cathode-lamp-for-neodymium-analysis.html.

place. Different fuel/oxidant combinations yield different flame temperatures as indicated in **Table 4.5**.

Table 4.5: Properties of AAS flames.

Fuel	Oxidant	Temperature (°C)
Acetylene	Air	2100-2500
Acetylene	Nitrous oxide	2600-2800

The metal ions in a solution are then converted to their atomic state by the flame. An alternative vaporization method is used by graphite furnace activation. In this technique a graphite coated tube is heated which vaporize and atomize the analyte. The monochromotor isolates a specific wavelengths of light from other wavelengths that was emitted from HCL (**Figure 4.15**). The resultant intensity of the emitted wavelength is measured by the detection system and indicated as a read-out in concentration units.

Table 4.6: The advantages and disadvantages of AAS.[149]

Techniques	Advantages	Disadvantages
FAAS	Robust technique	Manually operated due to toxic and flammable gases used
	Easy to use	Precision is 0.1 - 1 %
	Analysis take few second per sample	Refractory elements requiring hotter flame causes high LODs
GFAAS	LOD is 10 to 100 times lower than FAAS	Takes 2 minutes per sample to analysis
	Automatically operated	Require more operating skills and maintaince
		Precision is 1 - 5 % in homogenous solutions
		Single-element analysis
		Wet analysis only

4.4.2 INDUCTIVELY COUPLED PLASMA OPTICAL EMISSION SPECTROMETRY (ICP-OES)

4.4.2.1 INTRODUCTION

The first plasma-based spectrometers were developed by Greenfield *et al* in the mid-1960's more or less the same time as the introduction of FAAS and FAES.[150,151] This

[149] F Settle, Handbook of instrumental techniques for analytical chemistry, *National Science Foundation, Arlington, Virginia, Prentice Hall PTR (ECS Professional),* 1997, pp373-389.

[150] F Dunnivant and J Ginsbach, Flame atomic absorbance and emission spectroscopy and inductively coupled spectrometry - mass spectrometry, *Whitman College*, 2009, pp75-80.

[151] G Gauglitz and T Vo-Dinh, Handbook of spectroscopy. *WILEY-VCH, Verlag GmbH & Co. KGaA*, 2003, pp473-494.

first generation of the plasma-based instrument used microwave-induced (MI) and direct current (DC) to produce the plasma.[152] These instruments never gain much popularity due to the plasma instability and interference effects, therefore the sales of analytical equipment were dominated by the flame-based instrument.

The limitations of these first generation plasma source spectrometers were later overcome by the introduction of inductively coupled plasma (ICP) equipment. The ICP based equipment gained popularity in the 1980's due to advantages such as labour and time saving considerations as well as lower cost and increased accuracy during analyses.[152] ICP-OES and ICP-MS are currently the most important analytical tools which are being used in a wide range of scientific disciplines. These techniques permit multi-element determination with high levels of accuracy and precision for most elements. It also provide low detection limits, rapid analysis, reduced interferences with lower matrix background and large dynamic ranges compared to other instrumental analytical methods. ICP-OES uses a plasma with temperature between 6000 to 10000 K, allowing the complete atomization of the elements and minimizing potential chemical interferences in a sample. This method can be used to analyse over 70 elements simultaneously and its measurements rely on the characteristic emission of light at specific wavelengths from excited atoms and/or ions which are unique for each element. Concentrations from parts per billion (ppb) to weight % can be determined without dilution or pre-concentration.

4.4.2.2 ICP-OES INSTRUMENTATION

The main components of an ICP-spectrograph include a nebulizer, a spray chamber, a plasma torch and a detector. The plasma torch and its design is one of the most important aspects of ICP technology (**Figure 4.16**). This torch consists of three concentric quartz tubes, an outer, intermediate, and inner tube. Argon gas enters the intermediate and outer tubes through tangentially arranged entry points. The outer tube carries the argon at a flow rate of 10 - 15 $Lmin^{-1}$ which sustains the high temperature plasma, as well as preventing the torch quartz walls from melting. The intermediate argon flow (0 - 15 $Lmin^{-1}$) is optional and its function is to lift the plasma

[152] D A Skoog, F J Holler and S R Crouch, Principles of instrumental analysis, *Thomson Brooks/Cole*, 2007, pp254-276.

slightly as well as diluting the inner flow when organic solvents are present. The inner tube carries the sample into the center of the plasma at a flow rate of 0.5 - 1.5 L min^{-1} and helps to sustain the shape of the plasma.

The nebulizer introduces the sample (solid, liquid or gas) into the central channel of the ICP. The nebulizer converts the sample into an aerosol or vapour which is transported into the plasma while large droplets are removed as waste (**Figure 4.17**).[153]

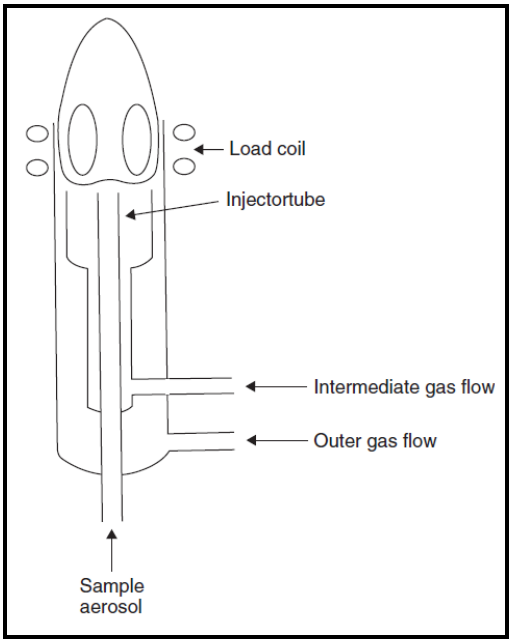

Figure 4.16: Schematic presentation of the ICP torch.[154]

The open end of an outer tube is surrounded by a water cooling induction coil connected to the radio-frequency (RF) generator. RF power passes through the copper coil which results in the formation of alternating current which moves back and forth inside the coil at a rate corresponding to the frequency of the RF generator. This oscillating current in the coil causes electric and magnetic fields (RF) whose lines of force are axially orientated inside the plasma torch and follow elliptical paths outside the induction coil. The plasma is initiated by argon gas flowing through the

[153] L Ebdon, E H Evans, A S Fisher and S J Hill, An introduction to analytical atomic spectrometry, *John Wiley & Sons, Inc.,* 1998, pp83-108.

[154] J R Dean, Atomic absorption and plasma spectroscopy, ACOL series, *John Wiley & Sons, Limited*, *Chichester, UK*, 1997. 2nd Edition, pp258-299.

plasma torch. A spark from a Tesla coil is used to initiate the reaction to produce electrons and ions in the argon gas inside the load coil region.

$$Ar \xrightarrow{spark} Ar^{+} + e^{-} \qquad 4.9$$

These ions and electrons are accelerated by the RF field, causing further ionization to produce the plasma with temperatures of 6000 - 10000 K.

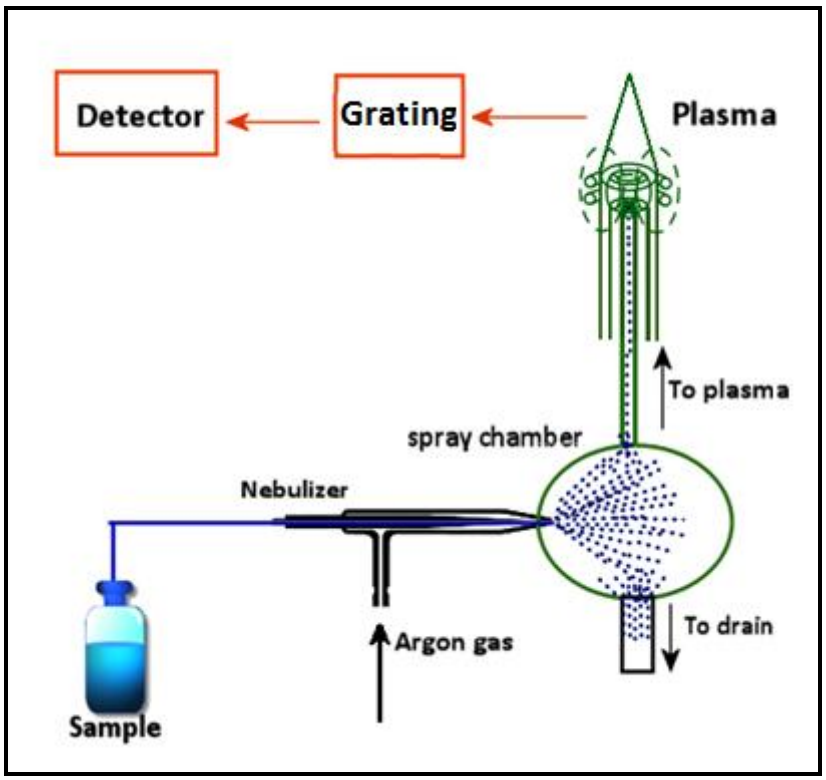

Figure 4.17: Schematic presentation of sample introduction into the ICP-OES.[155]

In the quantification step, the excited atoms and ions leave the hot portion of the plasma. The excited valence electrons relax (cascade back to ground state) and emit their characteristic radiation (photons) which is collected by a grating monochromator that arrange the radiation by obtained wavelengths. The radiation is measured by an array detector (photomultiplier) and converted into electronic signals that can be used to calculate the concentration of that particular element in the sample by comparing it with calibration standards.[145]

[155] Inductively coupled plasma optical emission spectrometry (ICP-OES), [Accessed 03-10-2013]. Available from: http://www.chemiasoft.com/chemd/node/52.

Table 4.7: Advantages and disadvantages of ICP-OES.[149]

Advantages	Disadvantages
Simultaneous multi-element analysis	Wet analyses only
Few chemical interferences	Expensive
Robust interface	Spectral interferences due to the line rich spectra of most elements
Low detection limits (1 - 10 ppb range),	Volatile organic solves may burn the plasma
Good precision (RSD 0.5 - 2 %)	Does not quantify the halogens, gaseous elements and carbon
Easy and rapid qualitative analysis	
Wide linear dynamic range (10^5 - 10^6 orders of magnitude)	
High sensitivity	

The detection limits achievable by FAA, GFAA, ICP-OES and ICP-MS for different elements are vital in different elements. Typical detection-limit ranges for these major atomic spectroscopy techniques are given in **Figure 4.18**. In general, the detection limits decrease from FAAS (in the sub-ppm range) followed by ICP-OES (of the order of 1 - 10 ppb) then GFAAS, (usually in the sub-ppb range) and finally ICP-MS produces the best detection limits (typically 1 - 10 ppt (parts per trillion)).

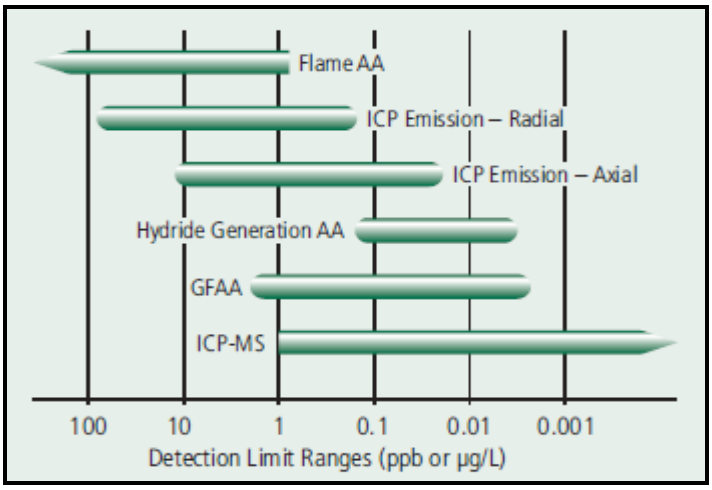

Figure 4.18: The detection limit ranges for the atomic spectroscopy techniques.[156]

4.5 METHOD VALIDATION

The final step in the whole analytical process involves the validation or quality assessment process. The results obtained in an analytical lab can be affected by several factors such as instrument sensitivity and stability of solution. To ensure reproducible analytical results and good accuracy it is essential that the proposed procedure is validated for its intended application. Typical method validation should consider the following parameters: accuracy, linearity, precision, range, robustness, selectivity, specificity, limit of detection (LOD) and quantification (LOQ) (**Figure 4.19**).[157] The different parameters will be discussed in the following section.

[156] World leader in AA, ICP-OES and ICP-MS, [Accessed 24-10-2013]. Available from: http://www.perkinelmer.com/CMSResources/Images/4474482bro_WorldLeaderAAICPMSICPMS.pdf.

[157] C C Chang, H Lam, Y C Lee and X Zhang, Analytical method validation and instrument performance verification, *A John Wiley & Sons, Inc., publication*, 2004, pp27-51.

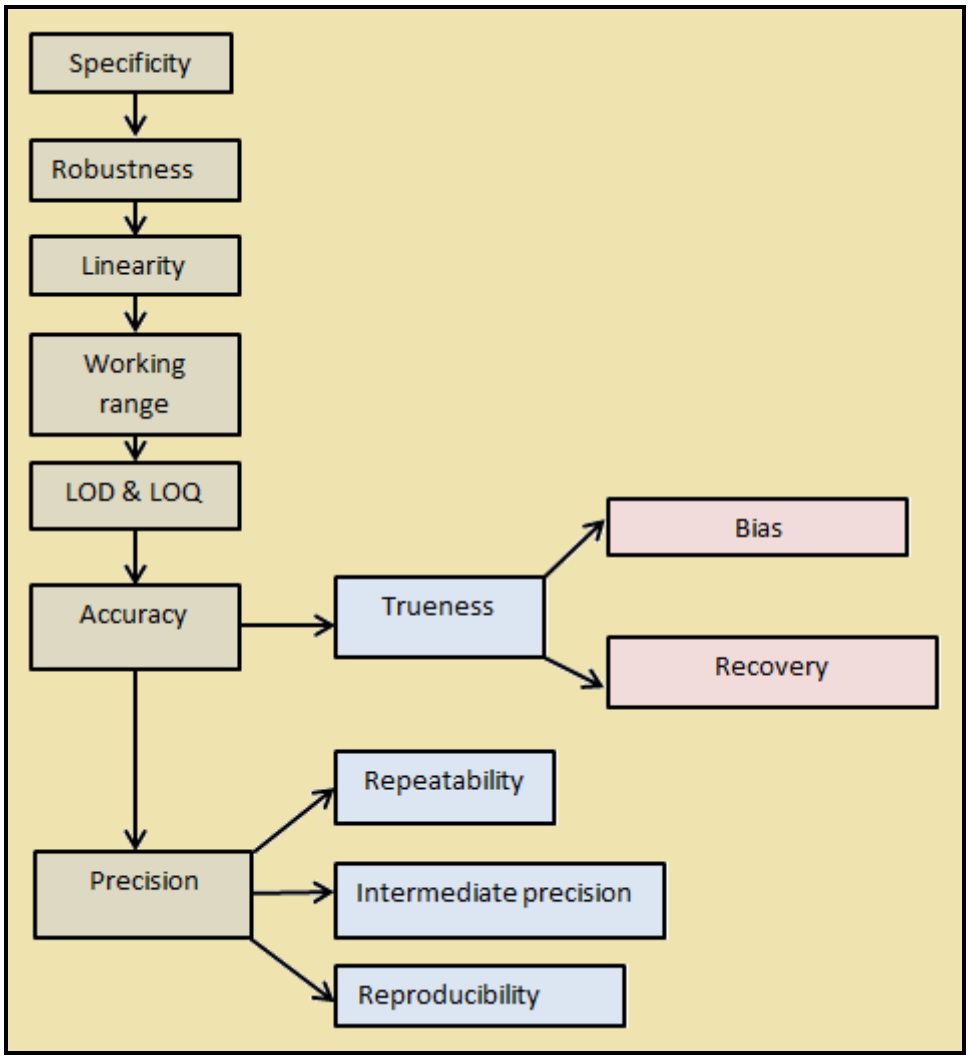

Figure 4.19: Steps in method validation.[158]

4.5.1 ACCURACY

Accuracy describes the closeness of the mean of the test results produced by the method to the true value or the concentration of the analyte.[159,160] The result (average) of replicate analyses of samples compared to the known concentrations (CRM) of the analyte, is expressed as the percentage recovery. Even the spiked placebo recovery and standard addition methods can be used to determine the

[158] S Bratinova, B Raffael, and C Simoneau, Guidelines for performance criteria and validation procedures of analytical methods used in controls of food, *European Commission Joint Research Centre Institute for Health and Consumer Protection contact materials*, 2009, pp1-74.

[159] D A Skoog, D M West, F J Holler and S R Crouch, Fundamentals of analytical chemistry, *Thomson learning,* 8th edition, pp90-146.

[160] D Reaggec 1.0 A guide to method validation*, Diagnostics Ltd*., 2003, pp1-16.

accuracy by comparing the obtained results with the expected results. The *t*-test is one of the most important tools or parameters to decide if there is any statistical difference between the expected and experimentally obtained results, e.g. the accuracy of the analysis. Two totally opposite hypothesis are assumed in the *t*-test, namely, the null hypothesis (H_0) which state that there is no statistical difference between the results while the alternative hypothesis (H_1) assumes that there is a statistical difference between results at a certain probability or confidence level. A new *t*-test value is calculated (**see Equation 4.10**)[159] and compared with the theoretical value (tabulated) and then one of the assumptions is accepted. Values between the two confidence levels are regarded as accurate ($-t_{crit} < t < t_{crit}$) while values outside of these values, $-t_{crit} < t$ and $t < t_{crit}$ are regarded as not accurate.

$$t = \frac{\mu - \bar{x}}{s/\sqrt{N}} \qquad 4.10$$

t = The *t*-statistic value

μ = The true mean

N = The number of replicate measurements

$\bar{x}$ = Mean or average

Another way to get an indication of the accuracy is to find the absolute or relative error of the obtained results compared to that of the theoretical or expected value.

Absolute error (E)

E is expressed as the difference between the true value and the mean (or average) as indicated in **Equation 4.11**[159].

$$E = \bar{x} - x_t \qquad 4.11$$

$\bar{x}$ = Mean or average

x_t = True or accepted value

Relative error (E_r)

The relative error, E_r is expressed as a percentage or parts per thousand (ppt) of the difference of the true value and the experimentally obtained value. The percent and ppt E_r is given by **Equation 4.12**[159] and **Equation 4.13**[159] respectively.

$$E_r = \frac{\bar{x} \quad x_t}{x_i} \times 100\% \qquad 4.12$$

x_i = The i-th measurement

or

$$E_r = \frac{\bar{x} - x_t}{x_i} \times 1000\,\text{ppt} \qquad 4.13$$

A minimum of at least three concentrations and three replicated determinations for each concentration is normally considered as good practice to determine the accuracy of an analysis covering a specified range. Acceptable criteria:

- Within the linearity range (working range)
- Recovery must be within 98 to 102 %
- Precision must be < 2 %

4.5.2 PRECISION

Precision is the closeness (grouping) of agreement among a series of measurements obtained from multiple aliquots of the same homogeneous sample under specified conditions.[161] Standard deviation is the parameter which gives an indication of the precision of a set of the replicates and can be expressed as SD or RSD (relative standard deviation). The coefficient of variance (CV) is also a parameter which can be used to express precision. The SD, RSD and CV can be calculated by **Equation 4.14**[159], **Equation 4.15**[159] and **Equation 4.16**[159] respectively.

[161] Analytical method validation, [Accessed 02-01-2014]. Available from: www.intechopen.com.

Standard deviation

$$S = \sqrt{\frac{\sum_{i=1}^{N}(x_i - \bar{x})^2}{N-1}} \qquad 4.14$$

N = The number of measurements

$\bar{x}$ = The arithmetic mean

Relative standard deviation

$$RSD = \frac{S}{\bar{x}} \times 1000 \text{ ppt} \qquad 4.15$$

Coefficient of deviation

$$CV = \frac{S}{\bar{x}} \times 100\% \qquad 4.16$$

Precision depend on concentration and should be determined within the working range at different concentrations.

4.5.1 SELECTIVITY AND SPECIFICITY

Selectivity and specificity are parameters that measure the reliability of measurements in the presence of interferences. Selectivity involves an experimental procedure to differentiate and measure the analyte in a complex mixture (matrix) with the possibility of interference from other components in a sample. The intercept of the calibration curve may also be used to get an idea of the selectivity of an analytical process. Specificity involves the recovery of specific compound in the presence of other compounds that are expected to be present in the sample.

4.5.2 LINEARITY AND RANGE

Linearity is the procedure to obtain results within a given range that are directly proportional to the analyte concentration in samples. Linearity is normally demonstrated by the dilution of a standard solution to at least 5 different concentrations. Linearity is assessed by the linear regression coefficient (r) which is obtained from a plot of the signals as a function of the concentration of analyte. The data from the standard calibration curve (**Equation 4.17**)[162] is used to determine a regression coefficient, slope (m) and intercept (c). The slope of this calibration curve is also known as the sensitivity of the analysis.

Linear calibration curve

$$y = mx + c \qquad 4.17$$

y = Detector response
m = Slope
x = Concentration of the analyte
c = Intercept on the y-axis

The linearity regression coefficient can be calculated using **Equation 4.18**[163]

$$r^2 = \frac{(n(\sum xy) - (\sum x \sum y))^2}{(n(\sum x^2) - (\sum x)^2)(n(\sum y^2) - (\sum y)^2} \qquad 4.18$$

The r^2 values should be larger than 0.997 to be considered as acceptable linear. Acceptable and not acceptable linearity is shown in **Figure 4.20**.

[162] Linear equation, [Accessed 02-04-2014]. Available from: http://en.wikipedia.org/wiki/Linear_equation.

[163] Correlation coefficient, [Accessed 03-04-2014]. Available from: http://math.tutorvista.com/statistics/correlation-coefficient.html.

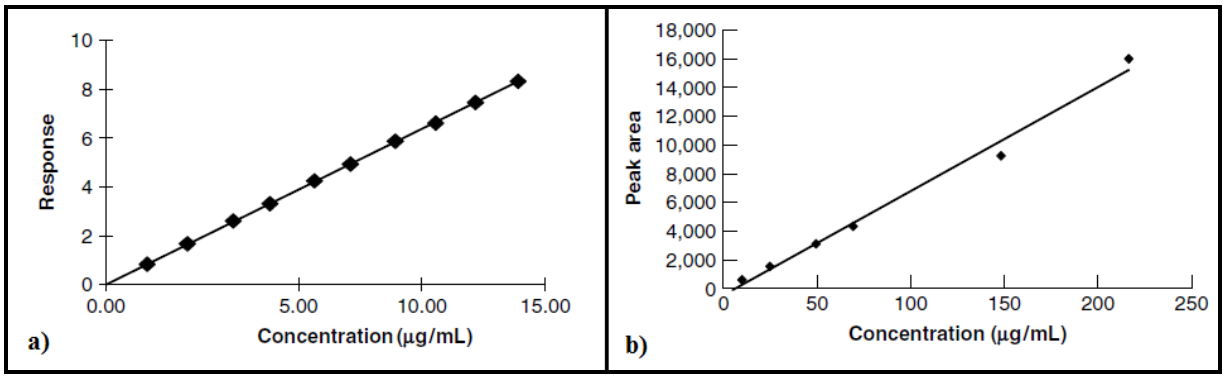

Figure 4.20:a) linearity with correlation coefficient $\geq$0.997 b) linearity with correlation coefficient $\leq$0.997.[157]

The working range of a calibration curve is normally the range between the upper and lower concentration of analyte in the sample which produce suitable precision, accuracy, and linearity.[164]

4.5.3 ROBUSTNESS

The robustness of an experimental procedure is determined by the influence of small but deliberate differences in method under standard laboratory conditions on accuracy and precision of the required compound. Variations such as filter effect, stability of the analytical solutions, pH, temperature, columns and extractions times are normally investigated as part of the study.[165]

4.5.4 LIMIT OF DETECTION (LOD) AND OF QUANTIFICATION (LOQ)[166]

Limit of detection (LOD) is the lowest analyte concentration that can be detected with certainty, but not necessarily be quantitated as an exact value. Limit of quantification (LOQ) is the lowest quantity that can be determined with great accuracy, employing the stated experimental conditions. Detection limits differ widely for several analytical

[164] Guidelines for the validation of analytical methods for active constituent, agricultural and veterinary chemical products, [Accessed 03-04-2014]. Available from: http://www.apvma.gov.au.

[165] O Mcpolin, Validation of analytical methods for pharmaceutical analysis, *Mourne training service*, 2009, p55.

[166] Guidance for industry q2b validation of analytical procedures: methodology, [Accessed 24-10-2013]. Available from: http://www.fda.gov/cder/guidance/index.htm.

methods, and from one element or compound to another. The signal-to-noise or standard deviation approaches can be used to determine both LOD and LOQ.

4.5.4.1 SIGNAL-TO-NOISE APPROACH

In this approach the LOQ corresponds to the analyte concentration in the sample that will give a signal-to-noise (S/N) ratio of 10:1 while the LOD corresponds to a 3:1 ratio.

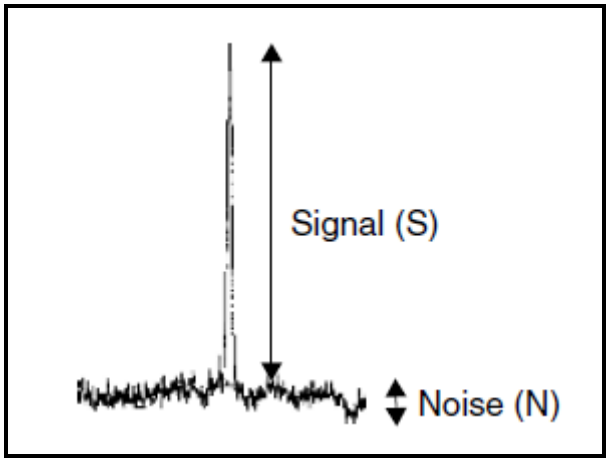

Figure 4.21: Chromatogram of candesartan in the lower LOD sample.[157]

Two different factors in the process, namely detection, sensitivity and sample preparation accuracy can affect both the LOD and LOQ at low concentrations. In this process a solution is prepared according to a certain method (procedure) and analyzed repeatedly to determine the S/N ratio. From the analyses the average S/N ratio is used to calculate LOD or LOQ as indicated in **Equation 4.19**[157] and **Equation 4.20**[157]:

$$LOQ = \frac{x}{S/N} \times 10 \qquad 4.19$$

$$LOD = \frac{x}{S/N} \times 3.3 \qquad 4.20$$

x = The concentration of an analyte

%S/N = Average at each concentration

The constant k is a factor of the confidence level, where k = 3.29 (3.3) which corresponds to a confidence interval of 99.9 %.

4.5.4.2 STANDARD DEVIATION APPROACH

In the standard deviation approach the LOD and LOQ can be determined by the recording of the standard deviation of the response, based on the slope of the calibration curve at low concentration as indicated by the following equations:

$$LOD = \frac{s}{m} \times 3.3 \qquad 4.21$$

$$LOQ = \frac{s}{m} \times 10 \qquad 4.22$$

or

$$LOQ = LOD \times 10 \qquad 4.23$$

s = Standard deviation of the response at low concentration
m = Slope of the linearity curve (sensitivity)

where s is equal to the average of at least 10 blank solutions. The slope obtained as indicated in **Equation 4.19**[157] and **Equation 4.20**[157] is also known as the instrument sensitivity for the specific analyte. The LOD and LOQ are therefore functions of instrument sensitivity and when these values are defined this way, it is not a universal property of the method, but a function of the instrument or from analyte to analyte.

4.6 CONCLUSION

It is clear from this discussion that numerous analytical methods for the dissolution and identification of inorganic chemical compounds exists. In this study, dissolution of the different REE was attempted using microwave and acid dissolution and identification was established using IR and UV/Vis spectroscopy. ICP-OES, with all its advantages were used for the quantification of all three REE in the different types of samples.

5 METHOD DEVELOPMENT AND VALIDATION FOR EARLY REE QUANTIFICATION

5.1 INTRODUCTION

A pre-requisite for the accurate quantification of REE in refractory minerals and especially at trace levels of REE, is the complete dissolution of these minerals. The quantification of the REE is further complicated by the presence of a number of these REE present in the mineral which have similar chemical and physical properties which may cause severe spectral and non-spectral interferences during the quantification process. Numerous separation processes, which include cation exchange, solvent extraction or chelating resin separation have been employed to isolate the REE's from the matrix to allow for accurate quantification.

This study involves an in-depth experimental study of the accurate quantification of the REE using ICP-OES. The study involves the development of an analytical procedure that can accurately determine and quantify the early REE (lanthanum, cerium and neodymium) in pure REE metal, in inorganic compounds and organometallic complexes as well as mixtures containing all three elements. The presence of up to 30 % of Th available in monazite mineral samples necessitated the preparation of a synthetic mixture that was used in this study. The study involved the employment of different acid mediums such as sulphuric acid, nitric acid and hydrochloric acid as well as to determine the influence of the different acids on the lanthanum, cerium and neodymium recoveries. Different analytical techniques, such as inductively coupled plasma optical emission spectrometry (ICP-OES), CHNS-micro analyser and infrared spectroscopy (IR) were used to characterise and quantify the REE in the different samples. The validation parameters such as accuracy, precision, linearity, sensitivity, etc., as discussed in **Chapter 4** were also evaluated to

determine the suitability of the developed methods for the digestion and analysis of REE.

5.2 GENERAL EXPERIMENTAL METHODS

5.2.1 **GENERAL EQUIPMENT**

5.2.1.1 SHIMADZU ICPS-7510 ICP-OES

A computer controlled Shimadzu ICPS-7510 ICP-OES sequential plasma spectrometer (**Figure 5.1**) was used for the qualitative and quantitative analysis of lanthanum, cerium and neodymium in aqueous solutions. The standard operating conditions of the ICP-OES during this study are reported in **Table 5.1**.

Figure 5.1: Shimadzu ICPS-7510 radial-sequential plasma spectrometer.

Table 5.1: ICP-OES operating conditions.

Parameter	Condition
RF power	1.2 kW
Coolant gas flow	14.0 L/min
Plasma gas flow	1.2 L/min
Carrier gas flow	0.7 L/min
Sample uptake method	Peristaltic pump
Spray chamber	Glass cyclonic
Type of nebuliser	Concentric

5.2.1.2 MICROWAVE DIGESTION

An Anton Paar Perkin-Elmer Multiwave 3000 microwave digester (**Figure 5.2 a**) equipped with an 8SXF 100 rotor and eight polytetrafluoroethylene (PTFE) reaction vessels (**Figure 5.2 b**) were used for the acid dissolution of the pure cerium metal samples as well as the TPPO complexes. An internal program for the digestion of the platinum group metals (PGM XF100-8) was selected with conditions as set in **Table 5.2**.

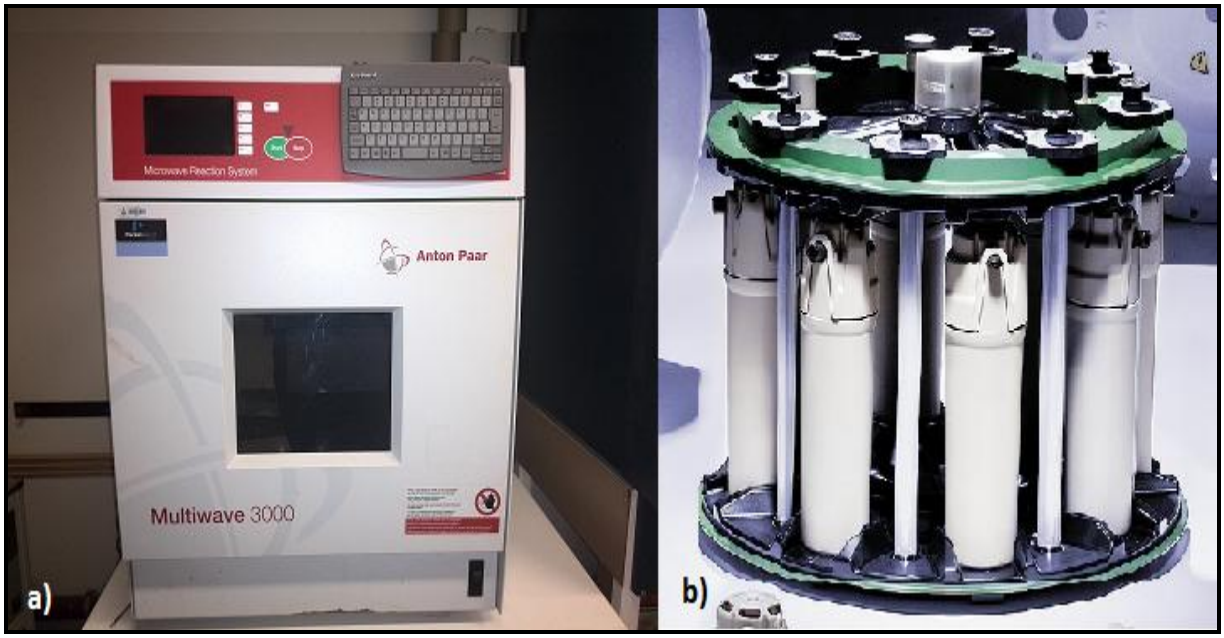

Figure 5.2: a) Anton Paar Perkin-Elmer Multiwave 3000 microwave systems and b) an 8SXF 100 rotor and 8 PTFE reaction vessels.

Table 5.2: Microwave digestion conditions.

Parameter	Condition
Power	600 Watts
Ramp	15 min
Hold	45 min
Pressure rate	0.5 bar/sec
Infra-red (IR)	240 °C
Pressure	60 bar
Weight	0.5 g
Volume of the acid	8.00 mL
Reagents	98 % H_2SO_4, 65 % HNO_3, 32 % HCl

5.2.1.3 WEIGHING

All the samples were accurately weighed to 0.1 mg at 20 °C ± 2°C using a Shimadzu AW320 electronic balance (**Figure 5.3**) certified under ISO 9001. All experimental samples and reagents used in the study were weighed by adding a sample in a pre-weight poly top glass vial.

Figure 5.3: Analytical Balances - AW Series.

5.2.1.4 BENCH-TOP MAGNETIC STIRRER EQUIPMENT

A Heidolph MR Hei-Tec magnetic stirrer/hotplate (**Figure 5.4**) obtained from Labotec was used to assist with the open vessel (beaker) digestion of the pure REE metals and the inorganic compounds and was also used during the synthesis of the organometallic complexes (25 ºC and 170 ºC).

Figure 5.4: HEIDOLPH Magnetic Stirrer with Heating.

5.2.1.5 PREPARATION OF ULTRA-PURE WATER

Ultra-pure water was prepared in the laboratory with an ultra-reverse osmosis system (**Figure 5.5 a**) bought from AJD Traders. The conductivity of tap, pure and ultra-pure water using a Hanna DIST 3 (HI98304S) conductivity meter was measured as 0.24, 0.05 and 0.00 mS/cm respectively.

Figure 5.5: **a)** Ultra reverse osmosis system **b)** ultra-pure water storage tanks.

5.2.1.6 MICRO-PIPETTES

Brand Transferpettes type (1000 µL and 10 mL) micro-pipettes with an accuracy of ±0.01 mL bought from Lasec, were used to accurately transfer solutions into Blau brand volumetric flasks.

5.2.1.7 GLASSWARE

The Schott Duran type (50, 100 and 250 mL) beakers and round bottom flasks were used for the sample digestion and synthesis respectively. The Blau brand grade (A) glass type (100 mL) Blau brand volumetric flasks were used for sample dilutions. The average of three replicate analyses for the results in this study are reported as elemental content with the standard deviations (s) to indicate the uncertainty in the last digit of the value.

5.2.2 **MATERIALS AND REAGENTS**

All chemicals and reagents were obtained commercially and used as received without further purification. These chemicals and reagents, along with their purity and commercial supplier are listed in **Table 5.3**.

Table 5.3: Chemicals and reagents used.

Chemical	Formula	Purity	Supplier
Reagents			
Lanthanum nitrate	$La(NO_3)_3{\cdot}6H_2O$	99.9 %	Sigma-Aldrich
Neodymium nitrate	$Nd(NO_3)_3{\cdot}6H_2O$	$\geq$ 99.99 %	Sigma-Aldrich
Cerium nitrate	$Ce(NO_3)_3{\cdot}6H_2O$	99.9 %	Sigma-Aldrich
Lanthanum metal piece	La	99.9 %	Sigma-Aldrich
Neodymium powder metal	Nd	$\geq$ 99 %	Sigma-Aldrich
Cerium powder metal	Ce	99.9 %	Sigma-Aldrich
Acids			
Nitric acid (TG)	HNO_3	55 %	Merck
Nitric acid (AR)	HNO_3	65 %	Merck
Sulphuric acid (AR)	H_2SO_4	98 %	Sigma-Aldrich
Hydrochloric acid (AR)	HCl	32 %	Merck

TG - Technical grade, AR - Analytical reagent grade

5.2.2.1 ICP STANDARDS

The ICP-OES multi standard containing Ce, Eu La, Pr and Sm in HNO_3 (7 % v/v 1000.000 µg/mL) and an ICP-OES Nd standard solution in HNO_3 (7 % v/v, 1000.000 µg/mL) were purchased from Inorganic Ventures Inc.

5.2.2.2 CLEANING OF APPARATUS

All glassware were soaked in 55 % HNO_3 acid for 24 hours and then rinsed with ultra-pure water and dried in a dust-free environment prior to use.

5.2.3 **PREPARATION OF ICP-OES CALIBRATION SOLUTIONS AND MEASUREMENTS**

5.2.3.1 PREPARATION OF CALIBRATION CURVES

All standards were prepared by the appropriate dilution of the 1000 ppm ICP-OES standard solutions of Nd in 7 % HNO_3. The multi-REE (Ce, Eu La, Pr and Sm) were also prepared in 7 % HNO_3. Appropriate volumes (0.0, 0.1, 0.2, 0.3, 0.5 and 1 mL) of the ICP-OES standard solutions and 10 mL of 98 % H_2SO_4, 65 % HNO_3 or 32 % HCI were transferred to different 100.0 mL volumetric flasks using the "Transferpette" micro-pipette. The volumetric flasks were filled to the mark with ultra-pure water to yield 0.0, 1.0, 2.0, 3.0, 5.0, and 10.0 ppm standards or calibration standards. A blank solution was prepared by adding 10.0 mL of the appropriate acid and ultra-pure water to the calibration mark of a 100.0 mL volumetric flask and was used for background corrections. The solutions were thoroughly mixed to obtain homogenized solutions and were allowed to stand for 24 hours before being used. Quantitative analyses were performed at 333.749 nm for La, 413.765 nm for Ce and at 401.225 nm for Nd. These are the most sensitive wavelengths in the analysis of lanthanum, cerium and neodymium.[167,168] The ICP-OES conditions indicated in **Table 5.1** were maintained throughout the study.

[167] N Velitchkova, S Velichkov, N Daskalova, *Spectrochimica Acta Part B,* 2007, 62, pp386-402.

[168] S G Johnson, J J Giglio, P S Goodall and D G Cummings, Applications of' high resolution icp-aes in the nuclear industry, *SPIE's Optoelectronics and High-Power Lasers & Applications*, 1998 pp1-13.

5.2.3.2 LOD AND LOQ

The correlation coefficient (r^2), slope (m), detector response (y-value) and concentration of the analyte (x-value) of the calibration curve were collected and calculated for each analyte. The LOD and LOQ for the three different REE in three different acids were calculated using **Equation 4.14**, **Equation 4.21** and **Equation 4.22** (**Chapter 4**) using the respective calibration curve and the standard deviation of the blank measurement for all the different acids and are reported in **Table 5.4**.

Table 5.4: Calculated LOD and LOQs for La, Ce and Nd.

H_2SO_4 (98 %)				
Element	**Standard deviation**	**Slope**	**LOD (ppm)**	**LOQ (ppm)**
La	0.0018	1.7965	0.0030	0.0298
Ce	0.0011	0.2887	0.0111	0.1114
Nd	0.0019	0.6994	0.0083	0.0832
HNO_3 (65 %)				
Element	**Standard deviation**	**Slope**	**LOD (ppm)**	**LOQ (ppm)**
La	0.0035	1.9688	0.0053	0.0530
Ce	0.0017	0.2748	0.0188	0.1881
Nd	0.0014	0.5738	0.0076	0.0757
HCl (32 %)				
Element	**Standard deviation**	**Slope**	**LOD (ppm)**	**LOQ (ppm)**
La	0.0018	1.7337	0.0031	0.0309
Ce	0.0011	0.2592	0.0124	0.1241
Nd	0.0019	0.7216	0.0081	0.0807

5.3 QUANTIFICATION OF REE IN PURE METAL SAMPLES

5.3.1 DISSOLUTION OF METAL SAMPLES

5.3.1.1 DISSOLUTION OF PURE METALS USING BENCH-TOP DIGESTION

A lanthanum ingot kept under oil (5 g) was cut into smaller pieces for the La determination. The La metal piece and Ce and Nd powder metal samples (0.0100 - 0.2942 g) were accurately weighed and quantitatively transferred to 100 mL glass beakers to yield approximate 5.0000 - 6.9500 ppm metal concentrations. 10 mL portions of the different acids (98 % H_2SO_4, 65 % HNO_3 or 32 % HCl) were added to each glass beaker and left in a fumehood for 5 hours to dissolve. Visual inspection indicated that both the La and Nd metal samples in the different acid solutions were completely dissolved after this digestion period. Visual inspection clearly indicates the presence of undissolved Ce in all the beakers. The reaction mixtures were then filtered to separate the soluble product from the undigested material. All the filtrates were then heated to almost dryness to remove the different acids. 10 mL portions of the different acids were then added to these samples to ensure acid matrix matching. These solutions were quantitatively transferred to 100.0 mL volumetric flasks and filled to the mark with ultra-pure water. 10.0 mL aliquots of these solutions were subsequently transferred to 100.0 mL volumetric flasks using micro-pipettes. These diluted metal containing solutions were analysed for La, Ce and Nd concentrations using ICP-OES and the results are presented in **Table 5.5**.

Table 5.5: La, Ce, and Nd recovery in different pure metals using H_2SO_4, HCl and HNO_3 by bench top dissolution.

H_2SO_4 (98 %)			
	La	**Ce**	**Nd**
Mass range of metal (g)	0.1003 - 0.1070	0.0118 - 0.0120	0.0100 - 0.0110
Theoretical metal content (ppm)	5.0150 - 5.3500	5.9000 - 6.0000	5.0000 - 5.5000
Recovery % (s)*	100.0(2)	95.30(8)	97.9(5)
RSD (%)	0.20	0.08	0.51
HCl (32 %)			
	La	**Ce**	**Nd**
Mass range of metal (g)	0.1120 - 0.1126	0.0118 - 0.0120	0.0121 - 0.0130
Theoretical metal content (ppm)	5.6000 - 5.6300	5.9000 - 6.0000	6.0500 - 6.5000
Recovery % (s)*	99.97(8)	81.37(9)	99.4(4)
RSD (%)	0.08	0.11	0.37
HNO_3 (65 %)			
	La	**Ce**	**Nd**
Mass range of metal (g)	0.2867 - 0.2942	0.0117 - 0.0139	0.0120 - 0.0132
Theoretical metal content (ppm)	5.7340 - 5.8840	5.8500 - 6.9500	6.0000 - 6.6000
Recovery % (s)*	99.5(3)	89.1(2)	99.7(3)
RSD (%)	0.26	0.23	0.28

*Average of 3 replicates

5.3.1.2 DISSOLUTION OF Ce METAL POWDER USING MICROWAVE-ASSISTED DIGESTION

The poor recovery of Ce using bench top digestion necessitated the use of the robust microwave digestion to enhance the recovery of the metal. 0.0102 - 0.0115 g of Ce powder were weighed accurately into a vial. The weighed samples were transferred to clean microwave PTFE vessels and 8 mL of 98 % H_2SO_4, 65 % HNO_3 or 32 % HCl was added to each vessel. After completion of the microwave program (digestion for 60 minutes) the samples were quantitatively transferred into 100.0 mL volumetric flasks. To ensure matrix matching 2 mL of 98 % H_2SO_4, 65 % HNO_3 and 32 % HCl were added to each volumetric flask. The solutions were thoroughly mixed until the samples were completely dissolved and then allowed to cool to room temperature. Visual inspection indicated complete dissolution of the Ce metal powder only in the nitric acid. The hydrochloric acid and sulphuric acid solution of the cerium mixtures were filtered to separate the soluble product from the undigested material. The filtrates were then heated at 70 °C to almost dryness to remove the acids. Hydrochloric acid and sulphuric acid were then added to these samples to ensure acid matrix matching. These solutions were quantitatively transferred to 100.0 mL volumetric flasks and then filled to mark with ultra-pure water. 5.0 mL aliquots of these solutions were subsequently transferred to 100.0 mL volumetric flasks using micro-pipettes. These diluted metal containing solutions were analysed for La, Ce and Nd concentrations using ICP-OES and the results are presented in **Table 5.6**.

Table 5.6: Ce recovery in pure metal using H_2SO_4, HCl and HNO_3 by microwave digestion.

	H_2SO_4	**HCl**	**HNO_3**
Mass range of metal (g)	0.0105 - 0.0115	0.0102 - 0.0108	0.0103 - 0.0106
Theoretical metal content (ppm)	5.2500 - 5.7500	5.1000 - 5.4000	5.1500 - 5.3000
Recovery % (s)*	98.7(3)	96.5(1)	99.6(3)
RSD (%)	0.32	0.14	0.28

*Average of 3 replicates

5.4 QUANTIFICATICION OF REE IN SAMPLES OF INORGANIC COMPOUNDS

5.4.1 DISSOLUSION OF INORGANIC COMPOUND SAMPLES

5.4.1.1 DISSOLUSION OF INORGANIC COMPOUNDS BY BENCH TOP DIGESTION

The REE (La, Ce and Nd) nitrates were commercially available and used without further purification. The REE nitrates are easy dissolved with H_2O.

Figure 5.6: a) $La(NO_3)_3{\cdot}6H_2O$ b) $Ce(NO_3)_3{\cdot}6H_2O$ and c) $Nd(NO_3)_3{\cdot}6H_2O$.

0.0101 - 0.0123 g of $Ln(NO_3)_3{\cdot}6H_2O$ (Ln = La, Ce, Nd) were accurately weighed (to 0.1 mg) and quantitatively transferred to a 100.0 mL volumetric flasks. To each volumetric flask, 10 mL of different acids (such as 98 % H_2SO_4, 65 % HNO_3 or 32 % HCl) was added while the 98 % H_2SO_4 solution was left to cool and then filled to the mark with ultra-pure water. A 10.0 mL aliquot of this solution was subsequently transferred to a 100.0 mL volumetric flask. These dilute solutions were analysed for La, Ce and Nd concentrations using ICP-OES and the results are presented in **Table 5.7**.

Table 5.7: La, Ce, and Nd recovery in different inorganic compounds using H_2SO_4, HCl and HNO_3 by bench top dissolution.

H_2SO_4 (98 %)			
	La	**Ce**	**Nd**
Mass range of metal (g)	0.0107 - 0.0113	0.0101 - 0.0110	0.0114 - 0.0122
Theoretical metal content (ppm)	3.4325 - 3.6250	3.2564 - 3.5465	3.7509 - 4.0142
Recovery % (s)*	98.6(2)	98.91(5)	98.0(2)
RSD (%)	0.22	0.05	0.21
HCl (32 %)			
	La	**Ce**	**Nd**
Mass range of metal (g)	0.0100 - 0.0103	0.0103 - 0.0129	0.0102 - 0.0109
Theoretical metal content (ppm)	3.2079 - 3.3041	3.3208 - 4.1591	3.3561 - 3.6193
Recovery % (s)*	100.2(2)	99.7(2)	100.0(1)
RSD (%)	0.17	0.19	0.11
HNO_3 (65 %)			
	La	**Ce**	**Nd**
Mass range of metal (g)	0.0100 - 0.0110	0.0100 - 0.0120	0.0110 - 0.0123
Theoretical metal content (ppm)	3.2079 - 3.5287	3.5465 - 3.8689	3.6456 - 4.1458
Recovery % (s)*	99.6(2)	100.6(1)	100.0(2)
RSD (%)	0.22	0.13	0.16

*Average of 3 replicates

5.4.1.2 ANALYSIS OF REE MIXTURE USING BENCH-TOP DIGESTION

Individual portions of the inorganic compounds $Ln(NO_3)_3 \cdot 6H_2O$ (La 0.0756 - 0.0788g, Ce 0.1568 - 0.1589g and Nd 0.0573 - 0.0579g) were accurately weighed and each transferred to a 100 mL Schott Duran glass beaker. 20 mL portions of ultra-pure water were added to each glass beaker and left in a fumehood to allow the complete dissolution of the individual inorganic salts. Visual inspection indicated that the inorganic compound were completely dissolved and the three solutions (La, Ce and Nd) were quantitatively transferred to the same (one) 100.0 mL volumetric flask to yield a synthetic mixture with a La:Ce:Nd ratio (1:3:1) which mimic their natural abundance of these early REE in the monazite minerals. 10 mL of 65 % HNO_3 was added to the volumetric flask and filled to the mark with ultra-pure water. A 1.0 mL aliquot of this solution was subsequently transferred to a 100.0 mL volumetric flask. This diluted solution was analysed for La, Ce and Nd concentrations using ICP-OES and the results are presented in **Table 5.8**.

Table 5.8: La, Ce, and Nd recovery in a synthetic mixture of inorganic compounds using HNO_3 by bench top dissolution.

	La	**Ce**	**Nd**
Mass range of metal (g)	0.0756 - 0.0788	0.1568 - 0.1589	0.0573 - 0.0579
Theoretical metal content (ppm)	2.4252 - 2.5279	5.0624 - 5.1302	1.8870 - 1.9067
Recovery % (s)*	99.3(3)	99.4(6)	98.7(3)
RSD (%)*	0.32	0.57	0.28

*Average of 3 replicates

5.5 QUANTIFICATION OF REE IN DIFFERENT ORGANOMETALLIC COMPOUNDS

5.5.1 INTRODUCTION

The purpose of this study was to develop the analytical method for lanthanum, cerium and neodymium determination and validate this method by determining the La, Ce, and Nd content in different organometallic complexes. In this study $La(NO_3)_3{\cdot}6H_2O$, $Ce(NO_3)_3{\cdot}6H_2O$ and $Nd(NO_3)_3{\cdot}6H_2O$ were used as the starting materials while acetyl acetone (acac), nitrilotriacetic acid (nta), iminodiacetic acid (imda), dimethylaminopyridine (dap) and triphenylphosphine oxide (TPPO) were used as ligands (**Figure 5.9**).

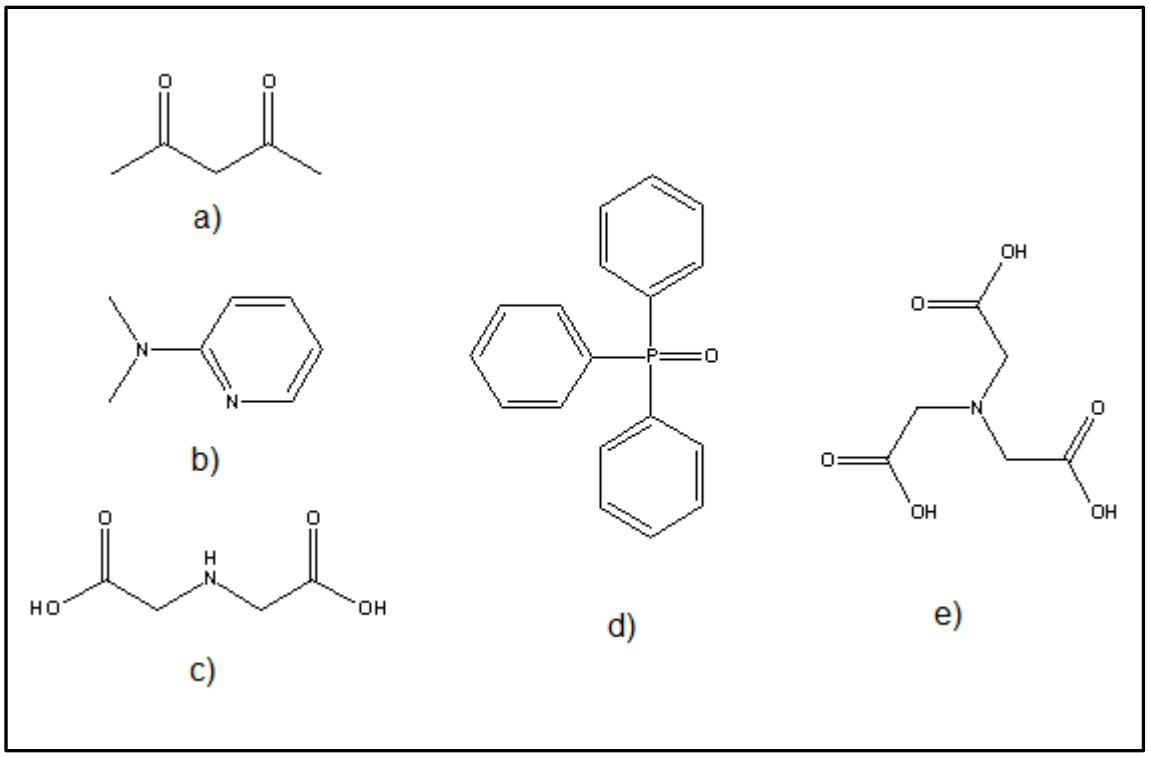

Figure 5.7: Ligands a) acetyl acetone (acac) b) dimethylaminopyridine (dap) c) iminodiacetic acid (imda) d) triphenylphosphine oxide (TPPO) and e) nitrilotriacetic acid (nta).

All the different products obtained from these syntheses such as powders or crystals as well as coloured solutions were characterized using analytical techniques such as

the CHN micro-analyser, IR and UV/Vis spectrophotometer to obtain the metal to ligand stoichiometry and the identity of the isolated compounds.

The external calibration method which proved to produce excellent results for all the previous quantitative analyses was chosen as the preferred method of analysis. The same experimental conditions for the ICP-OES lanthanum, cerium and neodymium determination were applied on the organometallic samples. Dissolution by the microwave-assisted and bench top digestion method using acids such as sulphuric acid, nitric acid and hydrochloric acid was used for sample dissolution for all the organometallic complexes.

5.5.2 **GENERAL EQUIPMENT**

5.5.2.1 IR-SPECTROSCOPY

IR spectra in the range of 4000 - 200 cm^{-1} were recorded on a Digilab Scimitar Series spectrometer (**Figure 5.7**). Samples were directly analysed on the IR spectrometer.

Figure 5.8: FTIR spectrometer.

5.5.2.2 TRUSPEC MICRO CHNS EQUIPMENT

A TruSpec Micro CHNS (**Figure 5.8**) bought from LECO was used for the elemental C, H and N analyses.

Figure 5.9: Leco CHN/CHNS TruSpec Micro Series.

Procedure

1. Perform maintenance and leak checks, etc after opening different gases (He, O_2 and N_2).
2. Analyse numerous blanks until the different detectors N, C, H and S are stable).
3. Analyse control samples in triplicate using the following procedure.
   a. Weigh ~2 mg of a calibration standard (sulfamethazine, EDTA etc.) into a tin capsule, crimp capsule, and analyse.
   b. Evaluate results and perform a calibration drift if needed.
4. Analyse different samples for C, H, N and S content.
5. Repeat step 3 - analyse calibration standards to verify the stability (accuracy) of the analyses.
6. Repeat the whole process if the results of the control samples differ significantly or perform more comprehensive maintenance such as replacing catalyst.

5.5.3 MATERIALS AND SOLVENTS

All chemicals and reagents were obtained commercially and used as received without further purification. These chemicals and reagents, along with the purity and commercial supplier are listed in **Table 5.9**.

Table 5.9: Materials and solvents.

Chemical	Formula	Purity	Supplier
Ligand			
Acetyl acetone (acac)	$C_5H_8O_2$	99.5 %	Riedel-de Haen AG
Nitrilotriacetic acid (nta)	$C_6H_9NO_6$	≥ 99 %	Sigma-Aldrich
Iminodiacetic acid (imda)	$C_4H_7NO_4$	98 %	Sigma-Aldrich
Dimethylaminopyridine (dap)	$C_7H_{10}N_2$	> 99 %	Merck
Triphenylphosphine oxide (TPPO)	$C_{18}H_{15}OP$	98 %	Sigma-Aldrich
Base			
Potassium hydroxide	KOH	≥ 90 %	Sigma-Aldrich
Solvent			
Ethanol	C_2H_5OH	99.5 %	Merck

Silicone oil used for heating in the oil bath (from - 50 °C to > 200 °C) was bought from Sigma-Aldrich.

5.5.4 SYNTHESES OF ORGANOMETALLIC COMPLEXES

5.5.4.1 SYNTHESIS OF [Ln(acac)$_3$]·n(H$_2$O) (Ln = La, Ce, Nd; n = 0 or 1)[169]

The solution of Ln$(NO_3)_3$·6H_2O (1 mmol; 0.4395 g for La, 0.4328 g for Ce and 0.4374 g for Nd) in 10 mL of ultra-pure water was added to the solution of acac (2 mmol, 0.2113 g for La, 0.1844 g for Ce and 0.1844 g Nd) in 10 mL of ultra-pure water. The pH of the solution was adjusted to approximately 5.5 with KOH [0.3 M] and was left stirring at 25 °C for 24 hours and resulted in precipitate formation. The crystalline material was filtered and dried in a desiccator for 24 hours. The crystalline material were collected (yield: light yellow [La$(acac)_3$] 0.3185 g, 71.50 %, light brown [Ce$(acac)_3$]·(H_2O) 0.3358 g, 73.54 % and purple [Nd$(acac)_3$]·(H_2O) 0.3792 g, 82.21 %).

5.5.4.1.1 BENCH-TOP DIGESTION FOR acac COMPLEXES

The acac complexes prepared in **Section 5.5.2.1** were weighed (0.0102 - 0.0124 g) and dissolved in 10 mL of a different acid such as 98 % H_2SO_4, 65 % HNO_3 or 32 % HCI each, then filled to the calibration mark of the volumetric flask with ultra-pure water. 10.0 mL aliquots of these solutions were subsequently transferred to 100.0 mL volumetric flasks and filled to the mark with ultra-pure water. These diluted solutions were analysed for La, Ce and Nd concentrations using ICP-OES and the results are presented in **Table 5.10**.

[169] J G Stites, C N Mccarty and L L Quill, *Journal of the American Chemical Society*, 1948, 70, pp3141-3142.

Table 5.10: La, Ce, and Nd recovery in different acac complexes using H_2SO_4, HCl and HNO_3 by bench top dissolution.

H_2SO_4 (98 %)			
	$[La(acac)_3]$	**$[Ce(acac)_3]\cdot H_2O$**	**$[Nd(acac)_3]\cdot H_2O$**
Mass range of metal (g)	0.0104 - 0.0121	0.0114 - 0.0117	0.0104 - 0.0124
Theoretical metal content (ppm)	3.2888 - 3.826373	3.6264 - 3.7219	3.3740 - 4.0229
Recovery % (s)*	100.01(9)	99.2(7)	100.1(9)
RSD (%)	0.09	0.72	0.92
HCl (32 %)			
	$[La(acac)_3]$	**$[Ce(acac)_3]\cdot H_2O$**	**$[Nd(acac)_3]\cdot H_2O$**
Mass range of metal (g)	0.0116 - 0.0123	0.0105 - 0.0109	0.0101 - 0.0102
Theoretical metal content (ppm)	3.6683 - 3.8896	3.3401 - 3.4674	3.2767 - 3.3091
Recovery % (s)*	99.4(3)	99.0(3)	101.6(3)
RSD (%)	0.32	0.31	0.27
HNO_3 (65 %)			
	$[La(acac)_3]$	**$[Ce(acac)_3]\cdot H_2O$**	**$[Nd(acac)_3]\cdot H_2O$**
Mass range of metal (g)	0.0108 - 0.0128	0.0102 - 0.0115	0.0104 - 0.0118
Theoretical metal content (ppm)	3.4153 - 4.0477	3.2447 - 3.4900	3.3740 - 3.8282
Recovery % (s)*	101.0(4)	100.3(2)	98.0(2)
RSD (%)	0.42	0.25	0.21

*Average of 3 replicates

5.5.4.1.2 ELEMENTAL ANALYSIS (CHN)

Three portions of the acac complexes prepared in **Section 5.5.2.1** were accurately weighed (approximately 2.0 mg) in tin capsules and then the CHN analyser was used for the determination of their C, H and N content. The metal (La, Ce and Nd) content in the metal complexes was determined by ICP-OES using sulphuric acid. The elemental analysis results for C, N, H and the REE content in the different complexes are given in **Table 5.11**.

Table 5.11: Analytical data for different metal acac complexes.

Molecular formula	Empirical formula	Metal (%)	C (%)	H (%)
		Found (Cald.)*•	Found (Cald.)*	Found (Cald.)*
$[La(acac)_3]$	$LaC_{15}H_{21}O_6$	31.84 (31.84)	40.54 (41.30)	4.64 (4.85)
$[Ce(acac)_3]\cdot H_2O$	$CeC_{15}H_{23}O_7$	30.52 (30.77)	38.86 (39.56)	4.81 (5.09)
$[Nd(acac)_3]\cdot H_2O$	$NdC_{15}H_{23}O_7$	31.42 (31.39)	38.56 (39.20)	4.73 (5.04)

*Average of 3 replicates

•ICP-OES analysed using H_2SO_4

5.5.4.1.3 INFRARED ANALYSIS

Infrared spectra of acac and their metal complexes prepared in **Section 5.5.2.1** were recorded with a Digilab Scimitar Series spectrometer. The spectra are very similar to each other, as illustrated in **Figure 5.10** and their important bands are reported in **Table 5.12**.

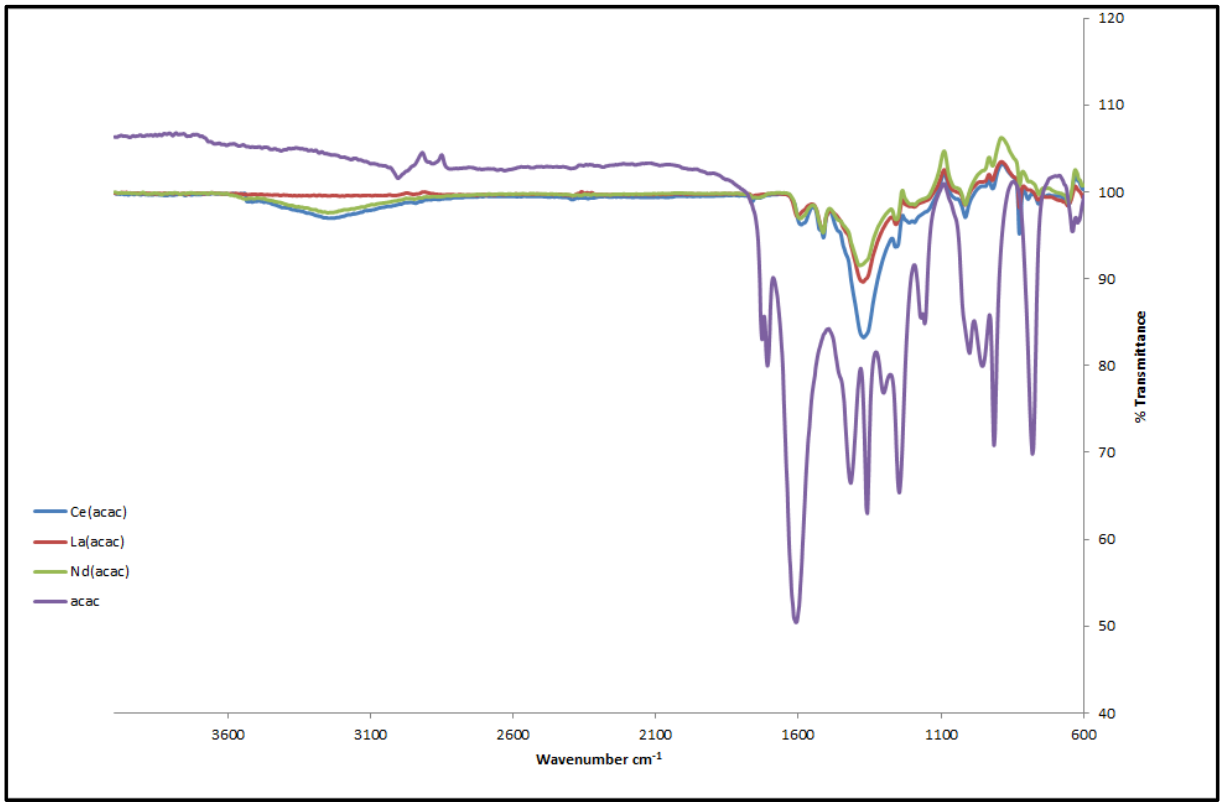

Figure 5.10: The IR spectra of acac and the different metal acac complexes.

Table 5.12: The IR stretching frequencies of acac and the different metal acac complexes.

Compound	ν (C=O)	ν (COO^-)	ν (C=O)+ δ (CH)	ν (CH)+ ν (C-C)	ν (OH)
Acac	1708.5	1608.4	1416.8	1246.4	
$[La(acac)_3]$	1761.0	1603.6	1513.7	1257.7	
$[Ce(acac)_3]\cdot H_2O$	1760.1	1590.6	1525.9	1254.8	3241.3
$[Nd(acac)_3]\cdot H_2O$	1760.0	1594.5	1514.0	1259.6	3243.9

5.5.4.2 SYNTHESIS OF [Ln(dap)(NO_3)$_3$] (Ln = La, Ce, Nd)

$Ln(NO_3)_3 \cdot 6H_2O$ (1 mmol, 0.4311 g for La, 0.4309 g for Ce, 0.4325 g for Nd) and dap (2 mmol, 0.2489 g for La, 0.2478 g for Ce and 0.2488 g for Nd) were dissolved in 10 mL ethanol, and the pH was recorded as 5.5 without any addition of base. The resulting solution was stirred for 30 minutes at 25 ºC, and then left to recrystallize at room temperature for 24 hours. Fine crystalline precipitate were collected by filtration, washed thoroughly with ethanol, and dried in a desiccator for 24 hours. Yield: light yellow [La(dap)(NO_3)$_3$] 0.4160 g, 60.48 %, light brown [Ce(dap)(NO_3)$_3$] 0.3973 g, 57.85 %and purple [Nd(dap)(NO_3)$_3$] 0.3748 g, 54.56 %).

5.5.4.2.1 BENCH-TOP DISSOLUTION FOR dap COMPLEXES

The dap complexes were accurately weighed (0.0101 - 0.0172 g) and transferred to different 100 mL glass beakers containing 10 mL of different acids (98 % H_2SO_4, 65 % HNO_3 or 32 % HCI). The solutions were stirred at 25 ºC until visual inspection confirmed complete dissolution (less than 10 min). The solutions were quantitatively transferred to 100.0 mL volumetric flasks and diluted to the mark with ultra-pure water. For ICP-OES analyses, 10.0 mL aliquots of these solutions were pipetted into 100.0 mL volumetric flasks and filled to the mark with ultra-pure water. These dilute solutions were analysed for La, Ce and Nd concentrations using ICP-OES and the results are shown in **Tables 5.13**.

Table 5.13: La, Ce, and Nd recovery in different dap complexes using H_2SO_4, HCl and HNO_3 by bench top dissolution.

H_2SO_4 (98 %)			
	[La(dap)$(NO_3)_3$]	**[Ce(dap)$(NO_3)_3$]**	**[Nd(dap)$(NO_3)_3$]**
Mass range of metal (g)	0.0103 - 0.0104	0.0112 - 0.0122	0.0109 - 0.0116
Theoretical metal content (ppm)	3.2003 - 3.2313	3.5007 - 3.8133	3.4752 - 3.6984
Recovery % (s)*	88.1(5)	95.5(3)	98.29(7)
RSD (%)	0.60	0.30	0.07
HCl (32 %)			
	[La(dap)$(NO_3)_3$]	**[Ce(dap)$(NO_3)_3$]**	**[Nd(dap)$(NO_3)_3$]**
Mass range of metal (g)	0.0117 - 0.0128	0.0111 - 0.0172	0.0105 - 0.0109
Theoretical metal content (ppm)	3.6352 - 3.9770	3.4695 - 5.3761	3.3477 - 3.4752
Recovery % (s)*	90.0(4)	91.4(3)	99.3(2)
RSD (%)	0.48	0.36	0.25
HNO_3 (65 %)			
	[La(dap)$(NO_3)_3$]	**[Ce(dap)$(NO_3)_3$]**	**[Nd(dap)$(NO_3)_3$]**
Mass range of metal (g)	0.0101 - 0.0123	0.0111 - 0.013	0.0115 - 0.0129
Theoretical metal content (ppm)	3.1381 - 3. 8217	3.4695 - 3.5320	3.6665 - 4.1129
Recovery % (s)*	90(2)	91.4(5)	98.3(2)
RSD (%)	2.02	0.57	0.18

*Average of 3 replicates

5.5.4.2.2 ELEMENTAL ANALYSIS (CHN)

The free dap ligand and the different metal complexes prepared in **Section 5.5.2.2** were accurately weighed and analysed with the CHNS analyser to determine their C, H and N content. The ICP-OES was used to quantify metal (La, Ce and Nd) content from the metal complexes with sulphuric acid. The elemental analysis results for C, N, H and the metal (lanthanum, cerium and neodymium) content of the complexes are given in **Table 5.14**.

Table 5.14: Analytical data for pure dap and the different metal complexes.

Molecular formula	Empirical formula	Metal (%)	N (%)	C (%)	H (%)
		Found (Cald.)*•	Found (Cald.)*	Found (Cald.)*	Found (Cald.)*
dap	$C_7H_{10}N_2$		20.73 (22.93)	70.56 (68.82)	7.65 (8.25)
[La(dap)$(NO_3)_3$]	$LaC_7H_{10}N_5O_9$	27.37 (31.07)	15.02 (15.66)	18.21 (18.81)	2.55 (2.25)
[Ce(dap)$(NO_3)_3$]	$CeC_7H_{10}N_5O_9$	29.85 (31.26)	15.19 (15.62)	17.34 (18.76)	2.54 (2.25)
[Nd(dap)$(NO_3)_3$]	$NdC_7H_{10}N_5O_9$	31.34 (31.89)	14.55 (15.48)	17.12 (18.59)	2.43 (2.23)

*Average of 3 replicates

•ICP-OES analysed using H_2SO_4

5.5.4.2.3 INFRARED ANALYSIS

Infrared spectra of the free dap ligand and the different metal complexes were recorded with a Digilab Scimitar Series spectrometer. The assignment of the most important vibrational bands of dap and their complexes are illustrated in **Figure 5.11** and **Table 5.15**.

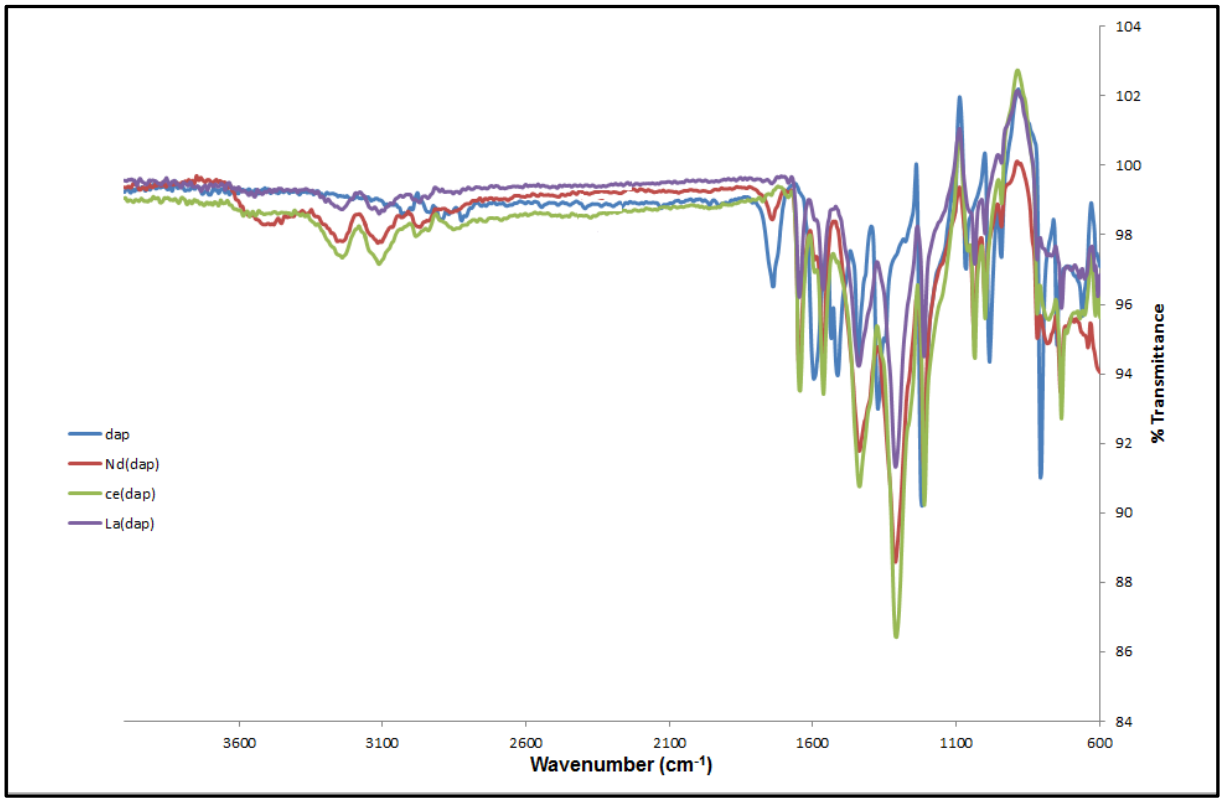

Figure 5.11: The IR spectra of dap and the different metal dap complexes.

Table 5.15: The IR stretching frequencies of dap and the different metal dap complexes.[170]

Compound	*v* (C=N)	*v* (C=N, C=C)	*v* (NO_3)	*v* (NO_3)	*v* (NO_3)
dap	1595.5	1513.6			
$Y(NO_3)_3{\cdot}5H_2O$*			1489.9	1282.2	1028.6
$[La(dap)(NO_3)_3]$	1646.8	1563.7	1439.8	1310.9	1035.5
$[Ce(dap)(NO_3)_3]$	1645.1	1562.1	1437.0	1309.3	1034.4
$[Nd(dap)(NO_3)_3]$	1646.6	1563.7	1437.5	1312.4	1037.4

*NO_3 stretching frequency

[170] S M Rosendahl, B R Danger, J P Vivek and I J Burgess, *American Chemical Society*, 2009, 25 (4), pp2241-2247.

5.5.4.3 SYNTHESIS OF [Ln(imda)]·H_2O (Ln = La, Ce, Nd)[171]

A solution of $Ln(NO_3)_3$·$6H_2O$ (1mmol, 0.4341 g for La, 0.4355 g for Ce and 0.4335 g for Nd) in ultra-pure water (10 mL) was added to an ultra-pure water solution (10 mL) of the imda (2 mmol, 0.2677 g for La, 0.2663 g for Ce and 0.2659 g for Nd). The pH of the solution was adjusted to ±6 with KOH [0.3 M] and the resulting solution was then refluxed on an oil-bath at 160°C for 3 days and then cooled slowly to room temperature. The crystalline material was filtered and dried in a desiccator for 24 hours. The crystalline material were then collected and weighed (yield: white [La(imda)]·H_2O 0.1648 g, 56.70 %, yellow [Ce(imda)]·H_2O 0.1666 g, 57.06 % and for purple [Nd(imda)]·H_2O 0.1608 g, 57.20 %).

5.5.4.3.1 BENCH TOP DISSOLUTION FOR imda COMPLEXES

The [Ln(imda)]·H_2O (Ln = La, Ce or Nd) samples were dried in an oven at 120 °C for 12 hours prior to digestion. Samples of the imda complexes (0.0103 - 0.0149 g) were accurately weighed and each transferred into 100 mL glass beakers. 10 mL of different acids (98 % H_2SO_4, 65 % HNO_3 and 32 % HCl) were added to each glass beaker and left in fumehood to be completely dissolved. The solutions were then quantitatively transferred to 100.0 mL volumetric flasks and filled to the mark with ultra-pure water. 10.0 mL aliquots of these solutions were subsequently transferred to 100.0 mL volumetric flasks and filled to the mark with ultra-pure water. These diluted solutions were analysed for La, Ce and Nd concentrations using ICP-OES and the results are presented in **Table 5.16**.

[171] J Wang, X Zhang, X Ling, W Jia and H Li, *Journal of Molecular Structure*, 2002, 610, pp151-158.

Table 5.16: La, Ce, and Nd recovery in different imda complexes using H_2SO_4, HCl and HNO_3 by bench top dissolution.

H_2SO_4 (98 %)			
	[La(imda)]·H_2O	**[Ce(imda)]·H_2O**	**[Nd(imda)]·H_2O**
Mass range of metal (g)	0.0103 - 0.0115	0.0114 - 0.0133	0.0129 - 0.0149
Theoretical metal content (ppm)	4.0882 - 4.5645	3.3542 - 3.9132	3.8655 - 4.2550
Recovery % (s)*	100.0(9)	98.6(4)	100.3(7)
RSD (%)	0.93	0.44	0.72
HCl (32 %)			
	[La(imda)]·H_2O	**[Ce(imda)]·H_2O**	**[Nd(imda)]·H_2O**
Mass range of metal (g)	0.0112 - 0.0141	0.0104 - 0.0118	0.0105 - 0.0112
Theoretical metal content (ppm)	4.4454 - 5.5964	3.0600 - 3.4719	3.1463 - 3.3561
Recovery % (s)*	101.7(9)	99.0(2)	100.76(7)
RSD (%)	0.93	0.21	0.07
HNO_3 (65 %)			
	[La(imda)]·H_2O	**[Ce(imda)]·H_2O**	**[Nd(imda)]·H_2O**
Mass range of metal (g)	0.0127 - 0.0149	0.0120 - 0.0122	0.0139 - 0.0149
Theoretical metal content (ppm)	5.0408 - 5.9140	3.5307 - 3.5896	4.1651 - 4.4648
Recovery % (s)*	102(1)	98.7(8)	103.6(4)
RSD (%)	1.02	0.81	0.34

*Average of 3 replicates

5.5.4.3.2 ELEMENTAL ANALYSIS (CHN)

The different imda complexes prepared as described in **Section 5.5.3.2** were dried in an oven at 120 °C for 12 hours before micro-element analysis. The complexes were accurately weighed in tin capsules and analysed for C, H and N content, while the ICP-OES was used to determine metal content (La, Ce and Nd) using H_2SO_4. The elemental analysis results for C, N, H and the lanthanum, cerium and neodymium metal content in a complex are given in **Table 5.17**.

Table 5.17: Analytical data for pure imda and the different metal complexes.

Molecular formula	Empirical formula	Metal (%)	N (%)	C (%)	H (%)
		Found (Cald.)*	Found (Cald.)*	Found (Cald.)*	Found (Cald.)*
Imda	$C_4H_7NO_4$		9.09 (10.52)	36.18 (36.09)	5.12 (5.30)
[La(imda)]·H_2O	$LaC_4H_7NO_5$	48.23 (48.23)	4.96 (4.86)	16.94 (16.68)	2.51 (2.45)
[Ce(imda)]·H_2O	$CeC_4H_7NO_5$	47.77 (48.45)	4.58 (4.48)	16.95 (16.61)	2.48 (2.44)
[Nd(imda)]·H_2O	NdC_4HNO_5	49.33 (49.18)	4.82 (4.77)	16.88 (16.38)	2.45 (2.41)

*Average of 3 replicates

•ICP-OES analysed using H_2SO_4

5.5.4.3.3 INFRARED ANALYSIS

The dried imda complexes were characterized with IR spectroscopy. The most important stretching frequencies of the imda ligand and respective metal complexes are reported in **Figure 5.12** and **Table 5.18**.

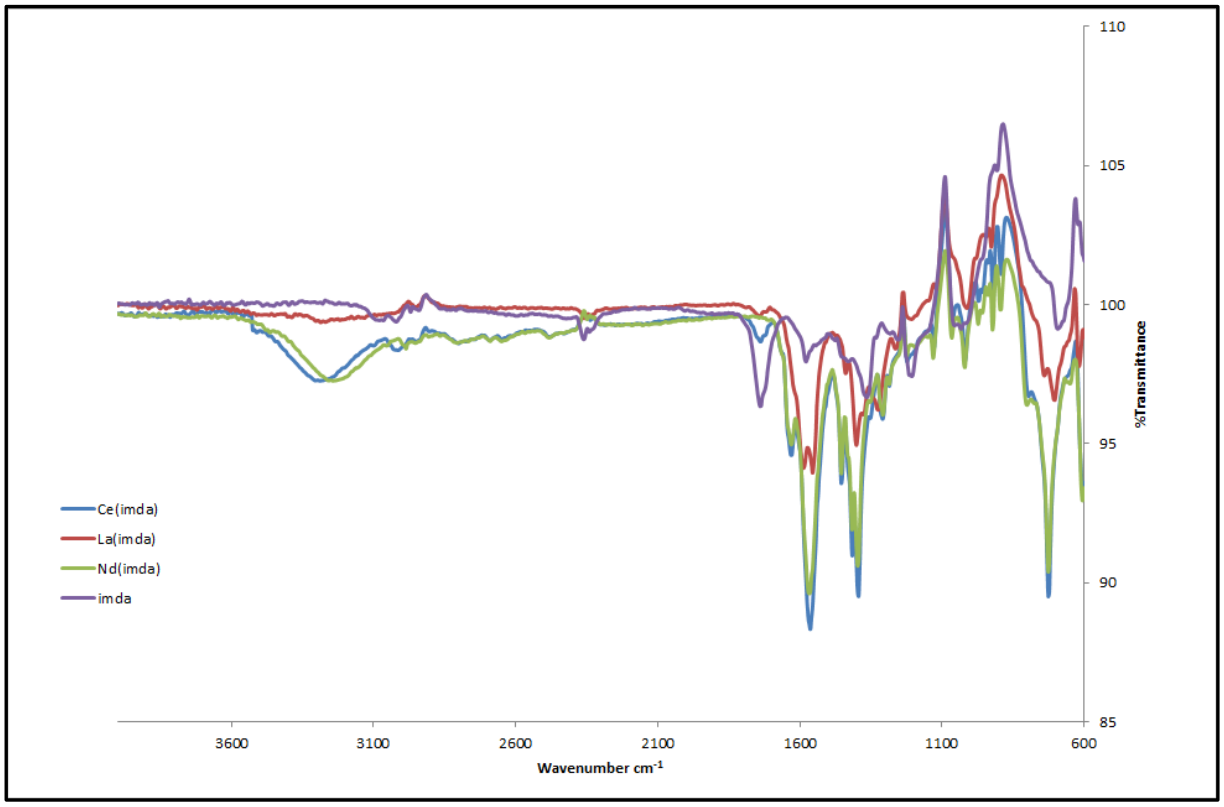

Figure 5.12: The IR spectra of imda and the different metal imda complexes.

Table 5.18: The IR stretching frequencies of imda and the different metal imda complexes.[172,173,174]

Compound	ν (C=O)	$\nu_{as}(COO^-)$	$\nu_{s}(COO^-)$	ν (OH)
Imda	1738.4	1578.0	1364.3	
[La(imda)]·H_2O	1743.6	1554.6	1400.6	3270.0
[Ce(imda)]·H_2O	1738.1	1563.2	1394.0	3023.4
[Nd(imda)]·H_2O		1566.5	1395.5	3454.4

[172] K Nakamoto, Infrared spectra of inorganic and coordination compounds, *Wiley-intersience, a division of John Wiley & Sons*, 2nd edition, 1963, p238.

[173] Y Li, F Liang, C Jiang, X Li and Z Chen, *Inorganica Chimica Acta,* 2008, 361, pp219-225.

[174] L Zhang, N Yu, K Zhang, R Qiu, Y Zhao, W Rong and H Deng, *Inorganica Chimica Acta,* 2013, 400, pp67-73.

5.5.4.4 SYNTHESIS OF [Ln(nta)]·nH$_2$O (Ln = La, Ce, Nd; n = 1 or 2)[171]

A solution of [Ln(NO$_3$)$_3$]·6H$_2$O (1mmol, 0.1300 g for La, 0.1299 g for Ce and 0.1309 g for Nd) in ultra-pure water (10 mL) was added to a water solution (10 mL) containing the nta ligand (3 mmol, 0.0579 g for La, 0.0599 g for Ce and 0.0575 g for Nd). The pH of the solution was adjusted to approximately 6 with KOH [0.3 M] and the resulting solutions were refluxed on an oil-bath at 160 °C for 3 days. Crystalline products were filtered and dried in a desiccator for 24 hours. Crystalline products were collected (yield: white [La(nta)]·2H$_2$O 0.0980 g, 93.83 %, white [Ce(nta)]·H$_2$O 0.0992 g, 94.98 % and purple [Nd(nta)]·H$_2$O 0.0905 g, 85.79 %)

5.5.4.4.1 BENCH TOP DISSOLUTION FOR THE nta COMPLEXES

The [Ln(nta)]·nH$_2$O (Ln = La, Ce or Nd; n = 1 or 2) complexes were dried in an oven at 120 °C for 12 hours prior to digestion. Samples (0.0104 - 0.0304 g) were accurately weighed in a glass vial and their masses recorded as shown in **Table 5.19**. The weighed samples were transferred into glass beakers in triplicate for each sample. 10 mL of different acids (98 % H$_2$SO$_4$, 65 % HNO$_3$ or 32 % HCl) was separately added to each glass beaker to completely dissolve the different metal complexes. The dissolved samples were quantitatively transferred into 100.0 mL volumetric flasks and the 98 % H$_2$SO$_4$ solution was left to cool while then filled to the mark with ultra-pure water. 10.0 mL aliquots of these solutions were pipetted into 100.0 mL volumetric flasks and filled to the mark with ultra-pure water. These diluted solutions were analysed for La, Ce and Nd concentrations using ICP-OES and the results are presented in **Table 5.19**.

Table 5.19: La, Ce, and Nd recovery in different nta complexes using H_2SO_4, HCl and HNO_3 by bench top dissolution.

H_2SO_4 (98 %)			
	[La(nta)]·2H_2O	**[Ce(nta)]·H_2O**	**[Nd(nta)]·H_2O**
Mass range of metal (g)	0.0225 - 0.0233	0.0109 - 0.0130	0.0165 - 0.0223
Theoretical metal content (ppm)	3.4437 - 3.5661	1.7651 - 2.1051	2.7172 - 3.6724
Recovery % (s)*	101.8(5)	98.4(4)	100(3)
RSD (%)	0.49	0.41	3.08
HCl (32 %)			
	[La(nta)]·2H_2O	**[Ce(nta)]·H_2O**	**[Nd(nta)]·H_2O**
Mass range of metal (g)	0.0227 - 0.0230	0.0105 - 0.0125	0.0170 - 0.0251
Theoretical metal content (ppm)	3.4743 - 3.5202	1.7003 - 2.0242	2.7996 - 4.1335
Recovery % (s)*	99.1(8)	99.39(6)	100.3(3)
RSD (%)	0.82	0.56	0.34
HNO_3 (65 %)			
	[La(nta)]·2H_2O	**[Ce(nta)]·H_2O**	**[Nd(nta)]·H_2O**
Mass range of metal (g)	0.0223 - 0.0227	0.0104 - 0.0162	0.0184 - 0.0304
Theoretical metal content (ppm)	3.4134 - 3.4743	1.6841 - 2.6233	3.0301 - 5.0063
Recovery % (s)*	100.6(4)	101.5(7)	100.8(7)
RSD (%)	0.43	0.72	0.70

*Average of 3 replicates

5.5.4.4.2 ELEMENTAL ANALYSIS (CHN)

The nta complexes were dried in an oven at 120 °C for 12 hours prior to micro-element analysis. 2.0 mg of the dried nta complexes as well as the pure nta ligand were analysed for C, H and N content. The ICP-OES results reported in **Table 5.20** are those dissolved using H_2SO_4. The elemental analysis results for C, N, H and the metal (lanthanum, cerium and neodymium) content in the different complexes are given in **Table 5.20**.

Table 5.20: Analytical data for pure nta and the different metal complexes.

Molecular formula	Empirical formula	Metal (%)	N (%)	C (%)	H (%)
		Found (Cald.)*•	Found (Cald.)*	Found (Cald.)*	Found (Cald.)*
nta	$C_6H_9NO_6$		6.32 (7.33)	37.57 (37.70)	4.48 (4.75)
[La(nta)]·2H_2O	$LaC_6H_{10}NO_8$	38.85 (38.16)	3.74 (3.85)	19.65 (19.85)	2.60 (2.78)
[Ce(nta)]·H_2O	$CeC_6H_8NO_7$	39.70 (40.35)	3.42 (4.03)	21.04 (20.81)	2.24 (2.33)
[Nd(nta)]·H_2O	$NdC_6H_8NO_7$	41.05 (41.05)	3.41 (3.99)	21.00 (20.57)	2.64 (2.74)

*Average of 3 replicates

•ICP-OES analysed using H_2SO_4

5.5.4.4.3 INFRARED ANALYSIS

The IR spectra of the free nta ligand and the dried different metal complexes ([La(nta)]·H_2O, [Ce(nta)]·H_2O and [Nd(nta)]·H_2O) were collected and are reported in **Figure 5.13 and Table 5.21**.

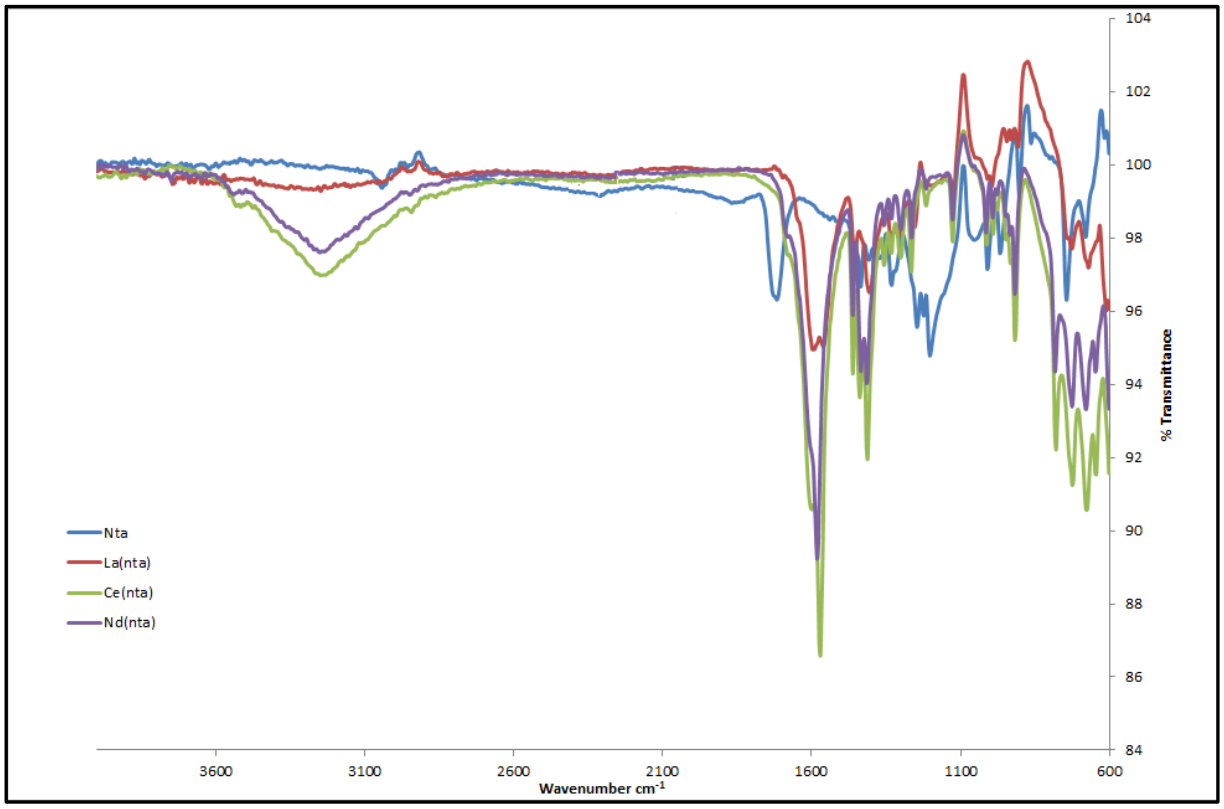

Figure 5.13: The IR spectra of nta and the different metal nta complexes.

Table 5.21: The IR stretching frequencies of nta and the different metal nta complexes.

Compound	ν (C=O)	$\nu_{as}(COO^-)$	$\nu_{s}(COO^-)$	$\nu_{as}(OH)$
nta	1715.5	1509.5	1331.3	
[La(nta)]·2H_2O		1591.2	1404.9	3237.1
[Ce(nta)]·H_2O		1571.1	1422.3	3241.3
[Nd(nta)]·H_2O		1587.4	1423.1	3243.3

5.5.4.5 SYNTHESIS OF [Ln(TPPO)$_3$(NO$_3$)$_3$] (Ln = La, Ce, Nd)[175]

A solution containing $Ln(NO_3)_3 \cdot 6H_2O$ (1 mmol; 0.2197 g for La, 0.1937 g for Ce and 0.5867 g for Nd) in 10 mL of ethanol was added to TPPO (3 mmol, 0.4234 g for La, 1.1282 g for Ce and 0.3694 g Nd) in 10 mL of ethanol. The solutions were covered with parafilm then left for 24 hours to crystalize at room temperature. The isolated crystals were separated and ethanol was evaporated using N_2 gas. Cubic-like crystals were collected and weighed (yield: white $[La(TPPO)_3(NO_3)_3]$ 0.4111 g, 69.86 %, yellow $[Ce(TPPO)_3(NO_3)_3]$ 1.4432 g, 78.80 % and purple $[Nd(TPPO)_3(NO_3)_3]$ 0.4057 g, 91.91 %).

5.5.4.5.1 BENCH TOP DISSOLUTION FOR THE TPPO COMPLEXES

Samples of the different TPPO complexes (0.2237 - 0.5182 g) were accurately weighed (to 0.1 mg) and quantitatively transferred into glass beakers. To each glass beaker 10 mL of a different acid (98 % H_2SO_4, 65 % HNO_3, 32 % HCl or *aqua regia* (HNO_3:HCl, 1:3)) was added, then stirred and left to dissolve. Only oily solutions were obtained from this dissolution, which could not be used for ICP-OES analysis. Hence dissolution using microwave digestion was attempted.

5.5.4.5.2 MICROWAVE-ASSISTED DISSOLUTION FOR TPPO COMPLEXES

8 mL of 98 % H_2SO_4 were added to portions (0.3437 - 0.6382 g) of the TTPO complexes and transferred into the clean microwave PTFE vessels. The microwave conditions indicated in **Table 5.2** were used for sample dissolution. Visual inspection indicated complete dissolution of all the samples after this digestion step with no appearance of any product or oily substances. The samples were then quantitatively transferred into 100.0 mL volumetric flasks. To ensure matrix matching 2 mL 98 % H_2SO_4 was added to each volumetric flask and homogenized. The volumetric flasks were then filled to the mark using ultra-pure water. The solutions were further diluted in order to ensure that the concentrations of La, Ce and Nd fall within the working range. 10.0 mL aliquots of these solutions were subsequently transferred to 100.0 mL volumetric flasks and filled to the mark with ultra-pure water. The solutions were analysed by ICP-OES and the results are given in **Table 5.22**.

[175] W Levason, E H Newman and M Webster, *Polyhedron*, 2000, Vol 19, pp2697-2705.

Table 5.22: La, Ce, and Nd recovery in different TPPO complexes using H_2SO_4 by microwave digestion.

	[La(TPPO)$(NO_3)_3$]	**[Ce(TPPO)$(NO_3)_3$]**	**[Nd(TPPO)$(NO_3)_3$]**
Mass range of metal (g)	0.3437 - 0.3500	0.6273 - 0.6382	0.3450 - 0.3440
Theoretical metal content (ppm)	4.0927 - 4.1676	7.5700 - 7.7015	4.2618 - 4.2742
Recovery % (s)*	98.66(4)	98.45(5)	99.4(2)
RSD (%)	0.04	0.05	0.16

*Average of 3 replicates

5.5.4.5.3 ELEMENTAL ANALYSIS (CHN)

Accurately weighed masses of the different TPPO complexes as well as pure TPPO were analysed for C, H and N content. The elemental analysis results for C, N, H and the lanthanum, cerium and neodymium metal content in the complexes are given in **Table 5.23**.

Table 5.23: Analytical data for pure TPPO and the different metal complexes.

Molecular formula	Empirical formula	Metal (%)	N (%)	C (%)	H (%)
		Found (Cald.)*•	Found (Cald.)*	Found (Cald.)*	Found (Cald.)*
TPPO	$C_{18}H_{15}OP$			79.86 (77.69)	5.21 (5.43)
$[La(TPPO)(NO_3)_3]$	$LaC_{54}H_{45}O_{12}P_3N_3$	11.82 (11.98)	3.49 (3.62)	57.66 (55.92)	3.88 (3.91)
$[Ce(TPPO)(NO_3)_3]$	$CeC_{54}H_{45}O_{12}P_3N_3$	11.88 (12.07)	3.43 (3.62)	57.74 (55.86)	3.80 (3.91)
$[Nd(TPPO)(NO_3)_3]$	$NdC_{54}H_{45}O_{12}P_3N_3$	12.31 (12.38)	3.44 (3.61)	56.28 (55.67)	3.85 (3.89)

*Average of 3 replicates

•ICP-OES analysed using H_2SO_4

5.5.4.5.4 INFRARED ANALYSIS

Infrared spectra of TPPO, $[La(TPPO)_3(NO_3)_3]$, $[Ce(TPPO)_3(NO_3)_3]$ and $[Nd(TPPO)_3(NO_3)_3]$ were recorded with a Digilab Scimitar Series spectrometer and they are reported in **Figure 5.14** and **Table 5.24**.

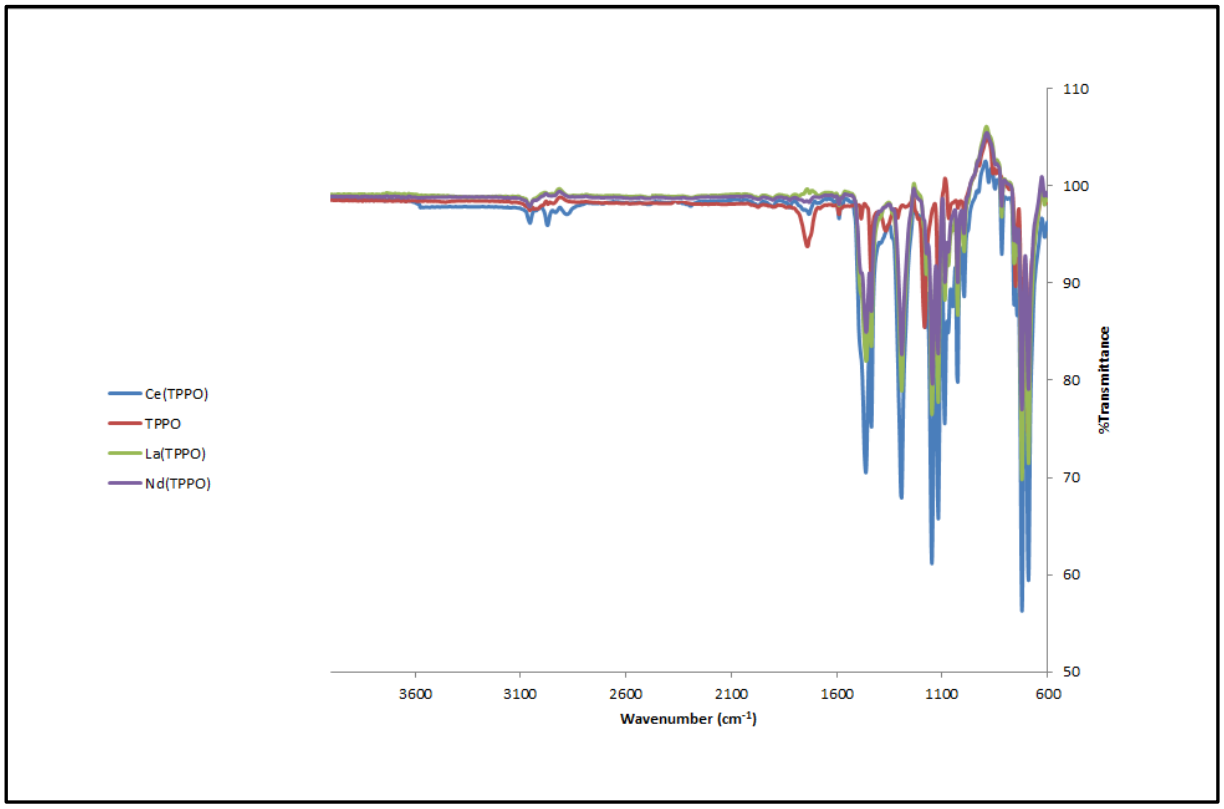

Figure 5.14: The IR spectra of TPPO and the different metal TPPO complexes.

Table 5.24: The IR stretching frequencies of TPPO and the different metal TPPO complexes.

Compound	ν (P=O)	ν (NO_3)	ν (NO_3)	ν (NO_3)
TPPO	1184.2			
$Y(NO_3)_3{\cdot}5H_2O$*		1489.9	1282.2	1028.6
$[La(TPPO)(NO_3)_3]$	1148.6	1460.7	1292.4	1087.2
$[Ce(TPPO)(NO_3)_3]$	1147.0	1464.5	1291.9	1086.8
$[Nd(TPPO)(NO_3)_3]$	1149.3	1463.1	1294.0	1088.4

*NO_3 stretching frequency

5.6 RESULTS AND DISCUSSION

5.6.1 LOD AND LOQ

The first step in this study was the determination of the LOD and LOQ of La, Ce and Nd using the ICP-OES prior to any analysis were done on the samples as discussed in **Section 5.2.3**. This La, Ce and Nd detection limits were obtained under ICP-OES instrument conditions and are reported in **Table 5.4**. In this study, the LOD was determined to range between 0.0030 - 0.0053 ppm for La, 0.0111 - 0.0188 ppm for Ce and 0.0076 - 0.0083 ppm for Nd while the LOQ were calculated as 0.0289 - 0.0530 ppm for La, 0.1114 - 0.1881 ppm for Ce and 0.0757 - 0.0832 ppm for Nd in the different acids used in this study. The LOD and LOQ were lower than the La, Ce and Nd concentrations that were quantified in this study.

Table 5.25: Comparison of LOD's in different studies.[176,177]

REE	This study•	Synthetic REE minerals	Biological samples	Water samples*	Geological materials
La	0.0030	0.0038	**0.1511**	0.3000	0.0079
Ce	0.0111	0.0094	**0.2950**	0.0060	0.0010
Nd	0.0083	0.0073	**0.2950**	0.0400	0.0339

*ppb

•H_2SO_4

The ICP-OES detection limits of this study compared favourably with the detection limits obtained for various samples (**Table 5.25**) in previous studies. According to the tabulated detection limits, only the REE detection limits of synthetic REE minerals studied[176] reported similar detection limits results as those obtained in this study

[176] S P Verma, E Santoyo and F Velasco-Tapia, *International Geology Review*, 2010, 44:4, p317.

[177] B Zawisza, K Pytlakowska, B Feist, M Polowniak, A Kita and Rl Sitko, *Journal of Analytical Atomic Spectrometry*, 2011, 26, pp2373-2390.

namely between 0.0038 - 0.0094 ppm, while biological samples studied were orders of magnitude larger[178] and water samples studied indicated LODs between 0.0400 and 0.3000 ppb.[177] Differences such as wavelengths and matrix matching may be attributed to these differences in the detection limits that were observed using ICP-OES for the REE quantification.

5.6.2 QUANTIFICATION AND CHARACTERISATION OF SAMPLES BY ICP-OES, IR AND CHN MICRO-ELEMENT ANALYSIS

5.6.2.1 PURE METALS

5.6.2.1.1 BENCH TOP DISSOLUTION AND MICROWAVE-ASSISTED DIGESTION

Bench top dissolution and microwave-assisted acid digestion were employed to dissolve the La metal pieces as well as Ce and Nd metal powder samples using HNO_3, HCl and H_2SO_4. The quantitative results are reported in **Table 5.5**. These results indicate the complete recovery of both La and Nd, but less successful recoveries for Ce. Complete dissolution of the La and Nd metal samples was generally achieved within 30 min in the different acids by bench top dissolution. The recovery for La ranged between 99.5(3) to 100.0(2) %, that for Ce between 81.37(9) to 95.30(8) % and between 97.9(5) to 99.7(3) % for Nd. The RSD for La were in the range of 0.08 - 0.26 %, for Ce between 0.08 - 0.23 % and that for Nd 0.28 - 0.51 %. These results showed acid effectiveness for Ce recovery in the order HCl < HNO_3 < H_2SO_4 as indicated by the recovery of the metal of 81.37(9) < 89.1(2) < 95.30(8) % respectively.

The microwave assisted acid digestion was mainly employed to improve the recovery of Ce metal as shown in **Table 5.6**. These results clearly show improved recovery of the Ce with % recovery ranging between 96.5 to 99.6 % for the different acids. The same order for metal recovery was obtained for the technique compared to the bench top dissolution HCl < HNO_3 < H_2SO_4. The Ce RSD in different acids (HNO_3, HCl and H_2SO_4) ranged between 0.28 %, 0.14 % and 0.32 %, and indicates a good precision of these determinations.

[178] Y Li and B Hu, *Journal of Hazardous Materials,* 2010, Vol 174, pp534-54.

5.6.2.2 INORGANIC SALTS

5.6.2.2.1 BENCH TOP DIGESTION FOR INORGANIC COMPOUNDS

Acid digestion was used to dissolve and quantify the La, Ce and Nd in inorganic nitrate salts using ICP-OES. The results in **Tables 5.7** indicated excellent recoveries for all three metals in these compounds. The recovery of La was found to be in the 98.6 to 100.2 % range, Ce in the 98.9 to 100.6 % range and that of Nd between 98.0 and 100.0 % for the different acids used in this study.

Both this set of results as well as those obtained for the pure metal quantification clearly indicate the experimental conditions employed (wavelengths, matrix matching, calibration curve and range) afforded the accurate quantification of the different metals in pure and well characterized samples.

5.6.2.3 MIXTURE OF INORGANIC SALTS

5.6.2.3.1 BENCH TOP DIGESTION FOR SYNTHETIC MINERAL

A bench top dissolution method was used to determine REE (La, Ce and Nd) in a mixture of the different inorganic nitrate salts using ICP-OES. The individual REE were mixed and HNO_3 (best recovery from previous results) was added prior to quantification. The REE recovery as recorded in **Tables 5.8** ranged from 98.7(3) to 99.4(6) % for the three REE. The RSD's were calculated to be between 0.28 to 0.57 %. These results clearly indicate that the REE can accurately be quantified in the presence of each other, employing the experimental conditions described in **Paragraph 5.4.1.2**.

5.6.2.4 QUANTIFICATION OF REE IN DIFFERENT ORGANOMETALLIC COMPLEXES

5.6.2.4.1 BENCH TOP DIGESTION FOR acac COMPLEXES

The analytical results obtained for the bench-top digestion of the $[Ln(acac)_3]\cdot nH_2O$ complexes using 98 % H_2SO_4, 65 % HNO_3 and 32 % HCI which are reported in **Table 5.10** indicate the complete digestion of these metal complexes. Excellent recoveries which are between 99.4(3) and 101.0(4) % for La, between 99.0(3) and 100.3(2) % for Ce and between 98.0(2) and 101.6(3) % for Nd in the different acids.

The RSD of La, Ce and Nd were calculated to be in the range of 0.09 - 0.42 %, 0.25 - 0.72 % and 0.21 - 0.92 % in the different acids respectively.

5.6.2.4.2 MICRO-ELEMENT ANALYSIS FOR acac COMPLEXES

The C, N, H and metal content obtained in this study and represented in **Table 5.11** are in good agreement with the proposed structures by Stites[169] (**Figures 5.15**). The elemental analysis of $[Ln(acac)_3]\cdot nH_2O$ (Ln = La, Ce, Nd; n = 0 for La, n = 1 for Ce, Nd) complexes shows 1:3 metal to ligand stoichiometry with anhydrous for La and monohydrate Ce and Nd complexes (see **Table 5.11**).[179] In addition, since there are three acac ligand rings and zero or one water molecule which are coordinated by the central Ln^{+3} ion it means that La is 8 and Ce and Nd 9 coordinated complexes. There are however conflicting data in the literature regarding the hydration of REE acac complexes. Pope *et al*[180] solved the problem of hydration number using x-ray diffraction and their results showed that acac complexes can accommodate mono-, di- and trihydrates. The hydration number of these complexes has been proved by chemical analyses, X-ray powder diffraction (XRD) patterns and infrared spectra.[181] Elemental analyses for example are relatively insensitive to the amount of water present in chelates. However, results reported by Koehler and Bos[182] indicated anhydrous acac complexes.

[179] A A Ansari, M Irfanullah and K Iftikhar, *Spectrochimica Acta Part A*, 2007, 67, p1179.

[180] G W Pope, J F Steinbach and W F Wagner, *Journal Inorganic and Nuclear Chem*istry, 1961, 20, p304.

[181] M F Richardson, W F Wagner and D E Sands, *Inorganic Chem*istry, 1968, Vol. 7, No. 12, pp2495-2500.

[182] J M Koehler and W G Bos, *Journal Inorganic and Nuclear. Chemistry Letters*, 1967, 8, p545.

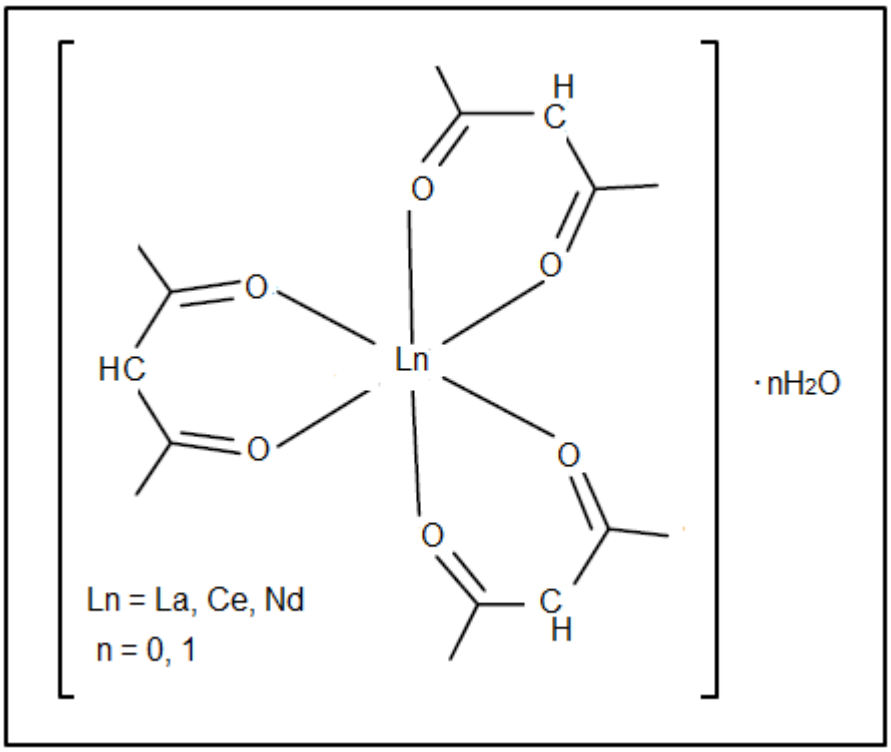

Figure 5.15: Proposed structure for the complexes.

5.6.2.4.3 INFRARED SPECTROSCOPY FOR acac COMPLEXES

The infrared spectrum of the acac was compared with $[Ln(acac)_3]\cdot nH_2O$ (Ln = La, Ce, Nd, n = 0, 1) complexes in order to ascertain the coordination sites that may be involved in chelation (**Table 5.12**). In the spectra of the free ligand (**Figure 5.10**), a band at 1708.5 cm^{-1} is assigned to ν(C=O) while the $[Ln(acac)_3]\cdot nH_2O$ complexes exhibit ν(C=O) stretching frequency at 1761.0 cm^{-1}. The carbonyl ν(CO) stretching vibration at 1608.4 cm^{-1} for the pure acac is shifted to lower frequency of about 1590.4 - 1603.6 cm^{-1} for the different metal complexes which indicates that the O atom of the ligand is coordinated to the central Ln^{+3} (La, Ce and Nd) ion. The coordination of acac ligand to the Ln^{+3} ion, promotes the reduction of the bond order of the carbonyl groups, hence the absorption shifts to lower stretching frequency.[183] It concludes that the electron cloud density of carbonyl becomes weaker. The ν(OH) absorption band in the $[Ln(acac)_3]\cdot H_2O$ (Ln = Ce, Nd) complexes at 3241.3 - 3243.9 cm^{-1} is attributable to water molecules. Abood and Ajam[184] reported that acac

[183] I G Zaitzeva, N P Kuzmina and L I Martynenko, *Journal of Alloys and Compounds*, 1995, 225, pp393-395.

[184] N A Abood and A F Ajam, *Journal of the Chemical Society of Pakistan,*1985, vol. 7, pp1-5.

has weak and strong bands at 1720 cm^{-1} and 1610 cm^{-1} respectively, which attributes the C=O stretching vibration of the keto form (a ketone or an aldehyde) and the C=O stretching vibration of the enol form (an alcohol). Kerim *et al*[185] also reported the carbonyl and OH stretching frequencies of the metal complexes ranged from 1608 - 1609 cm^{-1} and 3100 - 3600 cm^{-1} respectively.

5.6.2.4.4 BENCH TOP DIGESTION FOR dap COMPLEXES

Bench top dissolution as described in **Paragraph 5.5.2.2.1** was used for the quantification of the REE (La, Ce and Nd) in dap complexes by employing ICP-OES. The analytical results reported in **Table 5.13** indicated the complete digestion using H_2SO_4, HNO_3 or HCI by visual inspection. However their recovery results indicate the complete recovery of only Nd, but less successful recoveries for both La and Ce. The unsuccessful recovery of $[Ln(dap)(NO_3)_3]$ complexes may be due to the uncertainty regarding the accurate molecules structure of these complexes since no x-ray structure determination of this type of complexes has been reported. The proposed method enabled achieving recoveries ranging from 88.1(5) - 90.0(4) % for La, 91.4(3) - 95.5(3) % for Ce and 98.29(7) - 99.3(2) % for Nd together with the RSDs in the range of 0.48 - 2.02 % for La, 0.30 - 0.51 % Ce and 0.07 - 0.25 % for Nd.

5.6.2.4.5 MICRO-ELEMENT ANALYSIS FOR dap COMPLEXES

The ligand and its complexes were characterised in percentile content using a CHNO analyser and analytical data is summarised in **Table 5.14**. Different combinations of metal:dap:NO_3 have been calculated and final product $[Ln(dap)(NO_3)_3]$ was estimated to fit the reported C, N and H % recoveries the best for the composition of these complexes. This synthetic procedure predicted a $[Ln(dap)(NO_3)_3]$ complex formation with a 1:1 (M:L) stoichiometry. The analytical data of the ligand are not in good agreement since the experimental carbon content is slightly higher than the theoretical values while the nitrogen and hydrogen recoveries are lower than expected. **Figure 5.16** is proposed a scheme for the subsequent final product formation as predicted by the elemental analysis data presented in **Table 5.14**.

[185] F M Kerim, H F Aly and A El-Agramy, *Journal of Alloys and Compounds*, 1995, 225, pp393-395.

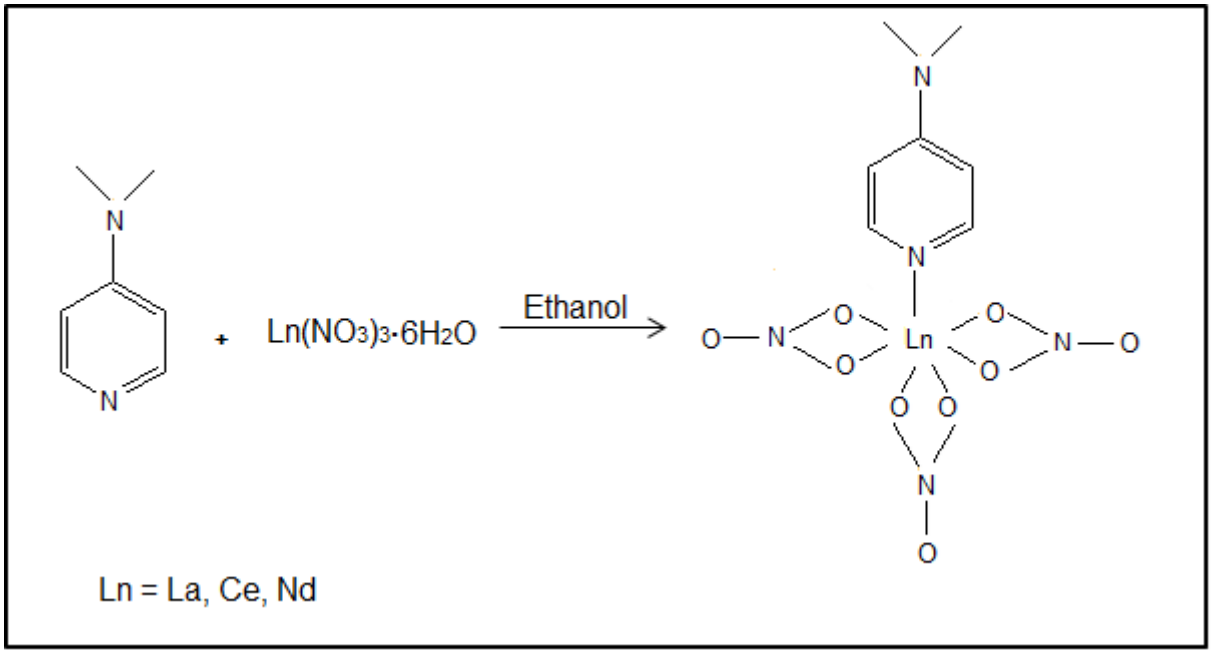

Figure 5.16: Schematic representation of a [Ln(dap)$(NO_3)_3$] complex.

5.6.2.4.6 INFRARED SPECTROSCOPY FOR dap COMPLEXES

The important IR stretching frequencies of dap and the different [Ln(dap)$(NO_3)_3$] (La, Ce and Nd) complexes are shown in **Table 5.15** and **Figure 5.11**. The strongest peaks at 1595.5 and 1513.6 cm^{-1} for dap can be attributed to ν(C=N) of the imine as well as ν(C=C) and ν(C=N) in the pyridinium ring respectively.[186] The C=C and C=N bands in all [Ln(dap)$(NO_3)_3$] complexes shifted to higher frequency at about 1645.1 - 1646.8 and 1562.1 - 1563.7 cm^{-1} due to the bond formation of the pyridyl nitrogen resulting in the change in C=C and C=N stretching modes. Hence the absorption shifts to higher stretching frequency. The IR spectra for all complexes show strong stretching frequencies that indicate coordinated nitrate groups within the complexes. The vibrations in the range of 1034.4 - 1035.5 cm^{-1}, 1309.3 - 1312.4 and 1437.0 - 1439.9 cm^{-1} are associated with the nitrate groups, suggesting that the nitrate groups form part of the ligand environment of the metal ions. The X-ray and neutron diffraction studies established that the nitrato groups have bidentate character for lanthanides (Ln = La, Pr, Nd, Sm, Gd, Dy, Dy or Ho) with the [N-(4-dimethylaminobenzalidene)amino]antipyrinethiosemicarbazone and pyridine complexes, hence the NO_3^- will occupy six coordinating positions, leaving only one position for dap. Dunstan and Khan[186] also reported the strong band at 1604 cm^{-1} in

[186] P O Dunstan and A M Khan, *Journal of the Chemical Thermodynamics*, 2013, 66, pp44-49.

the free ligand, attributed to ν(C=N) of imine. The nitrate complexes of REE metals show characteristic vibrational frequencies of the coordinated nitrate ions. Santhi and Namboori[187] reported stretching frequencies at 1430 cm^{-1}, 1310 cm^{-1} and 1073 cm^{-1} for the samarium complex which were not present in the ligand, and attributed them to nitrate ions vibrations.

5.6.2.4.7 BENCH TOP DIGESTION FOR nta COMPLEXES

The bench top dissolution method was used to determine the different REE (La, Ce and Nd) content in nta complexes. Excellent La, Ce and Nd recoveries were obtained from the complexes ranging from 99.1(8) to 101.8(5) %, 98.4(4) to 101.5(7) % and 100(3) to 100.8(7) % with the RSD 0.43 - 0.83 %, 0.41 - 0.72 % and 0.34 - 3.08 (**Table 5.19**) for La, Ce and Nd respectively.

5.6.2.4.8 MICRO-ELEMENT ANALYSIS FOR nta COMPLEXES

The different elemental analyses of the Ln(nta)·nH_2O (n = 1 for Ce, Nd, n = 2 for La) complexes indicated excellent C, H and N recovering as well as the metal for the complexes as predicted by the molecule structure in **Figure 5.17**. Combinations of metal:ligand (1:1) as well as one or two water molecules have been calculated, then compared with the final Ln(nta)·nH_2O product that Wang *et al*[171] obtained. The solid complexes prepared as showed by the 1:1 metal to ligand stoichiometry is confirmable by the elemental analysis as shown in **Table 5.20**. Analytical data of the ligand and its complexes are given in **Table 5.20**. A mechanism for the subsequent final product formation as reported by Wang's study is given by **Figure 5.17**. The [$Ln(nta)_n$]·nH_2O complexes are asymmetric units, hence trivalent Ce and Nd ions contain 8 coordinate metal centres based upon 3 oxygen and 1 nitrogen atoms from one ligand, 3 other oxygen atoms come from other ligands and 1 further oxygen atom come the water molecule. The La(III) ion on the other hand is 9-coordinated due to 1 additional oxygen atom from the water molecule.[188]

---

187 S Santhi and C G R Namboori, *International Journal of Chemical Technique Research*, 2013, Vol.5, No.4, pp1750-1755.

188 L Huanga, L Zhanga and L Jin, *Journal of Molecular Structure,* 2004, 692, pp121-126.

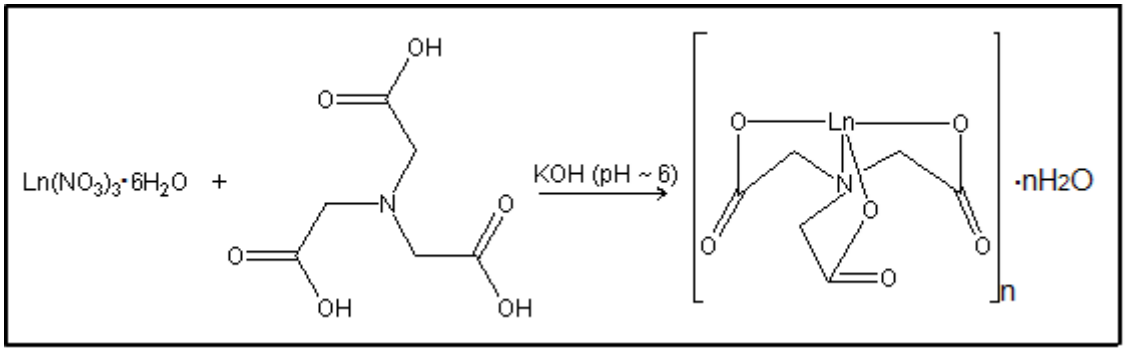

Figure 5.17: Schematic of representation of a $[Ln(nta)]_n \cdot H_2O$ complexes.

5.6.2.4.9 INFRARED SPECTROSCOPY FOR nta COMPLEXES

The infrared spectra of nta and $Ln(nta) \cdot nH_2O$ (Ln = La, Ce, Nd) complexes are presented in **Figure 5.13**. The carboxyl group is known to give a strong band at 1715.5 cm^{-1}, which is due to the C=O stretching frequency. The carboxylic group in nta at 1715.7 cm^{-1} disappeared in the different complexes, while ν_{as}(COO) at 1509.4 cm^{-1} and ν_s(COO) 1331.1 cm^{-1} of nta shifts to 1571.1 - 1591.2 and 1404.9 - 1423.1 cm^{-1} respectively in all metal complexes. Nakamoto *et al*[172] reported the un-ionized carboxyl group at 1720 - 1730 cm^{-1} in the free nta ligand. This confirms that the O atoms of all carboxylic groups are also coordinated to the Ln^{+3} ion and the wide (OH) bands at 3237.1 - 3243.3 cm^{-1}, showing the presence of H_2O in the complexes.[188] Wang *et al*[171] reported that the ν_{as}(COO) and ν_s(COO) stretching frequency at 1620 - 1584 cm^{-1} and 1340 - 1342 cm^{-1} for the free nta ligand and 1600 - 1610 cm^{-1} and 1410 - 1415 cm^{-1} for the Nd and Er complexes, respectively. The wide ν(OH) band showing the presence of H_2O in the complexes was found around 3460 - 3463 cm^{-1}.[189,190] Previously it was reported that a H_2O molecule is not coordinated to $[Nd(nta)_n]$. However, Huang and co-workers reported that the Nd^{+3} ion can coordinate with nta ligand and one or two water molecules.[191] The Visser *et al*[192]

[189] J Wang, Y Wang, Zh H Zhang, X D Zhang, X Zh Liu, G R Gao, X Y Liu and Y Zhang, *Russian Journal of Coordination Chemistry,* 2006, Vol. 32, No. 1, pp63-70.

[190] E J Salazar-Sandoval, M K G Johansson and A Ahniyaz, *The Royal Society of Chemitry Advances,* 2014, 4, pp9048-9055.

[191] Q Zhang, C Lu and W Yang, *Zeitschrift fuer Anorganische und Allgemeine Chemie*. 2004, 630, pp1550-1552.

[192] H G Visser, W Purcell and S S Basson, *Transition Metal Chemistry*, 2001, 26, p177.

study also showed that the ν(CO) stretching frequency in the nta ligand appears at about 1610 - 1670 cm^{-1} for the $[Co_2(nta)_2(\mu\text{-}OH)_2]_2$) complexes.

5.6.2.4.10 BENCH TOP DIGESTION FOR imda COMPLEXES

The analytical results obtained from the bench-top digestion of the $[Ln(imda)]\cdot H_2O$ complexes using H_2SO_4, HNO_3 and HCI indicated the complete digestion and recovering of the metal content. The analytical results reported in **Table 5.16** indicate excellent recoveries of 100.0(9) - 102(1) %, 98.6(4) - 99.0(2) % and 100.3(7) - 103.6(4) % with RSD of 0.93 - 1.02 %, 0.21 - 0.81 % and 0.07 - 0.72% for La, Ce and Nd respectively in all acids used in this study. A literature study[173] also indicated that lanthanide imda complexes can coordinate with H_2O molecules (see IR results in **Figure 5.12** and **Table 5.18** for predictable presence of H_2O). Hence The La, Ce and Nd complexes with imda ligand were prepared and their formula or composition are predicted to be $[La(imda)]\cdot H_2O$, $[Ce(imda)]\cdot H_2O$ and $[Nd(imda)]\cdot H_2O$.

5.6.2.4.11 MICRO-ELEMENT ANALYSIS FOR imda COMPLEXES

The $[Ln(imda)]\cdot H_2O$ (La, Ce, Nd) complexes were analyzed for C, H, N and metal content and the results are given in **Table 5.17**. On the basis of this data as well as those proposed as reaction product by Wang *et al*[176], indicated the successful preparation of the different $[Ln(imda)]\cdot H_2O$ complexes. These results show a 1:1 metal to ligand stoichiometry as well as the presence of a water molecule in the coordination sphere of the metal ion to produce (**Figure 5.18**), the type $[La(imda)]\cdot H_2O$, $[Ce(imda)]\cdot H_2O$ and $[Nd(imda)]\cdot H_2O$ complexes. The mechanism for the subsequent formation of the final product as reported by the Wang study is given in **Figure 5.18**. The $[Ln(imda)_n]\cdot H_2O$ complexes are asymmetric units as reported by the Huang[188] aminopolycarboxylic acids study. The $[Ln(imda)_n]\cdot H_2O$ complexes which contain six coordinate metal centres are based upon 2 oxygen and 1 nitrogen atoms from one ligand, with the other 2 oxygen atoms from other ligands and 1 oxygen atom from the water molecule.

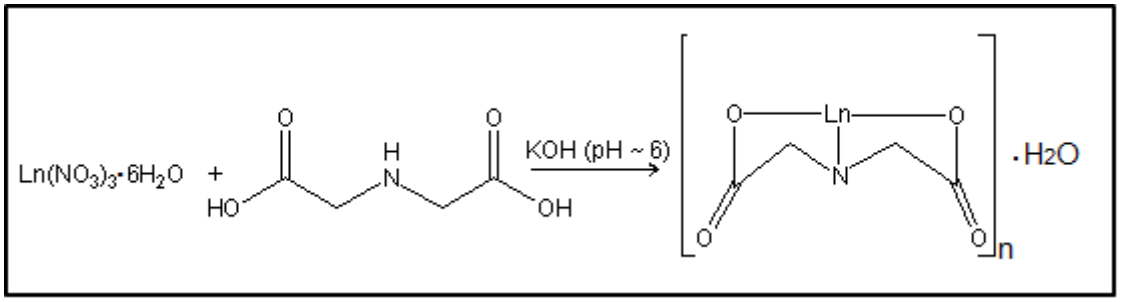

Figure 5.18: Schematic representation of a $[Ln(imda)]_n \cdot H_2O$ complexes.

5.6.2.4.12 INFRARED SPECTROSCOPY FOR imda OF COMPLEXES

Table 5.18 presents the most important infrared stretching frequencies of the pure imda and the respective REE complexes which were obtained from **Figure 5.12**. The stretching frequency of the imda at about 1738.4 cm^{-1} indicates the un-ionized and uncoordinated COO group stretching band. Nakamoto *et al*[193] reported the un-ionized carboxyl group at 1730 - 1710 cm^{-1} in the free imda ligand. This stretching frequency vanishes or shrinks in the case of metal complex formation as indicated in **Figure 5.12**. The imda ligand also exhibit $\nu_{as}(COO^-)$ and $\nu_s(COO^-)$ frequencies at 1578.0 cm^{-1} and 1364.3 cm^{-1}. These stretching frequencies shifted to 1554.6 - 1566.2 and 1394.0 - 1400.6 cm^{-1} respectively in the metal complexes. The ν(OH) absorption band in the $[Ln(imda)]\cdot H_2O$ complexes is observed at 3023.4 - 3454.4 cm^{-1} attributable to water molecules. Wang[194] also reported that $\nu_{as}(COO^-)$ and $\nu_s(COO^-)$ frequencies at 1636 - 1580 cm^{-1} and 1401 cm^{-1} in the imda ligand shifted to lower frequency at 1636 - 1559 and 1398 cm^{-1} respectively in the Nd complexes.

5.6.2.4.13 MICROWAVE-ASSISTED AND BENCH TOP DIGESTION OF TPPO COMPLEXES

Bench top dissolution of the different TPPO complexes using acids such as HCI, H_2SO_4, HNO_3 and *aqua regia* (HNO_3:HCI, 3:1) was attempted, but this method was not very successful. Visual inspection indicated the formation of oily products instead of clear solutions. ICP-OES analysis was not attempted on these mixed solutions

[193] K Nakamoto, Y Morimoto and A E Martell, *Organic and biological chemistry*, 1962, Vol. 84, pp2081-2084.

[194] L Wang, X Xu, D G Evans, X Duan and D Li, *Journal of Solid State Chemistry*, 2010, Volume 183, Issue 5, pp1114-1119.

fearing that the oily solutions may lead to carbon built-up in the ICP-OES torch leading to clogging or poor recoveries. Microwave assisted acid digestion was then employed to improve the dissolution of these complexes with the same series of acids mentioned above. Microwave assisted digestion using H_2SO_4 proved to be successful in dissolving all the TPPO complexes (**Table 5.26**). Dissolution of these complexes using the different acids solutions visually indicated poor recovery with the formation of decomposed products (burnt particles or a yellow-like gum substance) after the microwave digestion. ICP-OES recoveries of the different REE (La, Ce and Nd) are reported in **Table 5.22**.

Table 5.26: Comparison of the different REE TPPO complexes of the bench-top dissolution and microwave acid digestion.

TPPO complexes	Bench-top digestion				Microwave-assisted digestion			
	H_2SO_4	HNO_3	HCl	*Aqua regia*	H_2SO_4	HNO_3	HCl	*Aqua regia*
$[La(TPPO)_3(NO_3)_3]$	x	x	x	x	√√	x	x	x
$[Ce(TPPO)_3(NO_3)_3]$	x	x	x	x	√√	x	x	x
$[Nd(TPPO)_3(NO_3)_3]$	x	x	x	x	√√	x	x	x

√√- Successful dissolution

x- Not successful dissolution

The H_2SO_4 decomposition of the TPPO complexes using microwave digestion proved to be very successful with the selected REE recoveries ranging between 98.45(5) - 99.4(2) % and RSD in the range 0.04 - 0.16 % as shown in **Table 5.22**.

5.6.2.4.14 MICRO-ELEMENT ANALYSIS FOR TPPO COMPLEXES

The C, N and H recoveries for these isolated REE TPPO complexes are in excellent agreement with the predicted molecular or empirical formula as predicted by

Levason[180] and as confirmed by the crystal structure determined by Kuhn[195] as indicated in **Figure 5.19**. These proposed structures of the $[Ln(TPPO)_3(NO_3)_3]$ complexes show 1:3 metal to ligand stoichiometry **Table 5.23**. The analytical data obtained in this study compares extremely well with the X-ray crystal structures of the TPPO complexes that were obtained by Kuhn. The structures obtained by Kuhn indicated that these reactions produce $[Ln(TPPO)_3(NO_3)_3]$ type complexes in which the metal ion has a coordination number of nine and bonded to three phosphine oxides and three bidentately bonded nitrate ligands. The following mechanism in **Figure 5.19** is proposed for the formation of a 1:3 complex as well as for the subsequent $[Ln(TPPO)_3(NO_3)_3]$ complex formation.

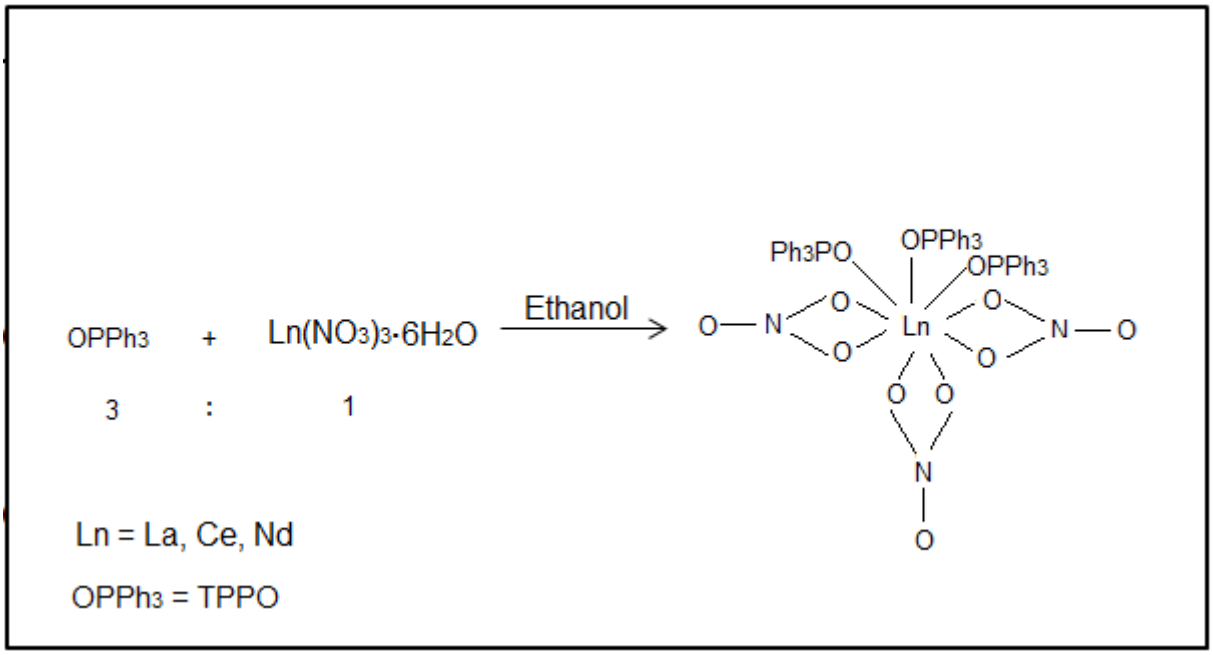

Figure 5.19: Schematic representation of a $[Ln(TPPO)_3(NO_3)_3]$ complex.

5.6.2.4.15 INFRARED SPECTROSCOPY FOR TPPO COMPLEXES

The important infrared stretching frequencies of the TPPO and the different REE complexes are shown in **Figure 5.14** and **Table 5.24**. The strongest peak at 1184.2 cm^{-1} for the free TPPO can be attributed to the free phosphine group, which then shifts to lower frequencies when coordinated as in all $[Ln(TPPO)_3(NO_3)_3]$

[195] K Kuhn, Submitted in partial fulfillment of the requirements for the degree, *Magister Scientiae at the Nelson Mandela Metropolitan University library*, 2012, pp21-22.

complexes to about 1147.0 - 1149.3 cm^{-1}. This demonstrates the involvement of the oxygen atom of the phosphine oxides coordinating to the metal ion. This P=O frequency in the complexes is explained by the nature of the lanthanide ion (the decrease of the ionic radius) and of the coordination number of the metal. The IR spectra also show bonding modes of the nitrate group in the metal complexes. The $\nu(NO_3)$ vibrations are in the range of 1460.7 - 1464.5, 1291.9 - 1294.0, and 1086.8 - 1088.4 cm^{-1}, and are associated with the nitrate groups. Literature indicated that the PO stretching frequency of $OPPh_3$ (1170 - 1200 cm^{-1}) decreases to lower stretching frequency by about 20 to 70 cm^{-1}, indicating a decrease in the stretching force constant of the P=O bond as a consequence of the complex formation which confirms that the TPPO are coordinated to the Ln^{+3} ion.[196] Similar results reported by Kuhn[195] give ν(PO) vibrations at 1195 and 1147 - 1149 4 cm^{-1} for the ligand and the three metal complexes respectively, while the absorption bands at 1460 - 1461, 1292 - 1294 and 1028 - 1029 4 cm^{-1} are attributed to $\nu(NO_3)$ vibrations of the complexes.[180]

5.7 CONCLUSION

Bench top dissolution yielded excellent results for all REE that were studied, namely La, Ce and Nd. Excellent recoveries were obtained from all the pure REE metal and inorganic compounds as well as the mixture containing all three elements, ranging from 97.9(5) to 100.6(1) % except for Ce. The pure Ce metal recovery ranged from 81.37(9) to 95.30(8) %. Microwave assisted acid digestion was employed in an effort to improve the recovery of Ce metal. The Ce recovery improved and the % Ce increased to between 96.5 and 99.6 % with the acid order HCI < HNO_3 < H_2SO_4. Excellent recoveries were also obtained for all the synthesised the organometallic complexes ranging from 98.0(2) to 103.6(4) %, except for [Ln(dap)$(NO_3)_3$ Ln = La, Ce] which varied between 88.1(5) and 95.5(3) % for these two metals. The successful recovery of the acac, imda, nta and TPPO complexes of the different metals is mainly due to the fact that they have been well characterised by X-ray

[196] K Nakamoto, Infrared spectra of inorganic and coordination compounds, *Wiley-intersience, a division of John Wiley & Sons*, 2nd edition, 1963, p186.

crystallography and have a known chemical structure. The exact chemical structure of the different dap complexes are still to be obtained which may explain the less than satisfactorily recoveries.

Characterisation of synthesised organometallic complexes and ligands using IR also played a huge role to identify if any coordination between the metal and the ligand exists. Significant changes in the stretching frequencies of the free ligand compared to that of the complexes, for example shifting to low or high wavenumber or disappearing or appearing indicate the successful bonding of the ligand to the metal centre.

The quantification results obtained for the pure REE metal, inorganic compounds as well as synthesised organometallic complexes samples clearly indicate that the experimental conditions employed during this study afforded the accurate quantification of the different metals. Excellent recovery of the elements is mainly attributed to careful wavelength selection which minimized or prevented any spectral overlap with that of the other elements and secondly to acid matrix matching.

5.8 METHOD VALIDATION

Method validation is the final step that is used to confirm whether the newly developed methods employed in this study was suitable for quantifying the REE (La, Ce and Nd) accurately in pure REE metal, inorganic compounds and organometallic complexes. All the analytical data obtained in this study for different samples are compiled to evaluate their reproducibility since it is important that the proposed procedure is validated for analytical purposes. Typical method validation should consider the following parameters: accuracy, linearity, precision, range, robustness, selectivity, specificity, limit of detection (LOD) and quantification (LOQ). These are evaluated for the La, Ce and Nd analyses performed in this study.

Statistical tests were performed at the confidence interval of 95 % for 3 experimental replicates. The *t*-test is one of the most important tools or parameters to decide if there is any statistical difference between the expected and experimentally obtained results e.g. the accuracy of the analysis. The t-crit is equal to ±4.30 depending on the number of replicates at 95 % confidence interval. A new *t*-test value is calculated by **Equation 4.10** in **Chapter 4** and compared with the theoretical value (tabulated) and then one at the assumptions is accepted or rejected using hypothesis testing criteria. If the calculated t-test value is larger than t-crit it means it will be rejected and *vice versa* the null hypothesis will be accepted. All the validation parameters evaluated using the ICP-OES for lanthanum, cerium and neodymium analysis in the various samples in the different acids used in this study are presented in **Table 5.27** to **Table 5.47**.

Table 5.27: Validation of La, Ce and Nd in pure metal using HCl.

Validation Criteria	Parameter	La	Ce	Nd
Recovery	Mean % (s)	99.97(7)	81.37(9)	99.4(4)
Precision	RSD (%)	0.08	0.11	0.37
Working Range	Calibration Curve	1 - 10 ppm		
Linearity	r^2	1	0.9999	0.9999
Sensitivity	Slope	1.7337	0.2592	0.5647
Selectivity	S_m	0.0028	0.0014	0.0028
Error of the Slope	Y-intercept	0.2469	0.0249	0.0503
Specificity	S_c	0.0149	0.0074	0.0149
t-crit at 95 % confidence interval		4.30		
t-value		-0.75	-354.98	-3.08
Null hypothesis		Accept	Reject	Accept

S_m = Standard deviation of the slope (also as S_a)

S_c = Standard deviation of the intercept (also as S_b)

Table 5.28: Validation of La, Ce and Nd in pure metal using HNO_3.

Validation Criteria	Parameter	La	Ce	Nd
Recovery	Mean % (s)	99.3(3)	89.1(2)	99.7(3)
Precision	RSD (%)	0.26	0.23	0.28
Working Range	Calibration Curve	1 - 10 ppm		
Linearity	r^2	0.9997	1	0.9997
Sensitivity	Slope	1.7765	0.2748	0.5738
Selectivity	S_m	0.0051	0.0007	0.0058
Error of the Slope	Y-intercept	-0.0039	-0.0025	0.0196
Specificity	S_c	0.0269	0.0037	0.0304
t-crit at 95 % confidence interval		4.30		
t-value		-3.37	-90.94	-2.05
Null hypothesis		Accept	Reject	Accept

Table 5.29: Validation of La, Ce and Nd in pure metal using H_2SO_4.

Validation Criteria	Parameter	La	Ce	Nd
Recovery	Mean % (s)	100.0(2)	95.30(8)	97.9(5)
Precision	RSD (%)	0.20	0.08	0.51
Working Range	Calibration Curve	1 - 10 ppm		
Linearity	r^2	0.9999	0.9997	0.9999
Sensitivity	Slope	1.7965	0.2887	0.6419
Selectivity	S_m	0.0080	0.0027	0.0040
Error of the Slope	Y-intercept	-0.1767	-0.0470	-0.0140
Specificity	S_c	0.0422	0.0143	0.0211
t-crit at 95 % confidence interval		4.30		
t-value		0.30	-27.80	-13.66
Null hypothesis		Accept	Reject	Reject

Table 5.30: Validation of Ce in pure metal using microwave assisted acid digestion.

Validation Criteria	Parameter	HCl	HNO_3	H_2SO_4
Recovery	Mean % (s)	96.5(1)	99.6(3)	98.7(3)
Precision	RSD (%)	0.14	0.28	0.32
Working Range	Calibration Curve	1 - 10 ppm		
Linearity	r^2	1	1	1
Sensitivity	Slope	0.2827	0.3012	0.2580
Selectivity	S_m	0.0009	0.0011	0.0005
Error of the Slope	Y-intercept	0.0021	0.0156	0.0014
Specificity	S_c	0.0049	0.0058	0.0027
t-crit at 95 % confidence interval		4.30		
t-value		-46.33	-2.44	-7.27
Null hypothesis		Reject	Accept	Reject

Table 5.31: Validation of La, Ce and Nd inorganic compounds using HCl.

Validation Criteria	Parameter	La	Ce	Nd
Recovery	Mean % (s)	100.2(2)	99.7(2)	100.0(1)
Precision	RSD (%)	0.17	0.19	0.11
Working Range	Calibration Curve	1 - 10 ppm		
Linearity	r^2	0.9999	0.9997	0.9999
Sensitivity	Slope	1.3511	0.2254	0.4704
Selectivity	S_m	0.0092	0.0023	0.0028
Error of the Slope	Y-intercept	0.1097	-0.0023	0.0096
Specificity	S_c	0.0486	0.0123	0.0150
t-crit at 95 % confidence interval		4.30		
t-value		0.09	-0.12	0.01
Null hypothesis		Accept	Accept	Accept

Table 5.32: Validation of La, Ce and Nd inorganic compounds using HNO_3.

Validation Criteria	Parameter	La	Ce	Nd
Recovery	Mean % (s)	99.6(2)	100.6(1)	100.0(2)
Precision	RSD (%)	0.22	0.13	0.16
Working Range	Calibration Curve	1 - 10 ppm		
Linearity	r^2	1	0.9999	0.9997
Sensitivity	Slope	1.2925	0.2231	0.4345
Selectivity	S_m	0.0045	0.0010	0.0047
Error of the Slope	Y-intercept	0.0922	0.0071	0.0168
Specificity	S_c	0.0239	0.0052	0.0246
t-crit at 95 % confidence interval		4.30		
t-value		-0.09	0.17	0.01
Null hypothesis		Accept	Accept	Accept

Table 5.33: Validation of La, Ce and Nd inorganic compounds using H_2SO_4.

Validation Criteria	Parameter	La	Ce	Nd
Recovery	Mean % (s)	98.6(2)	98.91 (5)	98.0(2)
Precision	RSD (%)	0.22	0.05	0.21
Working Range	Calibration Curve	1 - 10 ppm		
Linearity	r^2	0.9999	0.9997	0.9999
Sensitivity	Slope	1.3265	0.2236	0.4129
Selectivity	S_m	0.0068	0.0022	0.0024
Error of the Slope	Y-intercept	0.2117	-0.0063	-0.0066
Specificity	S_c	0.0360	0.0117	0.0126
t-crit at 95 % confidence interval		4.30		
t-value		-0.59	-0.20	-0.86
Null hypothesis		Accept	Accept	Accept

Table 5.34: Validation of La, Ce and Nd synthetic minerals using HNO_3.

Validation Criteria	Parameter	La	Ce	Nd
Recovery	Mean % (s)	99.3(3)	99.4(6)	98.7(3)
Precision	RSD (%)	0.32	0.57	0.28
Working Range	Calibration Curve	1 - 10 ppm		
Linearity	r^2	1	0.9999	0.9996
Sensitivity	Slope	1.8754	0.2970	0.5666
Selectivity	S_m	0.0052	0.0019	0.0068
Error of the Slope	Y-intercept	-0.0354	-0.0010	-0.0100
Specificity	S_c	0.0272	0.0099	0.0357
t-crit at 95 % confidence interval		4.30		
t-value		-3.93	-1.75	-8.61
Null hypothesis		Accept	Accept	Reject

Table 5.35: Validation of La, Ce and Nd in $[Ln(acac)_3]\cdot nH_2O$ using HCl.

Validation Criteria	Parameter	La	Ce	Nd
Recovery	Mean % (s)	99.4(3)	99.0(3)	101.6(3)
Precision	RSD (%)	0.32	0.31	0.27
Working Range	Calibration Curve	1 - 10 ppm		
Linearity	r^2	1	0.9999	0.9998
Sensitivity	Slope	1.7135	0.2542	0.4685
Selectivity	S_m	0.0070	0.0014	0.0036
Error of the Slope	Y-intercept	-0.0904	-0.0136	0.0334
Specificity	S_c	0.0369	0.0075	0.0188
t-crit at 95 % confidence interval		4.30		
t-value		-3.22	-5.85	10.22
Null hypothesis		Accept	Reject	Reject

Table 5.36: Validation of La, Ce and Nd in $[Ln(acac)_3]\cdot nH_2O$ using HNO_3.

Validation Criteria	Parameter	La	Ce	Nd
Recovery	Mean % (s)	101.0(4)	100.3(2)	98.0(2)
Precision	RSD (%)	0.42	0.25	0.21
Working Range	Calibration Curve	1 - 10 ppm		
Linearity	r^2	1	1	0.9999
Sensitivity	Slope	1.7213	0.2599	0.4793
Selectivity	S_m	0.0052	0.0008	0.0024
Error of the Slope	Y-intercept	0.0768	0.0016	0.0290
Specificity	S_c	0.0276	0.0044	0.0128
t-crit at 95 % confidence interval		4.30		
t-value		4.21	2.11	-16.27
Null hypothesis		Accept	Accept	Reject

Table 5.37: Validation of La, Ce and Nd in $[Ln(acac)_3]\cdot nH_2O$ using H_2SO_4.

Validation Criteria	Parameter	La	Ce	Nd
Recovery	Mean % (s)	100.01 (9)	99.2(7)	100.1(9)
Precision	RSD (%)	0.09	0.72	0.92
Working Range	Calibration Curve	1 - 10 ppm		
Linearity	r^2	0.9998	0.9999	1
Sensitivity	Slope	1.5348	0.2216	0.4128
Selectivity	S_m	0.0110	0.0014	0.0013
Error of the Slope	Y-intercept	-0.0386	0.0167	0.0100
Specificity	S_c	0.0578	0.0074	0.0066
t-crit at 95 % confidence interval		4.30		
t-value		0.22	-1.93	0.18
Null hypothesis		Accept	Accept	Accept

Table 5.38: Validation of La, Ce and Nd in [Ln(dap)$(NO_3)_3$] using HCl.

Validation Criteria	Parameter	La	Ce	Nd
Recovery	Mean % (s)	90.0(4)	91.4(3)	99.3(2)
Precision	RSD (%)	0.48	0.36	0.25
Working Range	Calibration Curve	1 - 10 ppm		
Linearity	r^2	0.9999	0.9999	0.9998
Sensitivity	Slope	1.8281	0.2704	0.6567
Selectivity	S_m	0.0102	0.0017	0.0056
Error of the Slope	Y-intercept	0.0530	0.0333	0.0070
Specificity	S_c	0.0536	0.0092	0.0295
t-crit at 95 % confidence interval		4.30		
t-value		-39.98	-44.80	-4.97
Null hypothesis		Reject	Reject	Reject

Table 5.39: Validation of La, Ce and Nd in [Ln(dap)$(NO_3)_3$] using HNO_3.

Validation Criteria	Parameter	La	Ce	Nd
Recovery	Mean % (s)	90(2)	91.4(5)	98.3(1)
Precision	RSD (%)	2.02	0.57	0.18
Working Range	Calibration Curve	1 - 10 ppm		
Linearity	r^2	0.9998	0.9998	0.9997
Sensitivity	Slope	1.8292	0.2625	0.5710
Selectivity	S_m	0.0140	0.0022	0.0057
Error of the Slope	Y-intercept	0.1123	-0.0213	0.0457
Specificity	S_c	0.0739	0.0117	0.0300
t-crit at 95 % confidence interval		4.30		
t-value		-9.69	-28.57	-17.34
Null hypothesis		Reject	Reject	Reject

Table 5.40: Validation of La, Ce and Nd in [Ln(dap)$(NO_3)_3$] using H_2SO_4.

Validation Criteria	Parameter	La	Ce	Nd
Recovery	Mean % (s)	88.1(5)	95.5(3)	98.29(7)
Precision	RSD (%)	0.60	0.30	0.07
Working Range	Calibration Curve	1 - 10 ppm		
Linearity	r^2	0.9999	1	0.9997
Sensitivity	Slope	1.7309	0.3049	0.6280
Selectivity	S_m	0.0091	0.0028	0.0018
Error of the Slope	Y-intercept	0.0646	-0.1248	-0.0670
Specificity	S_c	0.0480	0.0150	0.0092
t-crit at 95 % confidence interval		4.30		
t-value		-39.09	-27.50	-44.72
Null hypothesis		Reject	Reject	Reject

Table 5.41: Validation of La, Ce and Nd in [Ln(imda)]·nH_2O using HCl.

Validation Criteria	Parameter	La	Ce	Nd
Recovery	Mean % (s)	101.9(9)	99.0(2)	100.76(7)
Precision	RSD (%)	0.93	0.21	0.07
Working Range	Calibration Curve	1 - 10 ppm		
Linearity	r^2	0.9999	0.9999	0.9998
Sensitivity	Slope	1.8281	0.2704	0.6567
Selectivity	S_m	0.0102	0.0017	0.0056
Error of the Slope	Y-intercept	0.0530	0.0333	0.0070
Specificity	S_c	0.0536	0.0092	0.0295
t-crit at 95 % confidence interval		4.30		
t-value		-6.23	-5.65	18.73
Null hypothesis		Reject	Reject	Reject

Table 5.42: Validation of La, Ce and Nd in [Ln(imda)]·nH_2O using HNO_3.

Validation Criteria	Parameter	La	Ce	Nd
Recovery	Mean % (s)	102(1)	98.7(8)	103.4(4)
Precision	RSD (%)	1.02	0.81	0.34
Working Range	Calibration Curve	1-10 ppm		
Linearity	r^2	0.9998	0.9998	0.9997
Sensitivity	Slope	1.7309	0.3049	0.6280
Selectivity	S_m	0.0091	0.0028	0.0018
Error of the Slope	Y-intercept	0.0646	-0.1248	-0.0670
Specificity	S_c	0.0480	0.0150	0.0092
t-crit at 95 % confidence interval		4.30		
t-value		3.37	-3.05	-0.38
Null hypothesis		Accept	Accept	Accept

Table 5.43: Validation of La, Ce and Nd in [Ln(imda)]·nH_2O using H_2SO_4.

Validation Criteria	Parameter	La	Ce	Nd
Recovery	Mean % (s)	100.0(9)	98.6(4)	100.3(7)
Precision	RSD (%)	0.93	0.44	0.72
Working Range	Calibration Curve	1 - 10 ppm		
Linearity	r^2	0.9999	0.9997	1
Sensitivity	Slope	1.7309	0.3049	0.6280
Selectivity	S_m	0.0091	0.0028	0.0018
Error of the Slope	Y-intercept	0.0646	-0.1248	-0.0670
Specificity	S_c	0.0480	0.0150	0.0092
t-crit at 95 % confidence interval		4.30		
t-value		-0.35	-7.36	0.57
Null hypothesis		Accept	Reject	Accept

Table 5.44: Validation of La, Ce and Nd in [Ln(nta)]·nH_2O using HCl.

Validation Criteria	Parameter	La	Ce	Nd
Recovery	Mean % (s)	99.1(8)	99.4(6)	100.3(3)
Precision	RSD (%)	0.82	0.56	0.34
Working Range	Calibration Curve	1 - 10 ppm		
Linearity	r^2	0.9997	0.9998	0.9997
Sensitivity	Slope	0.6986	0.1434	0.2839
Selectivity	S_m	0.0140	0.0013	0.0042
Error of the Slope	Y-intercept	0.0197	-0.0165	-0.0455
Specificity	S_c	0.0739	0.0067	0.0219
t-crit at 95 % confidence interval		4.30		
t-value		-13.28	-2.46	0.87
Null hypothesis		Reject	Accept	Accept

Table 5.45: Validation of La, Ce and Nd in [Ln(nta)]·nH_2O using HNO_3.

Validation Criteria	Parameter	La	Ce	Nd
Recovery	Mean % (s)	100.6(4)	101.5(7)	100.8(7)
Precision	RSD (%)	0.43	0.72	0.70
Working Range	Calibration Curve	1 - 10 ppm		
Linearity	r^2	0.9999	1	0.9998
Sensitivity	Slope	1.0329	0.1171	0.1686
Selectivity	S_m	0.0062	0.0004	0.0015
Error of the Slope	Y-intercept	-0.031	0.0109	0.0005
Specificity	S_c	0.0328	0.0021	0.0079
t-crit at 95 % confidence interval		4.30		
t-value		-19.31	0.06	1.52
Null hypothesis		Reject	Accept	Accept

Table 5.46: Validation of La, Ce and Nd in $[Ln(nta)]\cdot nH_2O$ using H_2SO_4.

Validation Criteria	Parameter	La	Ce	Nd
Recovery	Mean % (s)	101.8(5)	98.4(4)	100(3)
Precision	RSD (%)	0.49	0.41	3.08
Working Range	Calibration Curve	1 - 10 ppm		
Linearity	r^2	1	0.9998	0.9993
Sensitivity	Slope	1.2660	0.1109	0.2551
Selectivity	S_m	0.0040	0.0008	0.0039
Error of the Slope	Y-intercept	-0.0625	-0.0282	-0.0429
Specificity	S_c	0.0215	0.0042	0.0203
t-crit at 95 % confidence interval		4.30		
t-value		-12.55	-1.39	-0.17
Null hypothesis		Reject	Accept	Accept

Table 5.47: Validation of La, Ce and Nd in $[Ln(TPPO)_3(NO_3)_3]$ complexes using H_2SO_4.

Validation Criteria	Parameter	La	Ce	Nd
Recovery	Mean % (s)	98.66(4)	98.45(5)	99.4(2)
Precision	RSD (%)	0.16	0.04	0.05
Working Range	Calibration Curve	1 - 10 ppm		
Linearity	r^2	0.9999	0.9997	0.9997
Sensitivity	Slope	1.2492	0.1581	0.2579
Selectivity	S_m	0.0042	0.0008	0.0014
Error of the Slope	Y-intercept	- 0.0071	- 0.0012	- 0.0043
Specificity	S_c	0.0168	0.0043	0.0072
t-crit at 95 % confidence interval		4.30		
t-value		-3.39	-2.50	-2.94
Null hypothesis		Accept	Accept	Accept

5.9 CONCLUSION

The results for the La, Ce and Nd in pure REE metal, inorganic compounds and organometallic complexes were validated with the use of the external calibration method. This proved to produce excellent results for all the previous quantitative analysis and was chosen as the preferred method of analysis were in the region of acceptance at 95 % confidence interval. Most of the results validated for the three metals content in different chemical substances with same conditions, rejected low percentile recovery results. The method validation done in **section 5.8** was considered satisfactory. All calibration curves showed good linearity by the excellent r^2 values which range between 0.9997 to 1 and their slopes were also fairly constant. In addition their LOD range between 0.0030 - 0.0188 ppm and their LOQ between 0.0289 - 0.1881 ppm in the different acids used in this study. It can be concluded that the La, Ce and Nd analyses were very successful for the analysis of the La, Ce and Nd content in pure REE metal, inorganic compounds and organometallic complexes and that the results met most of the guidelines within acceptable criteria, except for pure Ce metal and dap complexes.

6 EVALUATION OF THE STUDY AND FUTURE RESEARCH

6.1 INTRODUCTION

The main purpose of this chapter was to evaluate the achievements of this study compared to the objectives indicated in **Chapter 1**, **Paragraph 1.2** and secondly to identify possible future projects that may compliment the study.

6.2 EVALUATION OF THE STUDY

The objectives of this study as outlined at the beginning of this study were as follows:

- Perform an in-depth literature study on the analytical techniques for the analysis of REE.
- Develop an analytical procedure that can accurately determine and quantify lanthanum, cerium and neodymium in pure REE metal, inorganic compounds as well as in organometallic complexes.
- Determine the influence of different acids on the lanthanum, cerium and neodymium recoveries.
- Compare the results of different analytical techniques such as ICP-OES, IR and CHNS-micro analyser.
- Statistically validate the success of the most efficient analytical techniques.

This study has been successful in achieving all of the objectives as outlined in **Section 1.2** in **Chapter 1** and as reflected by the results obtained in **Chapter 5**. The different samples were successfully dissolved using different dissolution techniques and the efficiency of each technique was assessed using an ICP-OES analysis. The complete dissolution of the pure metal samples and inorganic nitrate salts was successfully accomplished using H_2SO_4, HNO_3 and HCI. However, low Ce recoveries

were obtained in these different acids under the said experimental conditions. Microwave assisted acid digestion was then employed to improve the recovery of Ce metal which yielded improved recovery in H_2SO_4. Bench top dissolution using H_2SO_4, HNO_3 and HCI was also attempted for the dissolution of different organometallic complexes. This dissolution method was successful in completely dissolving acac, dap, imda and nta complexes by visual inspection. In the case of TPPO complexes the bench top dissolution resulted in formation of oily solutions which were not suitable for ICP-OES analysis. Microwave assisted acid digestion was again employed to improve the dissolution of these complexes and recoveries of the metallic elements using the same acids used in the bench top dissolution. Complete sample dissolution and a clear solution was obtained using only H_2SO_4 microwave assisted digestion for a TPPO complex dissolution. The other acids formed jelly-like solutions with the TPPO complexes under microwave conditions. The results obtained showed that the developed analytical method of ICP-OES using external calibration is capable of accurately quantifying La, Ce and Nd content in pure REE metal, inorganic compounds and organometallic complexes in this study.

Validation of the ICP-OES and method showed the remarkable performance of ICP-OES as indicated by the validation parameters such as accuracy, precision, specificity, limit of detection, limit of quantitation and linearity. Most of the results from the pure REE metal, inorganic compounds and organometallic complexes by bench top dissolution method were found to be in the acceptable range of the hypothesis test at 95 % confidence interval, except for pure Ce metal and all the three metals in dap complexes (**Table 5.27** - **Table 5.47)**. Microwave digestion of pure Ce metal and TPPO complexes produced acceptable metal recoveries only in HNO_3 and H_2SO_4 respectively. It can therefore be concluded that all the objectives were successfully achieved as outlined in the beginning of this thesis (**Chapter 1**, **Paragraph 1.2**).

6.3 FUTURE RESEARCH

The study also revealed some potential projects which could be investigated following the current study. The following possible projects may be pursued to gain further understanding of the chemistry and quantification of the early REE.

- The potential X-ray crystallographic study for determining the structure of dimethylaminopyridine complex samples. The low metal recoveries may be due to the incorrect chemical structure predicted in this study. It is therefore believed that the determination of the correct chemical structure would indicate whether the low metal recoveries are due to the dissolution or analytical incapabilities. This study will also highlight the coordination chemistry of REE.
- Probably the most interesting future study could come from quantifying and characterizing different REE mineral ores containing these three metals (La, Ce and Nd). The presence of up to 30 % of Th (which this laboratory is not equipped to handle) in available monazite mineral samples limited the current study to only mimicking the ratios of the main elements in most of the mineral samples. However, the composition of the mineral will always be different and therefore, pose a different challenge.
- A comparative study on the use of complementary analytical techniques such as ultraviolet-visible absorption spectrometry (UV-Vis) and atomic absorption spectroscopy (AAS) to analyze all these metal samples quantitatively and for the characterization of some of the products isolated.
- Separation of REE using new and innovative methods are extremely important processes needed by industry for the beneficiation of these metals.

Summary

The aim of this study was to develop an analytical procedure to accurately quantify the early REE (La, Ce and Nd) in pure REE metal, in inorganic compounds as well as in a mixture containing all three elements and finally in organometallic complexes. The study involved the use of different inorganic acids such as H_2SO_4, HNO_3 and HCl as dissolution reagents and determination of their influence on the La, Ce and Nd recoveries. Both bench top and microwave dissolution were used in this study. Different analytical techniques such as inductively coupled plasma optical emission spectrometry (ICP-OES), CHNS-micro analyser and infrared spectroscopy (IR) were used to characterise and quantify the REE in the different samples. Validation parameters such as accuracy, precision, linearity, sensitivity, etc., using ICP-OES analysis were also evaluated (**Chapter 4**) to determine the suitability of the digestion and quantifying methods for REE analyses. Analytical lines (wavelengths) were carefully selected to minimize or prevent any spectral overlap with the other rare earth elements investigated in this study. Secondly, the acid matrix was strictly matched throughout the analytical process to ensure accurate analytical measurements and well controlled experimental conditions.

Bench top dissolution with 98 % H_2SO_4, 65 % HNO_3 or 32 % HCl yielded excellent La and Nd recoveries from the pure REE metal, inorganic compounds as well as in a mixture containing all three elements, ranging from 97.9(5) to 100.6(1) %. Ce recovery in the pure metal only ranged from 81.37(9) to 95.30(8) %. Microwave assisted acid digestion was employed to improve the recovery of Ce metal. The Ce recoveries improved to 96.5 and 99.6 % after microwave digestion. The efficiency of the acids in dissolving and recovering Ce in the pure metal sample was in the order HCl < HNO_3 < H_2SO_4. Excellent metal recoveries for the synthesised organometallic complexes ranging from 98.0(2) to 103.6(4) % for acac, imda and nta were obtained for the different organometallic complexes. ([Ln(dap)$(NO_3)_3$] Ln = La, Ce) yielded metal recoveries ranging from 88.1(5) to 95.5(3) % using bench top dissolution. The metal recoveries of TPPO complexes ranged between 98.45(5) and 99.4(2) % after microwave digestion.

The method validation done in **Section 5.8** was considered satisfactory. All calibration curves showed good linearity with excellent r^2 values which range between 0.9997 to 1 and fairly constant slopes. The elemental LODs ranged between 0.0030 - 0.0188 ppm and LOQ between 0.0289 - 0.1881 ppm in the different acid matrices used in this study. It can be concluded that the La, Ce and Nd analyses in pure REE metal, inorganic compounds and organometallic complexes were successful and the results met most of the guidelines within acceptable criteria as set out in ISO 17025.

The successful metal recoveries in acac, imda, nta and TPPO complexes were also due to the fact that these complexes have been crystallographically characterised and their chemical structures are well known, whereas the metal-dap complexes has not yet been fully characterised. Characterisation of synthesised organometallic complexes and ligands using IR also played a huge role in illustrating the possible coordination of the metal and ligands. The IR spectra were analysed by simple comparisons of the stretching frequencies between the unreacted samples and the reaction products. The shifting to low or high wavenumbers and disappearance or appearance of peaks was used as a measure for the possible formation of a new product.

Opsomming

Die doel van hierdie studie was om ‘n analitiese metode te ontwikkel wat die vroeë skaarse-aardmetale (REE) in suiwer metaliese, anorganiese verbindings, in mengsels van die drie aardmetaal (La, Ce en Nd) asook in organometaalverbindings akkuraat te kwantifiseer. Drie verskillende anorganiese sure, H_2SO_4, HNO_3 en HCl is as oplosmiddels gebruik en hulle invloed op die opbrengs van La, Ce en Nd ns die verskillende chemise verbindings is bepaal. Bankskaal bereiding sowel as ‘n mikrogolf is gebruik om monsters kwantatitief op te los. Verskillende analitiese tegnieke is gebruik om die nuut-bereide verbidings te karateriseer asook te kwantifiseer. Dit sluit onder andere optiese-emissie spektroskopie met behulp van induktief-gekoppelde plasma (ICP-OES), CHNS-mikro analise en infra-rooi spektroskopie (IR) in. Akkuraatheid, presisie, lineariteit, sensitiwiteit ens., deur middel van ICP-OES is geëvalueer (**Hoofstuk 4**) om die geskiktheid van die oplos- en kwantifiseringsmetodes vir die skaars-aardmetale te bepaal. Die golflengtes vir die drie elemente is baie noukeurig gekies om enige oorvleueling met mekaar of ander metale se spektrums te beperk of total te verhoed. Tweedens is die suurmatriks gedurende die analitiese proses noukeuring dieselfde gehou om akkurate analitiese metings en goed-gekontroleerde eksperimentele toestande te handhaaf.

Die verskillende monsters is op bankskaal met behulp van 98% H_2SO_4, 65% HNO_3 en 32% HCl opgelos en voortreflike resultate is vir La en Nd as suiwer elemente asook die anorganiese verbindings en die mengsel van die drie elemente verkry met opbrengste wat gewissel het tussen 97.9(5) % en 100.6(1) %. Die Ce-opbrengs tydens die studie vir die suiwer Ce metaal het tussen 81.37(9) % en 95.30(8) % gevarieer. Mikrogolf is vervolgens gebruik om die oplosproses te prober verbeter en die opbrengs het na 96.5 % en 99.6 % verhoog. Die doeltreffendheid van die sure in die oplos van die Ce metaal was in die volgende volgorde: $HCl < HNO_3 < H_2SO_4$. Baie goeie opbrengste is gevind vir die nuut bereide organometaalverbindings en het tussen 98.0(2) % tot 103.6(4) % vir acac, imda en nta gevarieer. Kleinskaal-bereidings van $[Ln(dap)(NO_3)_3]$ (Ln = La, Ce) het metaalherwinning van 88.1(5) % en 95.5(3) % gelewer terwyl TPPO-verbindings opbrengste tussen 98.45(5) % en 99.4(2) % na mikrogolfvertering gelewer het.

Metode validering aan die hand van ISO 17025 in **Paragraaf 5.8** dui op aanvaarbare valderingsparameters. Die kalibrasiekurwes toon almal goeie lineariteit met goeie r^2 waardes wat tussen 0.9997 en 1 varieer, en redelike konstante hellings. Die waarnemingslimiete in die verskillende suur-matrikse varieer tussen 0.0030 en 0.0188 dpm terwyl die kwantifiseringslimiete tussen 0.0289 en 0.1881 dpm varieer. Opsommend word die herwinning van La, Ce en Nd in die suiwer skaars-aardmetaal (REE), anorganiese verbindings en organometaalverbindings as uiters suksesvol beskou en die resultate voldoen grootliks aan die riglyne soos in ISO 17025 aangediu.

Die suksesvolle metaal-opbrengs in die acac, imda, nta en TPPO verbindings kan deels toegeskryf word aan die feit dat die verbindings reeds deur vorige studies kristallografies gekarateriseer is en dat hulle chemiese strukture (empiriese formules) bekend is. Die metaal-dap verbinding daarenteen is nog tot op hede nie ten volle gekarateriseer nie. Die karakterisering van die ligande en die nuut-bereide organometaalverbindings met behulp van infrarooi spektroskopie het ‘n groot rol in die karakterisering en odentifikasie van die bereide produkte gespeel. Vergelykings van die strekkingsfrekwensies van die ongekoördineerde ligande en die bereide komplekse is as maatstaf gebruik. ‘n Verskuiwing na ‘n hoër of laer energie of die laer golfgetal of die verdwying of verskyning van pieke is gebruik vir bevestiging van die sulksevolle bereiding van die nuwe produk.